Published in : ChemSusChem (2025), e202501565
DOI: 10.1002/cssc.202501565
Status : Postprint (Author's version)

REVIEW

CATALYTIC GENERATION OF NITROSOCARBONYLS UNDER MILD CONDITIONS: ADVANCES, CHALLENGES, AND OPPORTUNITIES

Yi-Hsuan Tsai

Center for Integrated Technology and Organic Synthesis (CiTOS), MolSys Research Unit, University of Liège, Liège, Belgium.

Carlotta Campalani

Center for Integrated Technology and Organic Synthesis (CiTOS), MolSys Research Unit, University of Liège, Liège, Belgium.

Thomas Toupy

Center for Integrated Technology and Organic Synthesis (CiTOS), MolSys Research Unit, University of Liège, Liège, Belgium.

Isaline Jacquemin

Center for Integrated Technology and Organic Synthesis (CiTOS), MolSys Research Unit, University of Liège, Liège, Belgium.

Jean-Christophe M. Monbaliu

Center for Integrated Technology and Organic Synthesis (CiTOS), MolSys Research Unit, University of Liège, Liège, Belgium – WEL Research Institute, Wavre, Belgique.

Abstract. Nitrosocarbonyl species (NOCs), also known as acylnitroso species, are highly reactive nitrogen-containing electrophiles. Since their first reports in the 1970s, they have shown significant synthetic potential for the preparation of aminated substrates. Their widespread adoption as versatile amination reagents began in the 2000s, driven by the development of new organometallic and organocatalytic systems. NOCs are typically generated in situ from stable precursors, such as hydroxamic acids and *N*-hydroxycarbamates, under oxidative conditions, in the presence of a scavenging substrate. This review highlights recent advances in NOC-based catalytic aminations over the past two decades. Specifically, their catalytic generation using oxygen, reactive oxygen species, and peroxides, followed by a subsequent capture through nitroso Diels–Alder, nitroso-ene, and nitroso-aldol reactions are comprehensively discussed. While most catalytic systems rely on Fe-, Co, Ni-, Cu-, Mo-, Ru-, and Ir-based catalysts, emerging approaches include organocatalysis, photoredox catalysis, electrochemistry, and enzymatic systems. Sustainability and innovative process technologies are also discussed as future directions.

Keywords. Catalytic oxidations | nitroso Diels–Alder | nitroso-aldol | nitroso-ene | nitrosocarbonyl.

Published in : ChemSusChem (2025), e202501565
DOI: 10.1002/cssc.202501565
Status : Postprint (Author's version)

1 | Introduction

Over the past two decades, catalytic oxidation protocols for generating nitrosocarbonyl compounds (NOCs, **1**, Figure 1a) have seen significant advancements. NOCs belong to a subclass of reactive *C*-nitroso intermediates bearing a geminal activation. Along with other reactive C-nitroso species, such as α-EWG-nitroso derivatives (**2**, Figure 1a) and nitrosoarenes (**3**, Figure 1a), their synthetic utility as versatile electrophilic amination reagents have been widely documented [1-3]. Owing to the sensitivity of the nitroso group to backbone modulation, NOCs are inherently the most reactive and, consequently, the most extensively studied members among the C-nitroso species [4].

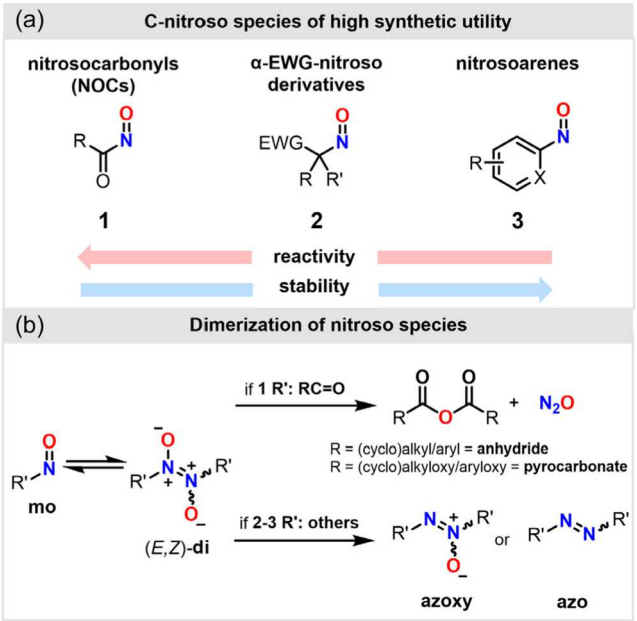

FIGURE 1 | (a) Main classes of C-nitroso compounds and relative reactivity. (b) Dimerization of C-nitroso compounds and corresponding potential competing decomposition pathways.

However, using nitroso species presents significant challenges due to their tendency to engage in a variety of competing side reactions (Figure 1b) [5]. Key factors like solvent, steric hindrance, and electronic effects strongly influence the equilibrium between the reactive monomeric nitroso species (**mo**) and their azodioxy dimers (**di**) [6]. While dimerization can serve as an inactive reservoir for the monomers, it can also lead to the formation of unwanted azoxy or azo side products (Figure 1b) [5].

In the case of NOCs, the formation of the dimer becomes even more problematic: with an estimated lifetime of just 1 ms at infinite dilution in organic solvents, the monomer is readily converted into the corresponding azodioxy dimers the decomposition of which is irreversible and almost instantaneous [7, 8]. This decomposition process typically results in the formation of nitrous oxide (N_2O) and the corresponding anhydride, or in some cases, a pyrocarbonate (Figure 1b) [4, 9].

Published in : ChemSusChem (2025), e202501565
DOI: 10.1002/cssc.202501565
Status : Postprint (Author's version)

NOCs were first reported *indirectly* in the early 1970s, either through the detection of their decomposition products or through capture with dienes [10]. Already in these early reports, dimerization was mitigated through low local concentration of NOCs. This is typically achieved by slow addition of an oxidizer to the NOC precursor in the presence of an excess of a good trapping agent [4, 11]. Direct detection of NOCs was not accomplished until 2002, about 30 years after their initial report, using time-resolved infrared spectroscopy [12].

NOCs are used in highly useful transformations. Figure 2 represents how, varying the nature of the trapping agent (diene or nucleophile), it is possible for NOCs to undergo hetero-Diels-Alder (hDA), nitroso-ene, and nitroso-aldol reactions among others [4, 11]. The trapping of NOCs with dienes through hDA reaction is both the historical landmark and the most represented synthetic application to date (Figure 2a) [4, 13]. This reaction, indeed, leads to a remarkably versatile heterocyclic platform, namely, the 3,6-dihydro-1,2-oxazine scaffold. Oxazine derivatives are interestingly used in biological applications [14, 15] and as versatile intermediates for the synthesis of 1,4-amino alcohols [4, 16], amino sugars [17, 18], oxazepinones [19], pyrroles [20, 21], pyrrolidines [4, 22, 23], γ-lactones [24], and many others [25–28].

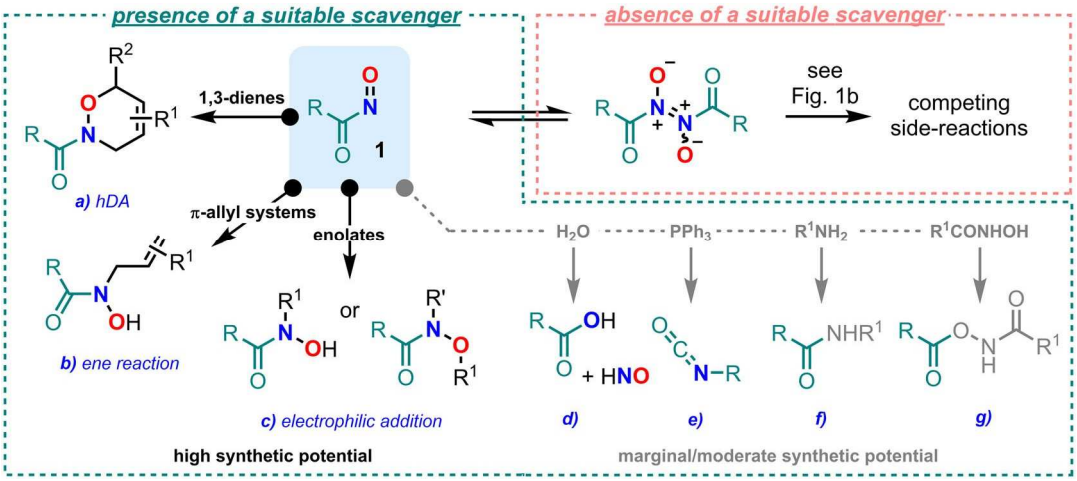

FIGURE 2 | Reactivity of NOCs in the presence of suitable scavengers. The main emphasis of this review concerns their wide synthetic applications in hDA, ene and nitroso-aldol reactions (electrophilic aminations). Other more marginal synthetic applications are presented as well (light gray).

It is important to note that the use of unsymmetrical dienes, such as 2-substituted-1,3-butadienes, can provide two regioisomers (Figure 3): the distal isomer, where the 2-substituent is positioned near the nitrogen atom of the resulting oxazine adduct, and the proximal isomer, where the 2-substituent is located near the oxygen atom of the cycloadduct. Achieving regiocontrolled scavenging of NOCs in this transformation is therefore crucial for the synthetic utility of the adducts.

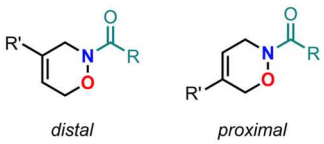

FIGURE 3 | Distal and proximal isomers from the hDA reaction of NOCs and unsymmetrical dienes.

Published in : ChemSusChem (2025), e202501565
DOI: 10.1002/cssc.202501565
Status : Postprint (Author's version)

In the presence of an allylic trapping reagent, NOCs undergo ene reaction to form *N*-allylhydroxamic acids (Figure 2b). Due to the sensitive character of this reaction that causes low selectivity and poor yields, its applications are rather narrow despite of its synthetic interest [29, 30]. Upon the addition of *C*-nucleophiles, NOCs undergo nitroso-aldol reactions (Figure 2c). Two possible regioisomers, namely, the *O*-selective α-aminoxylation and the *N*-selective α-hydroxyamination products, are expected. Hence, regioselective transformations have been developed [31], with additional efforts towards enantioselective C–O or C–N bond forming processes [32, 33]. The scope of the nitroso-aldol reaction of NOCs include enolizable ketones, aldehydes, β-dicarbonyl compounds, and β-ketophosphonates [34]. Subsequent transformations result in valuable aminated intermediates [32, 35, 36]. Other applications for NOCs have been reported, such as their deoxygenation by phosphines to obtain isocyanates (Figure 2e) and their reaction with water, amines, and hydroxamic acids to produce the corresponding carboxylic acids, amides, and *O*-acylhydroxamates, respectively (Figure 2d,f,g). NOCs can also be used as HNO generators through hydrolysis or as acylating agent of DNA bases [37, 38].

Regardless of the final scavenger, several methods for the production of NOCs in situ (Figure 4) were reported. These methods typically rely on the oxidation of stable precursors, such as hydroxamic acids (**HA**) or *N*-hydroxycarbamates (**HC**). *N*-hydroxyureas, and nitrile oxides have also been marginally reported [4, 11, 39]. Stable NOC precursors can be oxidized with a wide range of organic and inorganic oxidizers such as periodate salts [11, 40], lead acetate [40], Dess-Martin periodinane [41], hypochlorites [40, 42], and manganese dioxide [42]. Additionally, the combination of benzoyl peroxide (BPO) and (2,2,6,6tetramethylpiperidin-1-yl)oxyl (TEMPO) [33] as well as modified Swern protocols [43] have also been reported. The use of weaker oxidizers than periodates is usually preferred to avoid the formation of side-products.

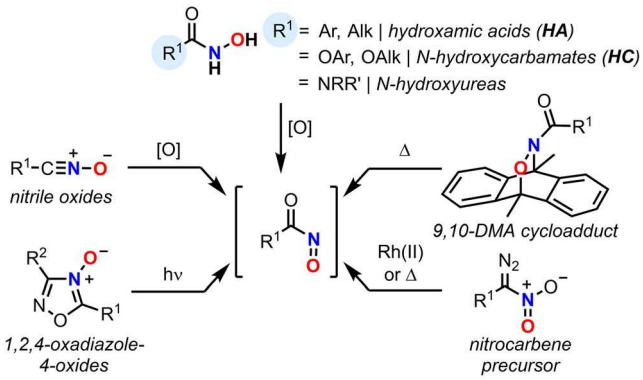

FIGURE 4 | Representative methods to prepare NOC intermediates in situ.

1,2,4-oxadiazole-4-oxides, and nitrocarbene compounds were also punctually reported as precursors of NOCs under photochemical or thermal activation [4, 11]. A common strategy to release NOCs in an oxidizer-free environment is the method developed by Keck and Kirby, which was predominant for more than three decades [10, 44]. Their original protocols, independently reported in the 1980s, relied on a 2 step *catch-and-release* method (Figure 5). During the first step (*catch*), a NOC precursor is oxidized and trapped with a reversible scavenger, such as 9,10-dimethylanthracene. The corresponding cycloadduct is isolable and purifiable. In the

Published in : ChemSusChem (2025), e202501565
DOI: 10.1002/cssc.202501565
Status : Postprint (Author's version)

second step (*release*), the purified reversible NOC cycloadduct is subjected to a thermal retro-Diels–Alder to release the NOC in the presence of the final scavenger. This two-step method is particularly useful for sensitive reactions that must be performed in oxidizer-free conditions. For instance, NOC ene and nitroso-aldol reactions yield products which can be overoxidized, leading to decomposition. This method however suffers from a poor atom economy, as it requires stoichiometric amounts of oxidant, a sacrificial diene, and a large excess of the final scavenger to outperform the reverse reaction.

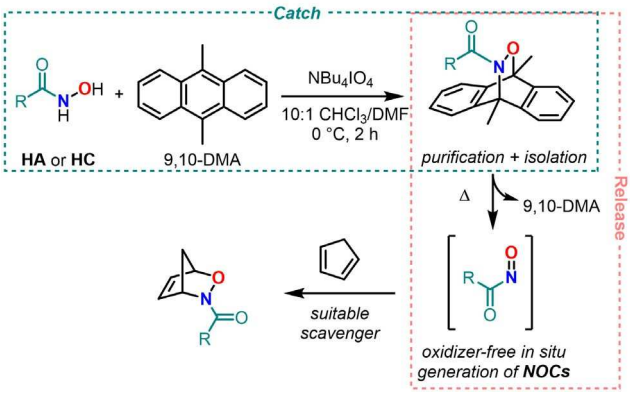

FIGURE 5 | Oxidizer-free stoichiometric generation of NOCs according to Keck and Kirby's protocol. This protocol is particularly suitable for reactions where competing oxidation is an issue.

In recent years, research efforts have increasingly targeted milder, more sustainable and cost-efficient ways toward NOCs (Figure 6). Low molecular weight oxidizers with a high atom economy, such as peroxides, oxygen, and reactive oxygen species (ROS), in conjunction with metal-, organo(photo)(electro)-, and enzyme-based catalytic systems are now defining the new norm. This review guides the chemist across these developing landscapes. It is divided in two main sections according to the type of primary oxidants (peroxides – Section 2, and oxygen/ROS – Section 3). In each subsection, the articles are clustered around the best performing metal catalyst, if concerned. If similar outcomes are obtained with different metals, the least expensive are emphasized, since they are also often the more abundant ones and thus the most pragmatic for large-scale applications [45].

Published in : ChemSusChem (2025), e202501565
DOI: 10.1002/cssc.202501565
Status : Postprint (Author's version)

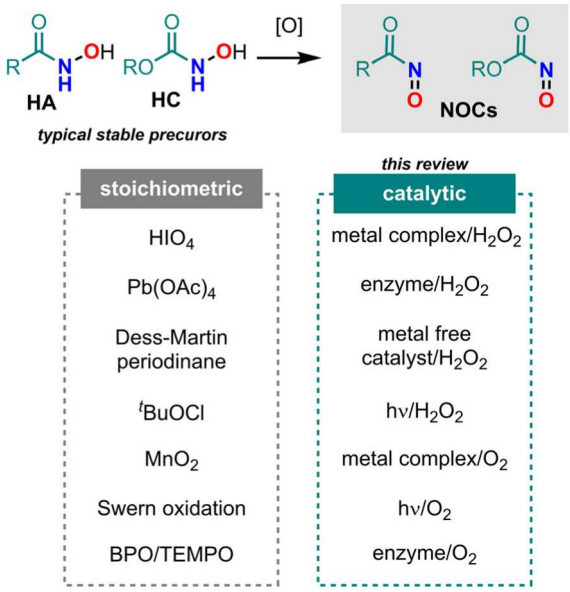

FIGURE 6 | Common protocols for the in situ oxidative preparation of NOCs. BPO = benzoyl peroxide; TEMPO = (2,2,6,6-tetramethylpiperidin-1-yl)oxyl.

The abbreviations used through the review are listed in Table 1 in alphabetical order.

Published in : ChemSusChem (2025), e202501565
DOI: 10.1002/cssc.202501565
Status : Postprint (Author's version)

TABLE 1 | Abbreviations used in this review.

Abbreviation	Definition
ANO	aziridine *N*-oxide
BINAP	2,2′-bis(diphenylphosphino)−1,1′-binaphthyl
Boc	*tert*-butyloxycarbonyl
BPO	benzoyl peroxide
Bpy	2,2′-bipyridine
Cap	caprolactamate
Cbz	benzyloxycarbonyl
CHP	cumyl hydroperoxide
Coe	cyclooctene
Cod	1,5-cyclooctadiene
D-Ala	D-alanine
D-Leu	D-leucine
D-Phe	D-phenylalanine
D-Trp	D-tryptophan
D-Val	D-valine
DCM	dichloromethane
DFT	Density Functional Theory
DMF	dimethylformamide
DMSO	dimethyl sulfoxide
dr	diastereomeric ratio
ee	enantiomeric excess
EPR	Electron Paramagnetic Resonance
EtOx	2-ethyloxazoline
Fmoc	9-fluorenylmethoxycarbonyl
GOx	glucose oxidase
HA	hydroxamic acid
HAT	hydrogen atom transfer
HC	*N*-hydroxycarbamates
hDA	hetero Diels–Alder
HOMO	Highest Occupied Molecular Orbital
HPLC	High-Performance Liquid Chromatography
HRMS	High Resolution Mass Spectroscopy
HRP	horseradish peroxidase
IR	infrared spectroscopy
LUMO	Lowest Unoccupied Molecular Orbital
m-CPBA	*m*-chloroperbenzoic acid
Moz	p-methoxybenzyloxycarbonyl
n-ESI-MS	nanoelectrospray ionization mass spectrometry
NBS	*N*-bromosuccinimmide
NIS	*N*-iodosuccinimmide
NMR	Nuclear Magnetic Resonance
NOC	nitrosocarbonyl
Nppoc	2-(2-nitrophenyl)-propyloxycarbonyl
PhBox	2,2′-(2,2-propanediyl)bis(4-phenyl-4,5-dihydro-1,3-oxazole)
PivOH	pivalic acid
PROPHOS	1,2-bis(diphenylphosphino)propane
Pybox	2,6-bis(4,5-dihydro-4-phenyl-2-oxazolyl) pyridine
Pydic	pyridine-2,6-dicarboxylate
Pyr	pyridine
RB	Rose Bengal
ROS	Reactive Oxygen Species
SAHA	suberoylanilide hydroxamic acid
TBA	tetra-*n*-butylammonium
TBAI	tetra-*n*-butylammonium iodide
TBADT	tetrabutylammonium decatungstate
TBHP	*t*-butyl hydroperoxide
TBS	*t*-butyldimethylsilyl
TEMPO	(2,2,6,6-tetramethylpiperidin-1-yl)oxyl
TFA	trifluoroacetic acid
TfOH	triflic acid
THF	tetrahydrofuran
TMS	tetramethylsilane
Troc	2,2,2-trichloroethoxycarbonyl chloride
TS	Transition State
UV-Vis	Ultraviolet-Visible

Published in : ChemSusChem (2025), e202501565
DOI: 10.1002/cssc.202501565
Status : Postprint (Author's version)

2 |Catalytic Oxidations Toward Nitrosocarbonyl Derivatives Using Peroxides

Peroxides have emerged as versatile and environmentally benign oxidants for the generation of NOC species, particularly from HA derivatives. Their broad availability, low cost, and ability to operate under mild conditions make them especially attractive for sustainable oxidation processes. Among the most widely used peroxides are hydrogen peroxide (H_2O_2) and t-butyl hydroperoxide (TBHP) both of which

can engage in single-electron or heterolytic oxidation pathways depending on the nature of the catalyst and reaction environment.

These oxidants can function in the presence of transition metals, organocatalysts, or biocatalysts, often facilitating the formation of reactive intermediates, such as NOC compounds, through mechanisms involving radical, ionic, or hypervalent species. Importantly, their compatibility with mild conditions (e.g., neutral pH, aqueous media, room temperature) aligns well with green chemistry principles.

This section explores the diverse catalytic systems used in peroxide-mediated NOC formation, including metal-catalyzed, metal-free, and enzyme-based systems, highlighting both mechanistic diversity and practical applications in synthesis.

2.1 | IRON CATALYSTS

In 2007, Adamo and Bruschi studied the oxidation of precursor **1a** in the presence of a diene (**2a**), of H_2O_2 as an oxidant and of different metal/amine complexes as catalysts (Figure 7) [46].

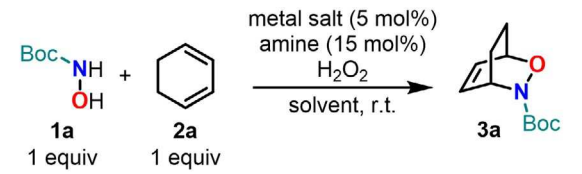

Metal salt	Amine	Solvent
$RuCl_3$ $CuCl$ $CuCl_2$ $FeCl_3$ $NiCl_2$	$HOCH_2CH_2NH_2$ NEt_3 $H_2NCH_2CH_2NH_2$	DCM THF

FIGURE 7 | Test experiments with five different catalytic systems on the hDA reaction between N-Boc-hydroxylamine **1a** and 1,3-cyclohexadiene **2a** using hydrogen peroxide as oxidant (see also Table 2).

Screening different metal salts and amines, the outcome of (Continues) the hDA reaction towards the cycloadduct (**3a**) was assessed.

As metal salts, the authors chose commercially available chlorides of Cu(I), Cu(II), Fe(III), and Ni(II), while ethanol amine, ethylene diamine, and triethylamine were tested as ligands to explore the possibility of ligand-accelerated

Published in : ChemSusChem (2025), e202501565
DOI: 10.1002/cssc.202501565
Status : Postprint (Author's version)

catalysis and to enhance the solubility of metal salts. THF (donor according to Guttman's scale) and DCM (nondonor solvent) were selected to study the effect of solvents that can (THF) or cannot (DCM) participate in metal ligation and their influence on catalytic efficiency.

$RuCl_3$ was used together with triethylamine in a test experiment, resulting in complete conversion in 20–30 min and isolated yields up to 78%. CuCl, $CuCl_2$, $FeCl_3$ and $NiCl_2$ were then studied in depth as more economical salts. All catalysts worked under mild conditions (low temperature) and demonstrated several additional distinctive advantages: strict atmosphere control was not mandatory, the diene was used under equimolar conditions, and no solubility issues were encountered. The following points were highlighted during the study:

1. In the presence of a ligand, the reaction was faster in DCM than in THF;
2. Cu(I), Cu(II), and Fe(III) salts were associated with a high activity, even without a ligand;
3. When the reaction proceeded without ligand, it was due to the ability of THF to act as a ligand (the possibility of compound **1a** acting as a ligand too was not excluded);
4. When used without ligands, Cu(I) and Cu(II) worked faster in THF than in DCM, but this trend was reversed in the presence of a ligand (amino alcohols resulted to be the best);
5. The use of enantiopure aminoalcohols as ligand still gave racemic product mixture suggesting the release of the corresponding NOC from the metal after oxidation, which aligns with Whiting´s observations regarding chiral Ru(II) salen catalysts (see below) [40];
6. Although Ni(II)-catalyzed reactions produced high yields cycloadducts, they were significantly slower, thus negatively impacting the overall productivity.

The scope was then explored using both cyclic and acyclic dienes **2b-f** in the presence of Cu(I), Cu(II), and Fe(III) catalysts (Table 2) and NOC precursor **1a**. Complete conversion of **1a** was generally observed under 30 min, giving the corresponding cycloadduct **3** in good yields (54%–78%) [46]. The iron-based catalyst resulted to be more active than the others for the reaction involving dienes **2b**, **2c**, and **2f**.

The same year, Whiting reported three novel transition metal catalysts designed for the oxidation of HA to NOC species in the presence of dienes [47]. The aim of this research was to reach a stereoselective hDA process, but the authors reported the systematic formation of racemate cycloadducts. It was hypothesized that the dissociation rate of the NOC from the catalyst is faster than its cycloaddtion. To address this, extending the lifetime of the acylnitroso species/metal complex appeared crucial for achieving stereoselective hDA. In this context, the authors considered commercially available *N*-(benzyloxycarbonyl)hydroxylamine (*N*-Cbz-hydroxylamine **1b**) as a potential precursor to a bidentate NOC ligand. The corresponding NOC ligand can coordinate with the metal center through the oxygen of the nitroso function and with either the urethane oxygen or the carbonyl oxygen (Figure 8). Additionally, the resulting acylnitroso species might also form *hapto*-complexes via the π-donor benzene ring, providing further stabilization, and, thus, potentially enhancing asymmetric induction.

Published in : ChemSusChem (2025), e202501565
DOI: 10.1002/cssc.202501565
Status : Postprint (Author's version)

TABLE 2 | *N*-Boc-hydroxylamine (**1a**) hDA reaction with a library of dienes catalyzed by Cu(I), Cu(II), and Fe(III) catalysts using H_2O_2 as oxidant.

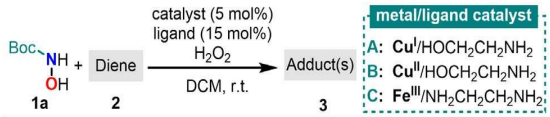

Entry	Diene	Adduct(s)	Catalyst/yield (%) A	B	C
1	2b	3b	63	64	78
2	2c	3c	74	70	76
3	2d	3d-I, 3d-II	70[a]	54[a]	54[a]
4	2e	3e-I, 3e-II	64[b]	70[b]	58[b]
5	2f	3f-I, 3f-II	58[c]	65[c]	64[c]

[a]Obtained as a 1:1.6 mixture of regioisomers.
[b]Obtained as a 1:3 mixture of diastereoisomers.
[c]Obtained as a 1:1 mixture of regioisomers.

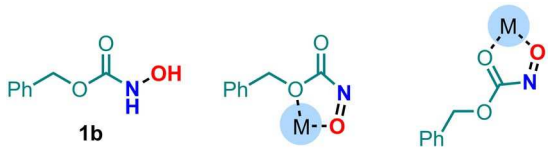

FIGURE 8 | *N*-Cbz-hydroxylamine (**1b**) as a bidentade ligand in metal chelation.

To achieve such distinct binding modes, the metal center requires at least two vacant coordination sites *cis* to each other. Therefore, metal complexes of ligand **4** (Figure 9) were chosen, since these would likely contain vacant *cis*-oriented sites suitable for acylnitroso coordination. Additionally, complexes of ligand **4** have an asymmetric three-dimensional structure which can restrict the approach of the diene to the bound acylnitroso species. Iron, ruthenium, and chromium were chosen as metals to form the complexes due to their rich redox and Lewis acid properties (Figure 9). The salen-ruthenium system (**8**), previously reported to effectively catalyze the oxidation of

Published in : ChemSusChem (2025), e202501565
DOI: 10.1002/cssc.202501565
Status : Postprint (Author's version)

HAs with *tert*-butyl hydroperoxide (TBHP), but unsuccessful in achieving enantioselective hDA reactions, was included for comparison [47, 48].

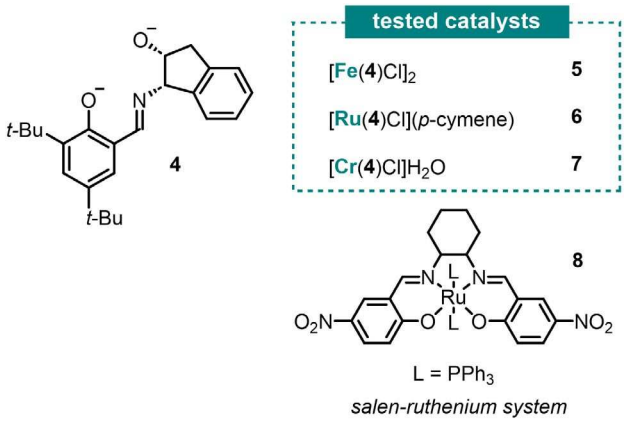

FIGURE 9 | Representation of ligand **4** and catalysts **5-8**.

Unlike catalyst **8**, complexes **5–7** were unable to oxidize the substrate to its corresponding acylnitroso species with TBHP, but they proved to be efficient with H_2O_2. If Ru- and Cr-based catalysts **6–7** led to lower yields than **8**, the iron complex **5** gave comparable results.

The catalytic activity of these complexes was evaluated through hDA reaction of a library of dienes and *N*-Cbz-hydroxylamine at room temperature for 16 h (Table 3). The low yields obtained some of the studied dienes (Table 3, entries 5, 6, 8, and 9) may be due to competing retro-DA reaction driven by the reversible behavior of the transformation. An increment in the catalyst loading from 0.1 mol% to 1 mol% improved the overall yields at decreased reaction rates but also increased the formation of side products from overoxidation. Finally, no asymmetric induction was observed in the cycloadducts probably due to the poor stability of the metal–acylnitroso complex. Indeed, the bidentate behavior of acylnitroso compounds could not be proven [47].

In 2011, Malkov and colleagues described a mild Fe(III)/H_2O_2 oxidation, compatible with an intramolecular nitrosocarbonyl ene reaction to yield valuable 1,2- and 1,3-amino alcohol derivatives [49]. In contrast with cycloaddtions, ene reactions are considerably slower and some conventional strong oxidants may degrade the ene adducts as well as the acylnitroso intermediates upon prolonged exposure [49]. While intramolecular allylic amination can be achieved using Pd(II) or Rh(II) catalysts, the use of the latter often leads to a mixture of products due to competing aziridination (Figure 10a) [50–52]. Alternatively, amination can be achieved using Kirby's protocol via the nitrosocarbonyl ene reaction, which involves a sacrificial diene and an additional isolation step to form the new C–N bond (Figure 10b) [8].

To enhance the efficiency of NOCs ene reactions, Malkov and coworkers tested $FeCl_3$ (4 mol%) as catalyst with H_2O_2 (1.2–6 equiv.) serving as the oxidant (Figure 10c).
The use of a stoichiometric amount of H_2O_2 resulted crucial for regenerating the catalytically active metal species, as evidenced by the absence of catalytic turnover without the oxidant. Notably, even though the Fe(III)/H_2O_2 catalytic system is known to promote epoxidation of alkenes, no epoxide was produced under these reaction

Published in : ChemSusChem (2025), e202501565
DOI: 10.1002/cssc.202501565
Status : Postprint (Author's version)

conditions [53]. The metal catalyst role was likely to participate in the oxidation of HAs to their corresponding nitroso intermediates.

TABLE 3 | Transition metal-catalyzed hDA reaction between *N*-Cbz-hydroxylamine and various dienes.

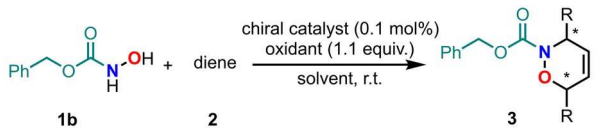

1b **2** **3**

Entry	Diene	Cycloadduct	Catalyst/yield (%)			
			5[a]	6[a]	7[a]	8[b]
1	**2a**	**3ba**	50;98[c]	45	23	53
2	**2b**	**3bb**	49	32	25	95
3	**2c**	**3bc**	42	40	22	69
4	**2e**	**3be**	22	7	28	25
5	**2f**	**3bf-I** **3bf-II**	10	14	9	14
6	**2g**	**3bg**	11	5	6	15
7	**2h**	**3bh**	23	6	10	16
8	**2i**	**3bi**	0	0	0	0[d]
9	**2j**	**3bj**	0	0	0	0[d]

[a] H_2O_2/Acetone.
[b] TBHP/DCM.
[c] Yields obtained from HPLC. [d] 1 mol% of catalyst used.

Published in : ChemSusChem (2025), e202501565
DOI: 10.1002/cssc.202501565
Status : Postprint (Author's version)

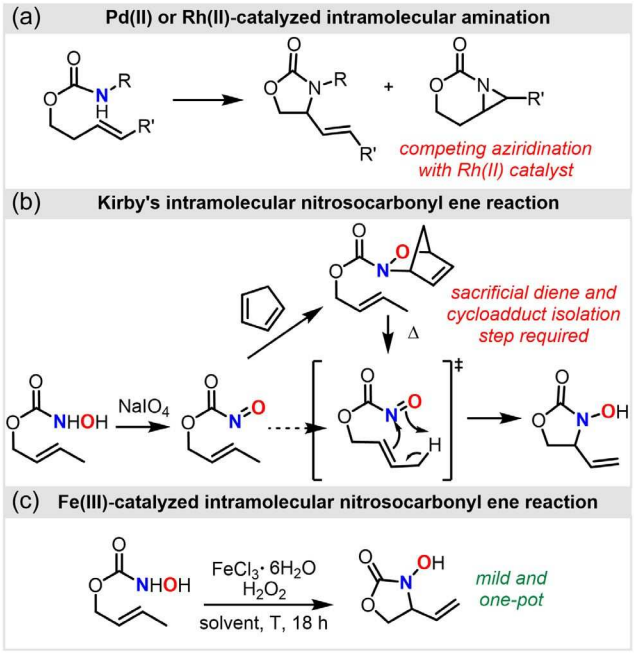

FIGURE 10 | Comparison of methods for intramolecular amination.

The reaction resulted to be stereospecific, as the (E)-crotyl alcohol derivative (**9a**) successfully produced the desired product **10a**, while the *Z*-analog did not yield any product (Figure 11a). Moreover, this process is also stereoselective, as seen with (*E*)-2-hexenol (**9b**), which gave product **10b** as an *E/Z* mixture enriched in the E-isomer. Raising the temperature from 60°C to 100°C improved both yield and the *E/Z* ratio from 4:1 to 6:1. Steric factors of the R^1 group significantly influenced reactivity, likely due to their impact on the removal of the allylic hydrogen. Reactivity decreased notably in the order Me > *n*-Pr > Bn > *i*-Pr.

In contrast, the bulkiness of the R^2 group does not appear to affect the reaction. Secondary crotyl analogs (**9e-h**) consistently produced **10e-h** adducts with a 2:1 *syn/anti* ratio, regardless of the size of the R^2 group (Figure 11b). Changes in solvent or catalyst did not influence on the *syn/anti* ratio. However, by lowering the temperature from room temperature (rt) to −20°C, the diastereoselectivity increased, as for the case of **10h** (2:1 → 5:1). The scope of this reaction was studied by using structurally diverse HAs (**9i-m**) to produce **10i-10m** (Figure 11c). Formation of 6-membered ring required more forcing conditions compared to the 5-membered counterpart [49].

Published in : ChemSusChem (2025), e202501565
DOI: 10.1002/cssc.202501565
Status : Postprint (Author's version)

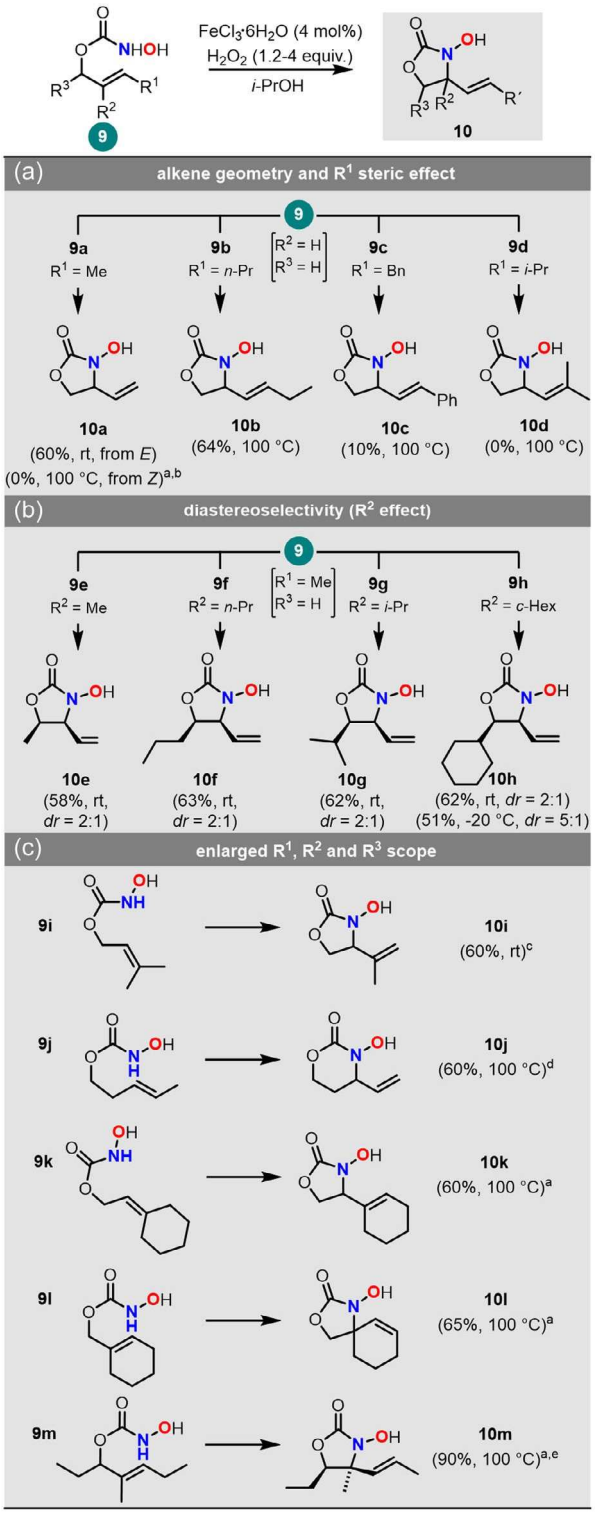

FIGURE 11 | Scope of intramolecular ene reaction in optimized conditions: $FeCl_3$ (4 mol%), aq H_2O_2 in i-PrOH, 18 h, indicated temperature. [a] H_2O_2 = 6 equiv. [b] precursor decomposed. [c] H_2O_2 = 1.2 equiv. [d] H_2O_2 = 3 equiv. [e] Major diastereoisomer (dr > 25:1).

Published in : ChemSusChem (2025), e202501565
DOI: 10.1002/cssc.202501565
Status : Postprint (Author's version)

2.2 | MAGNESIUM CATALYSTS

In 2014, Lu and coworkers reported a $MgCl_2$/TBHP-mediated α-amination of α-alkyl-β-ketoesters *via* oxidative *N*-acylnitrosoaldol reaction with HCs (Figure 12) [54]. Control experiments demonstrated the necessity of both $MgCl_2$ and TBHP to ensure the oxidation of the HC (**1a**) and enolization of β-ketoester **11a**. In the absence of TBHP, **1a** showed no conversion, whereas in the absence of $MgCl_2$, the desired reaction did not occur, even though **1a** was oxidized by TBHP, suggesting that the metal facilitates the enolization of **11a** (Figure 12).

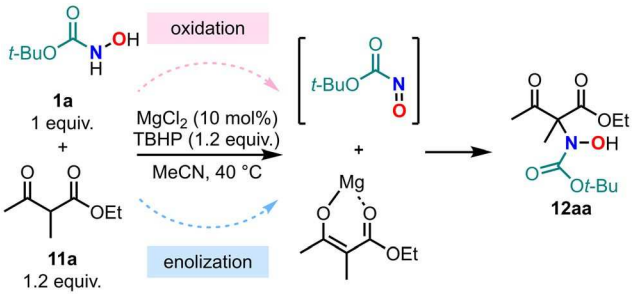

FIGURE 12 | $MgCl_2$-catalyzed *α*-amination of *α*-alkyl-*β*-ketoesters using HC.

Using the best conditions (10 mol% $MgCl_2$, 1.2 equiv. TBHP, in acetonitrile, T = 40°C), a broad range of substituted β-ketoesters and HCs resulted in high or excellent yields (Figure 13).

Published in : ChemSusChem (2025), e202501565
DOI: 10.1002/cssc.202501565
Status : Postprint (Author's version)

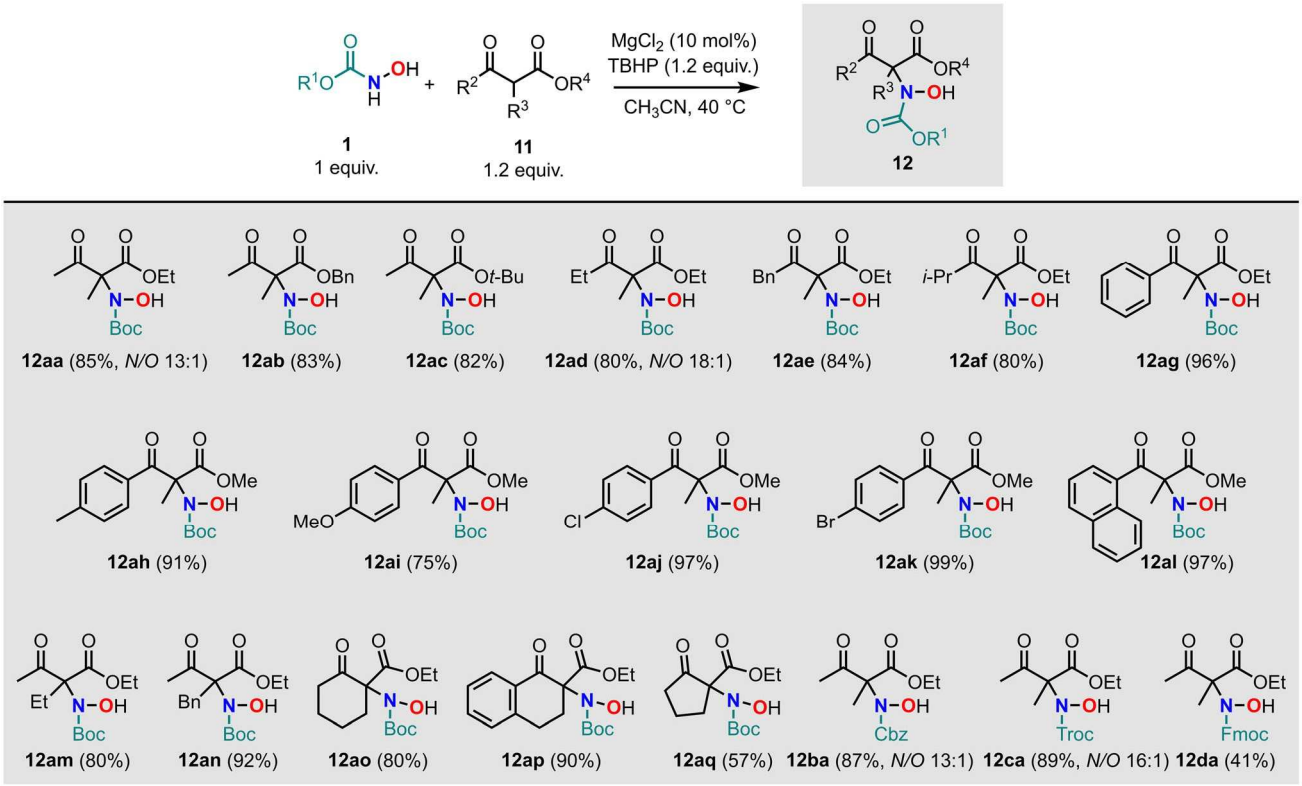

FIGURE 13 | Scope of the products obtained from the $MgCl_2$-catalyzed α-amination of *β*-ketoester using various HCs. The yields are the isolated yields and the *N/O* ratios were determined by ^1H NMR.

The reaction was predominantly *N*-selective except for some cases where the *O*-subproducts were observed with *N/O* ratios ranging from 13:1 to 16:1 (compounds **12ad**, **12ba**, and **12ca** in Figure 13).

To prove the robustness of the protocol, β-ketoesters with alkyl substituents (linear or branched) and aryl substituents (electron-rich or electron-deficient) at R^1 and protected hydroxylamines (with Cbz, Troc, and Fmoc) were successfully tested (Figure 13). However, reaction with β-ketoesters containing sterically hindered groups such as *tert*-butyl in R^1 position or isopropyl in R^2 position were particularly slow. In addition, the reaction of ethyl acetoacetate as unsubstituted β-ketoester, produced a mixture of products, probably due to transformations of the α-imino-β-ketoester intermediate with elimination of the β-hydroxyl group, as hypothesized by Read de Alaniz and coworkers [55]. The protocol established by Lu and colleagues was then tested for asymmetric α-amination but without success.

2.3 | COPPER CATALYSTS

In 2004, Iwasa and colleagues explored various metal-promoted oxidations of HCs using hydrogen peroxide to generate acylnitroso species [56]. These reactive intermediates were then trapped by alkenes through an ene reaction, followed by halocyclization, leading to the formation of oxazolidinones (Figure 14).

Published in : ChemSusChem (2025), e202501565
DOI: 10.1002/cssc.202501565
Status : Postprint (Author's version)

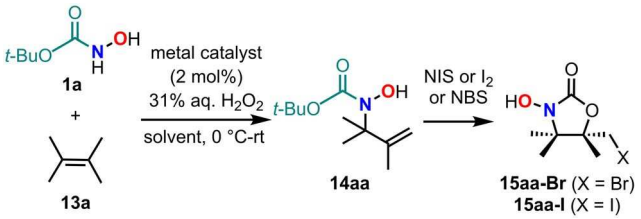

FIGURE 14 | Acylnitroso-ene reaction with further halocyclization.

The authors tested four different catalysts based on Ru(II), Ir(I), and Cu(I); the best conditions implied the use of 2 mol% of said catalyst together with 1.1–1.2 equiv. of 31% aqueous H_2O_2 (Table 4). The scope of the reaction was studied with a selection of aliphatic alkenes (**13a-c**) and two NOC precursors: HC **1a** and HA **1e**.

Interestingly, when **1e** was oxidized in the presence of trisubstituted alkene **13b**, the ene reaction produced a single regioisomer **14eb**, while **1a** under similar conditions led to the formation of two regioisomers, **14ab** and **16ab**. These were obtained in significantly higher yields (50%–86% for **1a** compared to 29%–40% for **1e**) and exhibited good to moderate regioselectivities (3:1–8:1). The major regioisomer, **14ab**, arose from allylic hydrogen abstraction at the more substituted side of the alkene.

Additional experiments with **1a** and other substrates demonstrated that the reaction is more favorable with more electron-rich alkenes. For example, under identical conditions, the disubstituted alkene **13c** produced lower yields compared to the tri- and tetrasubstituted alkenes **13b** and **13a**, respectively. In all cases, despite the unsymmetrical nature of the acylnitroso enophile, the reaction exclusively formed a C–N bond.

The catalytic activity observed for the formation of the NOC intermediate from **1a** followed the order: CuI > $[Ir(cod)Cl]_2$ > $[Ir(coe)_2Cl]_2$ > Ru(II)(pybox)(pydic) [56]. Generally, **1a** showed better performances than the HA **1e**: using the latter only Ru and Ir-based catalysts proved successful for the formation of the NOC intermediate (Table 4 entries 18–22).

Published in : ChemSusChem (2025), e202501565
DOI: 10.1002/cssc.202501565
Status : Postprint (Author's version)

TABLE 4 | Metal-catalyzed hydrogen peroxide oxidation of **1a** and **1e** and subsequent trapping of the NOCs with acyclic alkenes **13a-c** *via* an ene reaction.

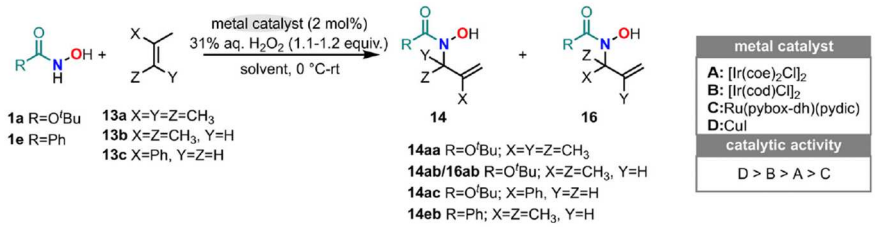

Entry	HA/HC	Alkene	Catalyst	Solvent	Time (h)	Product(s)[c]	Yield (%)[a]
1	**1a**	**13a**	A	THF	24	**14aa**	73
2	**1a**	**13a**	B	THF	8	**14aa**	87
3	**1a**	**13a**	C	THF	24	**14aa**	56
4	**1a**	**13a**	D	THF	4	**14aa**	91
5	**1a**	**13b**	A	THF	24	**14ab/16ab** 4:1	76[b]
6	**1a**	**13b**	B	THF	24	**14ab/16ab** 3:1	84[b]
7	**1a**	**13b**	C	THF	24	**14ab/16ab** 8:1	50[b]
8	**1a**	**13b**	C	MeOH	24	**14ab/16ab** 8:1	86[b]
9	**1a**	**13b**	D	THF	3	**14ab/16ab** 4:1	83[b]
10	**1a**	**13c**	A	THF	48	**14ac**	30
11	**1a**	**13c**	B	THF	16	**14ac**	31
12	**1a**	**13c**	C	THF	48	**14ac**	26
13	**1a**	**13c**	C	MeOH	24	**14ac**	12
14	**1a**	**13c**	C	MeOH	48	**14ac**	17
15	**1a**	**13c**	D	MeOH	5	**14ac**	78
16	**1a**	**13c**	D	THF	4	**14ac**	75
17	**1e**	**13a**	A	THF	40	**14ea**	38
18	**1e**	**13b**	B	THF	24	**14ea**	40
19	**1e**	**13b**	C	THF	24	**14ea**	29
20	**1e**	**13b**	C	MeOH	72	**14ea**	32
21	**1e**	**13b**	D	THF	24	**14ea**	0
22	**1e**	**13b**	D	MeOH	24	**14ea**	0

[a]Isolated yields.
[b]Combined yield of regioisomers.
[c]Regioisomeric ratios determined by ^{1}H NMR.

The generated acyclic ene products (**14**) were then used to perform a halocyclization to yield *N*-hydroxyhalosubstituted oxazolidinones (Table 5). As a proof of concept, compound **14aa** was subjected to iodolactonization using either N-iodosuccinimide (NIS) or iodine (I_2) and bromolactonization using *N*-bromosuccinimide (NBS). The resulting products, **15aa-I** and **15aa-Br**, are likely formed through a halonium ion intermediate that cyclizes with the carbonyl group of the carbamate [56].

Published in : ChemSusChem (2025), e202501565
DOI: 10.1002/cssc.202501565
Status : Postprint (Author's version)

TABLE 5 | Halocyclization of the ene product **14aa** using NIS, I_2 or NBS.

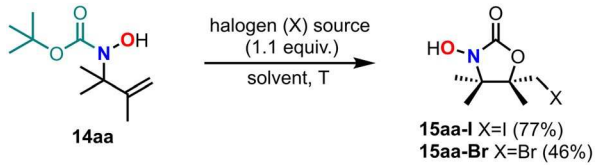

14aa

15aa-I X=I (77%)
15aa-Br X=Br (46%)

Entry	Halogen (X) source	Solvent	T (°C)	Yield (%)[a]
1	NIS (X = I)	Et_2O	rt	57
2	NIS (X = I)	Et_2O	0 - rt	70
3	NIS (X = I)	THF	rt	77
4	I_2 (X = I)	Et_2O	rt	77
5	NBS (X = Br)	THF	rt	46

[a]Isolated yields.

In another work from the same group, the catalytic oxidation of HC **1a** was applied to ene reaction with cyclic alkenes **13e** and **13f** using hydrogen peroxide and different Cu-, Ir-, and Ru-based catalysts (Table 6) [57]. Differently from the case with acylic alkenes [56], CuI resulted to be the least active catalyst but use of Cu(I) complexes (CuI(pybox-dh) and CuI-pybox-*i*Pr(*S, S*)) led to the highest yields of the desired product.

In 2005, Kalita and Nicholas reported the regioselective hydroxyamination of olefins using *N*-Boc-hydroxylamine (**1a**) and Cu(I) salts, yielding allyl-N(OH)(Boc) derivatives [58]. Initial studies with α-methyl styrene (**13c**) identified CuBr·SMe_2 (10 mol%) as the most effective catalyst (Conditions A, Table 7), affording the Boc-N-OH product (**14ac**) in 48% yield and $(Boc)_2NOH$ in 3%. Notably, this result contrasted with prior work where α-methyl styrene and arylhydroxylamines predominantly formed reduced *N*-aryl-*N*-allylamines [59–61].

The observed oxidation suggested Cu-catalyzed disproportionation of **1a**, generating the acylnitroso intermediate, which then underwent an ene reaction with the olefin. Supporting this, **1a** and 1,3-cyclohexadiene **2a**, heated with CuBr·SMe_2 (10 mol%), produced the Boc-NO-derived Diels–Alder adduct (**3aa**) (41% yield, 65 h). Notably, reaction efficiency improved significantly with a stoichiometric oxidant (e.g., 30% H_2O_2), enabling quantitative Diels–Alder conversion and 73% yield for **13c** hydroxamination at 20°C with CuCl catalysis (Table 7, entry 1, conditions B). Under these conditions, reactions with β-pinene (**13g**) and 1-octene (**13h**) afforded moderate yields of *N*-hydroxallyl amines **14ag** (43%) and **14ah** (24%), exhibiting typical enetype regioselectivity. [4 + 2]-Cycloadditions of transient acylnitroso are well documented, and the CuCl-H_2O_2 system provides an economical method for its generation.

Published in : ChemSusChem (2025), e202501565
DOI: 10.1002/cssc.202501565
Status : Postprint (Author's version)

TABLE 6 | Metal-catalyzed hydrogen peroxide oxidation of HC **1a** and subsequent trapping of the NOC species with cyclic alkenes *via* ene reaction.

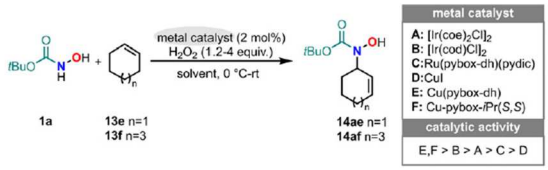

Entry	Alkene	Product	Catalyst	Solvent	Time (h)	Yield (%)[d]
1	**13e**	**14ae**	C[a]	THF	24	56
2	**13e**	**14ae**	A[a]	THF	24	55
3	**13e**	**14ae**	B[a]	THF	23	59
4	**13e**	**14ae**	D[a]	THF	4	43
5	**13e**	**14ae**	E[b]	MeOH	5	63
6	**13e**	**14ae**	F[a]	MeOH	3	73
7	**13f**	**14af**	C[c]	THF	24	39
8	**13f**	**14af**	A[c]	THF	24	47
9	**13f**	**14af**	B[c]	THF	24	60
10	**13f**	**14af**	D[c]	THF	5	47
11	**13f**	**14af**	F[a]	MeOH	3	69

[a]$H_2O_2 = 2.4$ equiv.
[b]$H_2O_2 = 4.0$ equiv.
[c]$H_2O_2 = 1.2$ equiv.
[d]Isolated yields.

Since Cu(I)X salts were ineffective in reducing Boc-*N*-hydroxy amines to Boc-*N*-allyl amines directly, ligand effects were explored. Among tested N- and P-based ligands, $CuBr/P(OEt)_3$ (10 mol%:100 mol%, 85°C (Table 7), conditions C) facilitated allyl amine **17ac** formation (37% yield). Similarly, β-pinene amination selectively yielded Boc-N-pinyl amine **17ag**, albeit in modest yield (13%).

Published in : ChemSusChem (2025), e202501565
DOI: 10.1002/cssc.202501565
Status : Postprint (Author's version)

TABLE 7 | Cu-catalyzed allylic hydroxyamination and amination of alkenes with N-Boc-hydroxylamine.

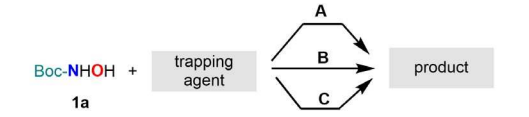

Conditions A	Conditions B	Conditions C
CuBr. SMe_2 (10 mol%) 90 °C, CH_2Cl_2/CH_3CN	CuCl (15 mol%), H_2O_2 (5 equiv.) 20 °C, CH_2Cl_2/CH_3CN	CuBr (10 mol%), $P(OEt)_3$ (1 equiv.) 80 °C, CH_2Cl_2/CH_3CN

Entry	Trapping agent	Cond.	Product	Yield (%)
1	 13c	A / B	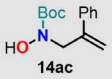 14ac	48 / 73[a]
2		C	 17ac	37
3	 2a	A	 3aa	41
4	 13g	A / B	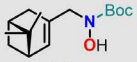 14ag	18 / 43[a]
5		C	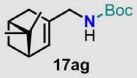 17ag	13
6	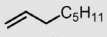 13h	A / B	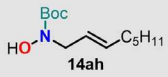 14ah	8 / 24[a]

[a]Yields of condition A/condition B.

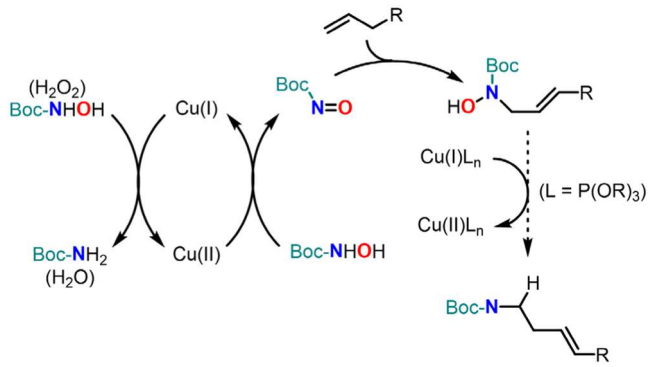

FIGURE 15 | Proposed catalytic cycle for the copper-catalyzed allylic amination reaction.

The proposed pathway for hydroxyamination (Figure 15) starts with the Cu-induced disproportionation of the HA or its oxidation in the presence of H_2O_2. This is followed by trapping of the acylnitroso intermediate with the olefin *via* an ene reaction to give the *N*-Boc-*N*-hydroxylamine. With the addition of $P(OEt)_3$, the Cu(I) Ln complex can reduce the hydroxylamine to the corresponding allylamine, regenerating the Cu(II) catalyst [58].

Published in : ChemSusChem (2025), e202501565
DOI: 10.1002/cssc.202501565
Status : Postprint (Author's version)

2.4 | VANADIUM CATALYSTS

In 2012, Honda and colleagues reported a vanadium-catalyzed oxidation of *N*-Boc-hydroxylamine using alkyl peroxides as terminal oxidants and in situ trapping of the corresponding nitrosoformate via hDA [62]. Their studies began with the reaction between BocNHOH (**1a**) and hexa-2,4-dien-1-ol (**2k**) using cumyl hydroperoxide (CHP) as the terminal oxidant (Table 8). In the absence of a catalyst, no cycloadduct was formed (Table 8, entry 1). However, with a catalytic amount of $VO(Oi\text{-}Pr)_3$ (1 mol%), cycloadducts **3ak-I** and **3ak-II** were obtained in 65% yield at −20°C after 1 h (Table 8, entry 2). Increasing the amounts of **1a** and CHP, along with the temperature, led to complete conversion and improved the yield from 65% to 99% (Table 8, entries 3–4). At room temperature and without excess of **1a**, only the corresponding epoxide was formed, whereas using 2 equivalents of **1a** yielded cycloadducts exclusively, without aldehyde or epoxide byproducts. These results suggest the formation of stable hydroxamate complexes between vanadium and HA, preventing concurrent coordination of dienol **2k** and of the oxidant to vanadium, thereby inhibiting epoxidation of the dienol itself. Notably, this approach slightly improved the yield and regioselectivity compared to a previous study using tetrabutylammonium periodate as a stoichiometric oxidant (80% yield with **3ak-I/3ak-II** 67:33 vs. 99% yield, **3ak-I/3ak-II** 72:28) [63]. The enhanced regioselectivity can be attributed to the concurrent coordination of the nitrosoformate and dienol **2k** to vanadium during the Diels–Alder reaction, which controls their orientation during bond formation.

The reaction was also tested using nonpolar solvents (e.g., toluene and cyclopentylmethylether) or $Ti(O\textit{i}\text{-}Pr)_4$ as the catalyst. Under these conditions, the reaction proceeded with satisfactory yields, but when using the Ti-based catalyst (Table 8, entry 7), significantly longer reaction times were required (12 vs. 1 h). Substituting CHP with TBHP as the oxidant gave similar results, whereas hydrogen peroxide was ineffective.

Published in : ChemSusChem (2025), e202501565
DOI: 10.1002/cssc.202501565
Status : Postprint (Author's version)

TABLE 8 | Optimization of the reaction conditions with the hDA reaction between *N*-Boc-hydroxylamine and hexa-2,4-dien-1-ol catalyzed by VO(O*i*-Pr) using ROOH as oxidant.

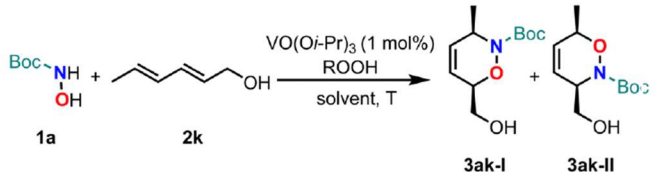

1a 2k 3ak-I 3ak-II

Entry	1a (equiv.)	ROOH (equiv.)	Solvent, T (°C)	Yield (%)[a]	3ak-I/ 3ak-II ratio[b]
1[c]	2	CHP (2)	CH_2Cl_2, -20	0	/
2	1	CHP (1)	CH_2Cl_2, -20	65	83:17
3	2	CHP (2)	CH_2Cl_2, -20	95	77:23
4	2	CHP (2)	CH_2Cl_2, rt	99	72:28
5	2	CHP (2)	Toluene, rt	99	79:21
6	2	CHP (2)	CPME, rt	80	71:29
7[d]	2	CHP (2)	CH_2Cl_2, rt	85	78:22
8	2	TBHP (2)	CH_2Cl_2, rt	91	77:23
9	2	H_2O_2 (2)	CH_2Cl_2, rt	27[e]	80:20

[a]Isolated yield of **3ak-I** and **3ak-II**.
[b]Ratio based on the isolated yields of the regioisomers.
[c]Without catalyst.
[d]With Ti(O*i*-Pr)$_4$ (1 mol%) as catalyst.
[e]Mixture of the products and BocNHOH.

The optimized conditions (VO(Oi-Pr)$_3$ (1 mol%), diene (1 equiv.), oxidant (1 equiv.), BocNHOH (2 equiv.), rt, 1 h) were applied to a library of cyclic and acyclic dienes, successfully yielding the corresponding cycloadducts (Table 9). The hDA reaction with silyl-protected dienoate ester **2p** gave lower yields compared to the unmasked hydroxy dienoate ester **2o**, likely due to steric repulsion between the triisopropylsilyl and *tert*-butoxycarbonyl groups [62].

Published in : ChemSusChem (2025), e202501565
DOI: 10.1002/cssc.202501565
Status : Postprint (Author's version)

TABLE 9 | hDA reaction between *N*-Boc-hydroxylamine and a library of cyclic and acyclic dienes catalyzed by VO(O*i*-Pr) using ROOH as oxidant.

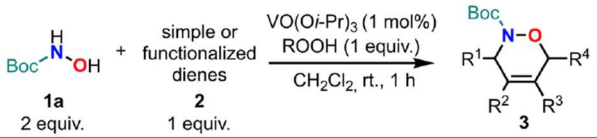

Entry	Diene	Oxidant	Cycloadduct	Yield (%)[a]
1[b]	 **2a**	CHP	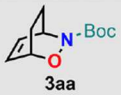 **3aa**	86
2[c]	 **2b**	CHP	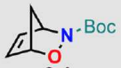 **3ab**	62
3	 **2f**	TBHP	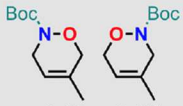 **3af-I** **3af-II**	46[d]
4	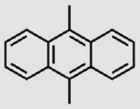 **2g**	TBHP	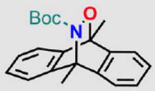 **3ag**	40
5	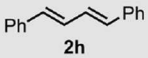 **2h**	CHP	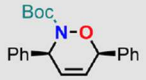 **3ah**	77
6	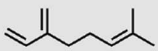 **2l**	CHP	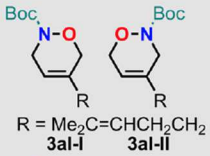 R = $Me_2C{=}CHCH_2CH_2$ **3al-I** **3al-II**	20[d]
7	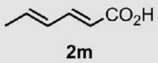 **2m**	CHP	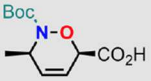 **3am**	44
8	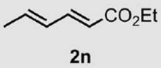 **2n**	TBHP	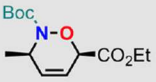 **3an**	70
9	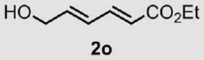 **2o**	CHP	 **3ao**	62
10	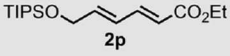 **2p**	TBHP	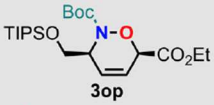 **3op**	20
11	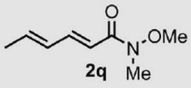 **2q**	TBHP	 **3aq**	79
12	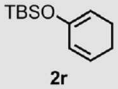 **2r**	CHP	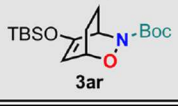 **3ar**	13[e]

[a]Isolated yield.
[b]Reaction in toluene.
[c]Reaction conducted at −20°C.
[d]Ratio 1:1 of regioisomers.
[e]The product is likely to desilylate on the silica gel to produce *N*-Boc-6-hydroxyamino-2-hexenone in 24% yield.

Published in : ChemSusChem (2025), e202501565
DOI: 10.1002/cssc.202501565
Status : Postprint (Author's version)

2.5 | RUTHENIUM CATALYSTS

In 2001, Whiting and colleagues reported the use of Ru(II) complexes to oxidize *N*-Boc-hydroxylamine **1a** in the presence of TBHP, generating the corresponding acylnitroso species [64]. This reactive intermediate was subsequently trapped via hDA reaction with 1,3-cyclohexadiene **2a**. Optimal conditions involved the use of 10 mol% of catalyst $RuCl_2(PPh_3)_4$ together with 3 equiv. of TBHP at room temperature for 30 min (Figure 16). ^{31}P NMR studies indicated that, within 10 min of reaction, all triphenylphosphine ligands were oxidized, suggesting that $RuCl_2(PPh_3)_4$ acts as a precatalyst and that catalytic turnover occurs via a Ru(II)/Ru(IV) redox cycle.

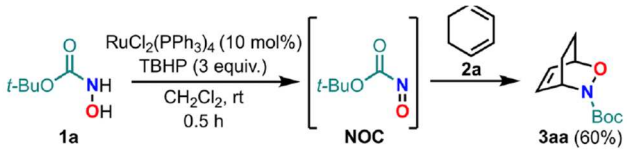

FIGURE 16 | hDA reaction between *N*-Boc-hydroxylamine and 1,3-cyclohexadiene catalyzed by $RuCl_2(PPh_3)_4$ using TBHP as oxidant.

A catalytic mechanism was proposed (Figure 17), beginning with oxidation of the PPh_3 ligands in $RuCl_2(PPh_3)_4$ to generate a Ru(II) oxo–chloride complex **18**, stabilized by phosphine oxide ligands. Further oxidation by TBHP affords the Ru(IV) complex **19**, which can oxidize the HA to generate compound **20**, containing an *N*-bound nitroso ligand. Complex **20** then undergoes cycloaddition reaction, forming compound **3aa** and regenerating complex **18** in the process [64].

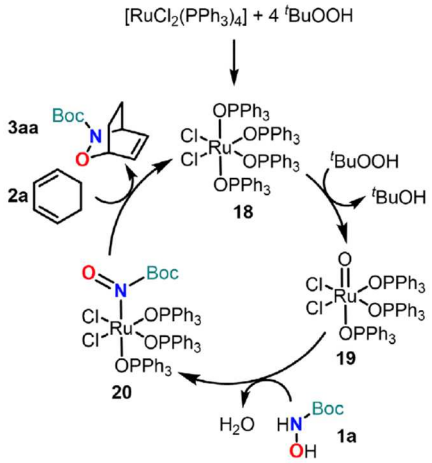

FIGURE 17 | Proposed catalytic cycle of Ru(IV) oxo complex-mediated oxidation of HA with phosphine oxide donors.

Based on this proposed cycle, the authors explored the use of chiral phosphine oxide ligands in an effort to achieve asymmetric hDA reactions [48]. However, the incorporation of chiral bidentate bis-phosphine ligands such as BINAP or PROPHOS did not lead to any enantiomeric enrichment. This lack of asymmetric induction may be attributed to the reaction conditions, which likely prevent the formation of discrete, diastereomerically pure ruthenium complexes.

Published in : ChemSusChem (2025), e202501565
DOI: 10.1002/cssc.202501565
Status : Postprint (Author's version)

To investigate whether a ruthenium-nitroso intermediate could induce enantioselectivity during the cycloaddition step, an alternative approach using a Ru–salen complex was explored (Table 10) [48]. This strategy aimed to fix all equatorial ligand positions, thereby producing an enantiomerically pure metal complex. Initial trials using racemic salen ligands to form the achiral complex **8a** showed a marked improvement over the $RuCl_2(PPh_3)_4$-catalyzed system. The new optimal conditions, using only 0.1 mol% of the Ru–salen complex **8a** and 1 equivalent of TBHP, yielded 81% of the product, compared to 60% under the original conditions (Table 10). This catalyst system was also effective with a range of other dienes.

TABLE 10 | hDA reaction between *N*-Boc-hydroxylamine and different dienes catalyzed by an achiral ruthenium (II) salen complex 8a with TBHP as oxidant.

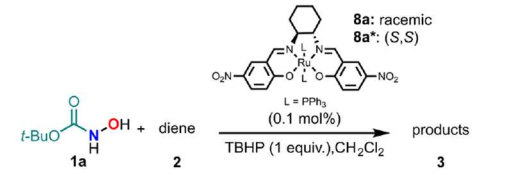

Entry	Dienes	Products	Yield (%)[a]
1	 2a	 3aa	81
2	 2b	 3ab	69
3	 2c	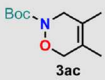 3ac	42
4	 2d	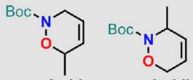 3ad-I 3ad-II	40[b]
5	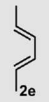 2e	 3ae	38
6	 2f	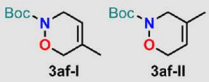 3af-I 3af-II	25[c]
7	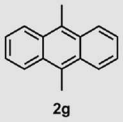 2g	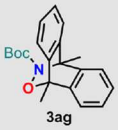 3ag	36
8	 2s	 3as	71
9	 2t	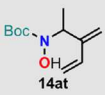 14at	19
10	 2u	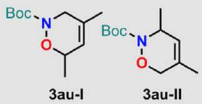 3au-I 3au-II	38[b]

[a]Isolated yields.
[b]1:2 inseparable regioisomers.
[c]1:1 inseparable regioisomers.

Published in : ChemSusChem (2025), e202501565
DOI: 10.1002/cssc.202501565
Status : Postprint (Author's version)

However, when the enantiopure chiral Ru–salen complex **8a*** was applied to the reaction with cyclohexadiene, no enantioselectivity was observed. This outcome suggests that, although an *N*-bound ruthenium nitroso complex may indeed form upon oxidation of HA **1a**, it is likely unstable and undergoes rapid dissociation. As a result, the free acylnitroso species reacts thermally with the diene, bypassing any potential for asymmetric induction. In other words, acylnitroso compounds appear to be poor ligands for Ru(II) complexes, rapidly dissociating into solution once formed.

Interestingly, when the Ru–salen complex **8a** was used without TBHP, a slow oxidation of the phosphine ligands by atmospheric oxygen was observed, resulting in the generation of the active catalyst form. A 10% yield was obtained after 6 days under air (Table 11, entry 1), compared to only 3% under an argon atmosphere (Table 11, entry 2). This observation also highlighted the capacity of the HA to act as a weak oxidant [48].

TABLE 11 | Effect of air on the oxidation of *N*-Boc-hydroxylamine catalyzed by the ruthenium (II) salen complex **8a** (0.1 mol equiv.) and subsequent hDA reaction with 1,3-cyclohexadiene. Time = 6 days.

Entry	Oxidation conditions	Yield (%)
1	Air, CH_2Cl_2	10
2	Argon, CH_2Cl_2	3
3	TBHP, air, CH_2Cl_2	27
4	TBHP, argon, CH_2Cl_2	15

Building on the hypothesis proposed by Whiting and coworkers [48], which suggests that successful Ru(II)-catalyzed asymmetric hDA reactions require the acylnitroso species to remain coordinated to the chiral catalyst during cycloaddition, Chow and Shea devised an alternative strategy [65]. Given the limited success of this approach in intermolecular systems, they proposed exploring intramolecular cycloadditions, which are more likely to proceed while the reactive intermediate is still within the coordination sphere of the ruthenium center (Figure 18). In essence, if dissociation of the NOC species or re-oxidation of the catalyst occurs faster than the hDA reaction, the product will be racemic. Conversely, if cycloaddition outpaces either dissociation or reoxidation, some degree of enantiomeric induction should be observed.

Published in : ChemSusChem (2025), e202501565
DOI: 10.1002/cssc.202501565
Status : Postprint (Author's version)

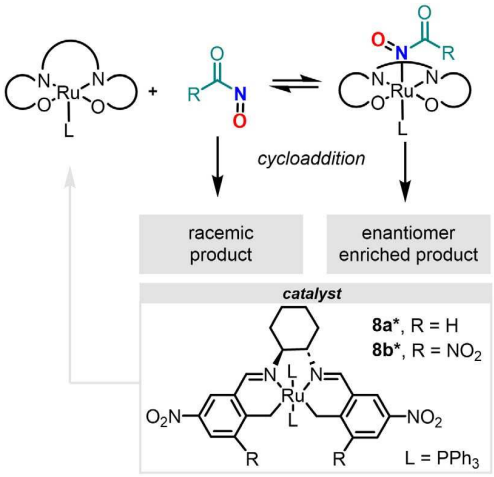

FIGURE 18 | Proposed mechanistic explanation for divergent outcomes in the Ru(II)-catalyzed hDA reaction.

To test this hypothesis, Ru(II) complexes **8a***, incorporating chiral salen ligands derived from (+)−1,2-diaminocyclohexane, were synthesized and evaluated as catalysts for both interand intramolecular hDA reactions (Figure 19). In agreement with Whiting's findings [48], the intermolecular reaction of *O-tert*-butyl-*N*-hydroxyformamide (**1a**) led to racemic cycloadduct **3aa** in 74% yield. As anticipated, the intramolecular cycloaddition of *N*-hydroxyformate ester **21a** furnished cycloadduct **22a** in 64% yield and with a detectable enantiomeric excess. Although the observed enantioselectivity was modest (9% ee), it confirmed that a portion of the cycloaddition occurred within the chiral environment of the Ru catalyst.

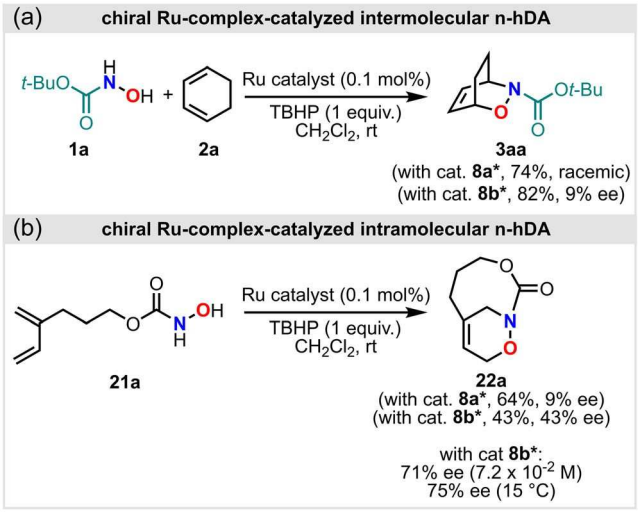

FIGURE 19 | Chiral Ru(II)-catalyzed hDA reaction of HAs in the presence of TBHP as oxidant.

Recognizing the importance of stabilizing the transient Ru–NOC intermediate to achieve higher asymmetric induction, the authors tried to use a more Lewis acidic catalyst. This led to the synthesis of the dinitro-substituted salen complex **8b***, which markedly improved the enantiomeric excess of cycloadduct **22a** to 43%, underscoring the role of intramolecular coordination in stereochemical

Published in : ChemSusChem (2025), e202501565
DOI: 10.1002/cssc.202501565
Status : Postprint (Author's version)

control. In contrast, the corresponding bimolecular reaction catalyzed by **8b*** afforded only 9% *ee* for **3aa**.

To further enhance enantioselectivity by extending the lifetime of the Ru–NOC complex and minimizing competing bimolecular reoxidation, the reaction conditions were optimized by lowering both the concentration and the temperature (Figure 19b, bottom right). The highest enantioselectivity (71% ee) was achieved at a concentration of 7.2×10^{-2} M. Further cooling the reaction from room temperature to 15°C increased the enantiomeric excess to 75% [65].

In 2008, Whiting and colleagues reported mechanistic insights into the Ru(salen)-catalyzed oxidation of *N*-protected HAs [66]. A combination of analytical techniques, including time-resolved infrared spectroscopy, mass spectrometry, and ^{1}H NMR spectroscopy, enabled the monitoring of both the ruthenium coordination environment and the catalytically active species. The model system involved the oxidation of HA **1b** in the presence of a Ru(salen) complex and a stoichiometric amount of TBHP as oxidant, with diene **2a** serving as the trapping agent. Consistent with previous observations, the use of enantiomerically pure catalyst **8a** in intermolecular hDA reactions (Figure 20a) yielded no enantiomeric enrichment [40].

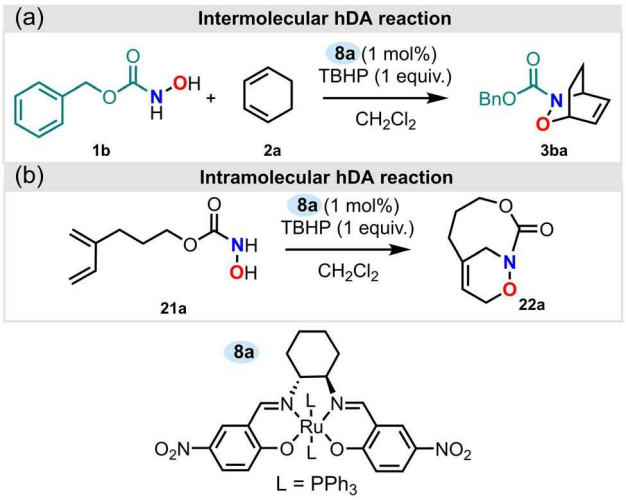

FIGURE 20 | Intermolecular and intramolecular Ru(II)-catalyzed hDA reactions of HAs in the presence of TBHP as oxidant.

However, upon investigating the asymmetric intramolecular reaction previously studied by Chow and Shea [65], the expected complete conversion of the starting material was not achieved (Figure 20b). Instead, NMR concentration profiles indicated an incomplete reaction, and the isolated product was racemic. Chow and Shea had initially hypothesized that the observed enantiomeric excess was due to the intramolecular Diels–Alder reaction occurring more rapidly than dissociation of the nitroso intermediate from the ruthenium center. However, if this were the case, complete conversion of the starting material into the cycloadduct would have been expected. The lack of full conversion suggests that dissociation of the acylnitroso species from the Ru-salen catalyst is faster than the intramolecular cycloaddition, allowing competing decomposition pathways to interfere. While both Chow and

Published in : ChemSusChem (2025), e202501565
DOI: 10.1002/cssc.202501565
Status : Postprint (Author's version)

Whiting works are influential, they differ in their findings and suffer from reproducibility issues, generating controversy.

No significant changes were detected in the IR spectrum when either **1b** or **2a** were mixed individually with the Ru catalyst, indicating no direct interaction. However, upon addition of TBHP, a new absorption band appeared at 1250–1300 cm^{-1}, consistent with the formation of $O=PPh_3$, alongside a weak band near 830 cm^{-1} attributed to Ru=O stretch. Mass spectrometry confirmed the formation of two key species in the reaction mixture: ion peaks at m/z = 529 and 791 were assigned to species **23** and **24**, respectively (Figure 21). Drawing on analogies with chromium(V) oxo(salen) species reported by Kochi [67], the active catalytic species was proposed to be Ru(oxo)(salen) **23**, likely formed by the dissociation of PPh_3 from complex **24**, which in turn derived from initial oxidation of the Ru(salen) complex **8a**.

Subsequent kinetic studies revealed that the overall process consists of three discrete steps (Figure 21): (1) oxidation of the metal complex to form the active catalyst, (2) oxidation of the HA to generate the acylnitroso intermediate, and (3) the cycloaddition of the nitroso species with the diene to yield the adduct [66]. The oxidation of complex **8a** to **24** was proposed to proceed via two possible mechanisms (Figure 21, square 1). In the first, an equilibrium exists between complex **8a** and a species in which PPh_3 has dissociated. Upon TBHP addition, both free PPh_3 and the Ru(salen)-PPh_3 complex are oxidized to triphenylphosphine oxide and complex **24**, respectively, driving the equilibrium to completion. In the second mechanism, PPh_3 is oxidized while still coordinated to the Ru center, followed by its dissociation.

Published in : ChemSusChem (2025), e202501565
DOI: 10.1002/cssc.202501565
Status : Postprint (Author's version)

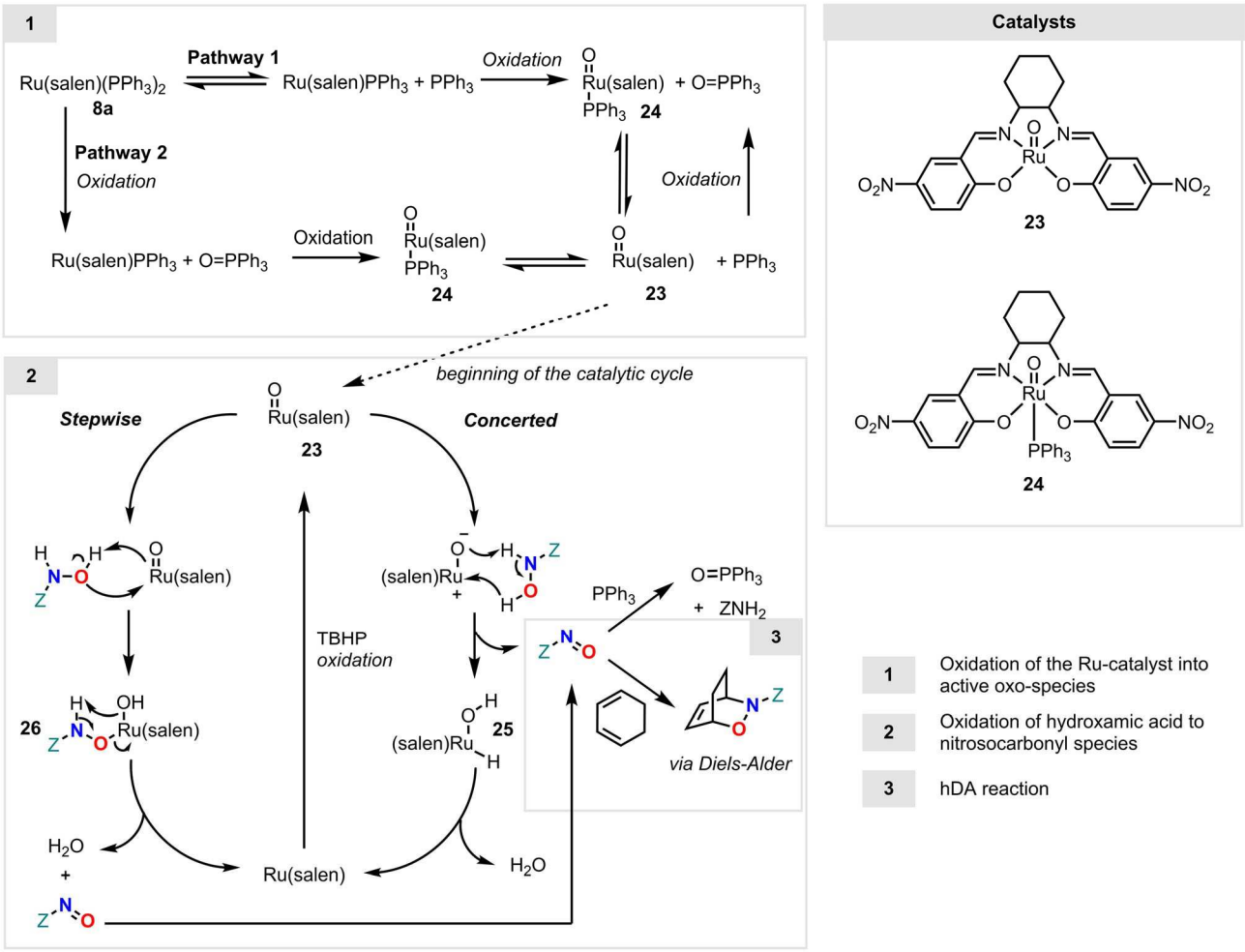

FIGURE 21 | Proposed mechanism for the Ru-catalyzed oxidation of HAs with in situ Diels–Alder trapping of the acyl nitroso derivative.

Once formed, the Ru(salen)-oxo complex catalyzes the oxidation of HA to the corresponding acylnitroso compound. This transformation may proceed via either a concerted or stepwise mechanism (Figure 21, square 2). In the concerted pathway, simultaneous deprotonation of the HA and hydride transfer to the metal center result in formation of the acylnitroso intermediate and a Ru(salen)–hydride complex (**25**). This hydride complex then eliminates water and is reoxidized by TBHP to regenerate the Ru(oxo)(salen) species. Alternatively, in the stepwise pathway, protonation of the Ru=O species by the HA leads to coordination via the terminal oxygen, generating intermediate **26**. This intermediate subsequently releases the acylnitroso species and water, allowing reoxidation of the metal center to complete the catalytic cycle. Regardless of the pathway, the result is a transient, free NOC intermediate that undergoes rapid cycloaddition with dienes (Figure 21, square 3). Since this step likely occurs outside the coordination sphere of the metal center, it provides a plausible explanation for the lack of enantioselectivity observed in the intermolecular hDA reactions [66].

In parallel with the work of Whiting et al., Iwasa and colleagues reported an alternative Ru(II)-catalyzed oxidation of HAs, using hydrogen peroxide as the terminal oxidant (Figure 22) [68]. Compared to the previously described oxidation systems, this method offers a significant environmental advantage, as

Published in : ChemSusChem (2025), e202501565
DOI: 10.1002/cssc.202501565
Status : Postprint (Author's version)

it generates only water as a byproduct. The optimal conditions involved the use of Ru(pybox-dh)(pydic) (11 mol%) in the presence of hydrogen peroxide (4 equiv.) as the oxidant, with either THF or a 1:1 mixture of CH_3OH/H_2O as the solvent, at temperatures ranging from 0°C to room temperature. These conditions were successfully applied to a range of HA substrates, with the transient acylnitroso intermediates efficiently trapped via hDA reactions with cyclopentadiene, affording cycloadducts in excellent yields (76%–99%). Notably, the catalyst loading could be reduced to as low as 1 mol% without compromising the efficiency of the transformation, highlighting the practicality and robustness of this catalytic system [68].

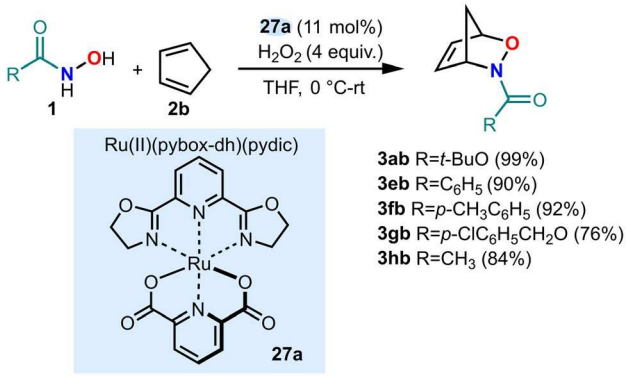

FIGURE 22 | Ruthenium-catalyzed hDA reaction between a library of HA derivatives and cyclopentadiene using hydrogen peroxide as oxidant.

Subsequently, the same research group developed an asymmetric hDA reaction involving transient acylnitroso species generated via Ru(II)- or Ir(I)-catalyzed hydrogen peroxide oxidation of HAs, in combination with optically pure *N*-dienyl-*L*-pyroglutamates (Table 12) [69]. Given that Ru(pybox)(pydic) complexes **27a-d** had previously demonstrated efficiency in the oxidation of HAs and phenolic substrates, they were selected as catalysts for this transformation, along with two Ir(I) complexes: $[IrCl(coe)_2]_2$ and $[IrCl(cod)]_2$ (**E** and **F**).

Different **HA**s were evaluated in the catalytic hDA reaction with chiral *N*-dienyl-*L*-pyroglutamates **2v-w** in either THF or methanol, affording the corresponding diastereomeric adducts **3-I** (major) and **3-II** (minor) with complete regioselectivity (**12**). Yields ranged from moderate to high (45%–98%), with good levels of diastereoselectivity (32%–72%). Methanol was identified as the optimal solvent for the Ru(II)-catalyzed reactions, whereas THF was preferred for Ir(I)-catalyzed systems due to better solubility of the catalysts in this medium. Notably, the Ru(II) catalysts not only provided superior asymmetric induction but also promoted faster reaction rates compared to their Ir(I) counterparts [69].

Published in : ChemSusChem (2025), e202501565
DOI: 10.1002/cssc.202501565
Status : Postprint (Author's version)

TABLE 12 | Ru(II)- or Ir(I)-catalyzed hydrogen peroxide oxidation of different HAs and subsequent hDA reaction with chiral *N*-dienyl-L-pyroglutamates.

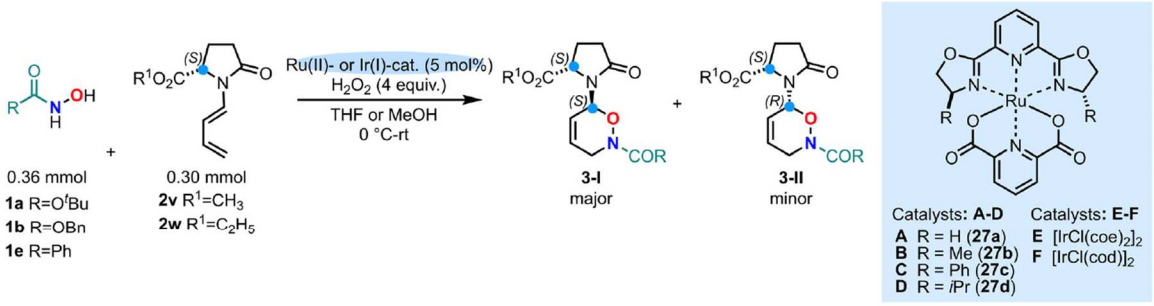

Entry	HA	Diene	Catalyst	Solvent	Adduct	Yield (%)[a]	3-I/3-II ratio[b]	d.e.
1	**1a**	**2v**	A	MeOH	**3av-I/3av-II**	73	79:21	58
2	**1a**	**2v**	C	MeOH	**3av-I/3av-II**	88	85:15	70
3	**1a**	**2v**	D	MeOH	**3av-I/3av-II**	81	82:18	64
4	**1a**	**2v**	E	THF	**3av-I/3av-II**	68	79:21	58
5	**1a**	**2v**	F	THF	**3av-I/3av-II**	67	79:21	58
6	**1a**	**2w**	D	MeOH	**3aw-I/3aw-II**	98	85:15	70
7	**1b**	**2v**	A	THF	**3bv-I/3bv-II**	59	73:27	46
8	**1b**	**2v**	A	MeOH	**3bv-I/3bv-II**	49	79:21	58
9	**1b**	**2v**	B	MeOH	**3bv-I/3bv-II**	74	78:22	56
10	**1b**	**2v**	C	MeOH	**3bv-I/3bv-II**	45	79:21	58
11	**1b**	**2v**	D	MeOH	**3bv-I/3bv-II**	63	79:21	58
12	**1b**	**2v**	E	THF	**3bv-I/3bv-II**	62	70:30	40
13	**1b**	**2v**	F	THF	**3bv-I/3bv-II**	51	69:31	38
14	**1e**	**2v**	A	MeOH	**3ev-I/3ev-II**	51	83:17	65
15	**1e**	**2v**	B	MeOH	**3ev-I/3ev-II**	87	83:17	644
16	**1e**	**2v**	C	MeOH	**3ev-I/3ev-II**	48	84:16	68
17	**1e**	**2v**	D	MeOH	**3ev-I/3ev-II**	64	84:16	66
18	**1e**	**2v**	E	THF	**3ev-I/3ev-II**	66	80:20	60
19	**1e**	**2v**	F	THF	**3ev-I/3ev-II**	52	82:18	64
20	**1e**	**2w**	D	MeOH	**3ew-I/3ew-II**	91	85:15	70
20	**1e**	**2w**	D	MeOH	**3ew-I/3ew-II**	70	86:14	72

[a]Yield of the two diastereoisomers.
[b]Determined by ^{1}H NMR.

The proposed stereochemical model suggests that the nitroso dienophile approaches the diene from its less sterically hindered face and *anti* to the ester moiety of the pyroglutamate derivative (Figure 23). Moreover, a *s*-trans conformation between the butadiene and the amide group is proposed in the transition state, enabling optimal π-orbital alignment and favorable orbital interactions to govern the stereochemical outcome of the cycloaddition [57, 69].

Published in : ChemSusChem (2025), e202501565
DOI: 10.1002/cssc.202501565
Status : Postprint (Author's version)

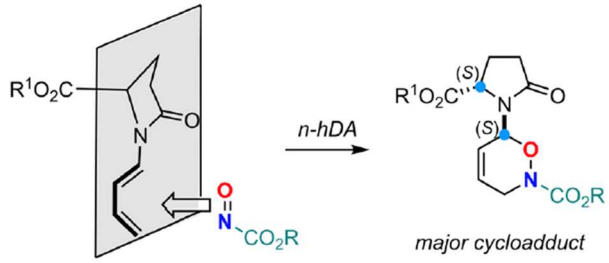

FIGURE 23 | Spatial approach of NOC to the pyroglutamate diene explaining the stereochemical outcome of the product.

2.6 | IRIDIUM CATALYSTS

In 2002, Iwasa and coworkers reported a highly efficient Ir(I)/ H_2O_2-based method for generating nitroso intermediates, followed by their subsequent hDA reaction with cyclopentadiene [70]. Among the various metal systems evaluated (Table 13), $[Ir(coe)_2Cl]_2$ was identified as the optimal catalyst due to its superior reactivity, favorable solubility, and ability to operate without the need for additional additives.

TABLE 13 | Metal-catalyzed oxidation of HAs using hydrogen peroxide as oxidant and subsequent hDA reaction with cyclopentadiene. Conditions: HA (0.15 mmol), catalyst (0.003 mmol), H_2O_2 (0.60 mmol), cyclopentadiene (0.75 mmol) at 0°C to room temperature.

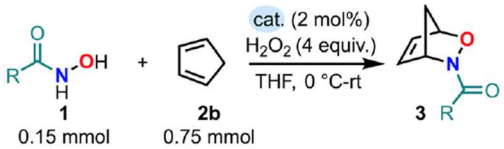

1a R=*t*-BuO
1e R=C_6H_5
1g R=*p*-$ClC_6H_4OCH_2$
1i R=*p*-$CH_3OC_6H_4$
1j R=*m*, *p*-di-$CH_3OC_6H_3$

Entry	HA	Catalyst	Additive (equiv.)	Yield (%)[a]
1	**1e**	$Co(acac)_2$	None	18
2	**1e**	$[Rh(OAc)_2]_2$	None	19
3	**1e**	$[Ir(cod)Cl]_2$	None	51
4	**1e**	CuI	None	60
5	**1e**	$[Ir(cod)Cl]_2$	KOH (0.3)	74
6	**1e**	$[Ir(coe)_2Cl]_2$	None	97
7	**1a**	$[Ir(coe)_2Cl]_2$	None	92
8	**1g**	$[Ir(coe)_2Cl]_2$	None	60
9	**1i**	$[Ir(coe)_2Cl]_2$	None	94
10	**1j**	$[Ir(coe)_2Cl]_2$	None	80

[a]Isolated yields.

Published in : ChemSusChem (2025), e202501565
DOI: 10.1002/cssc.202501565
Status : Postprint (Author's version)

The choice of solvent significantly influenced the reaction outcome, with THF affording the best results, although DMF, CH_2Cl_2, and 1,4-dioxane also proved effective. The most efficient reaction conditions used $[Ir(coe)_2Cl]_2$ (2 mol%), cyclopentadiene (5 equiv.), and hydrogen peroxide (4 equiv.) in THF, starting at 0°C and gradually warming to room temperature. Under these conditions, a small library of HAs was subjected to oxidation, yielding the desired cycloadducts in moderate to excellent yields (Table 13, entries 6–10). Notably, benzohydroxamic acid also reacted with alternative dienes such as 1,3-cyclohexadiene and α-terpinene, giving the corresponding adducts in 90% and 87% yield, respectively, with the latter exhibiting a 9:1 regioselectivity [70].

In a subsequent comparative study, the same group investigated the use of *N*-dienyl-lactams (**2x-z**) as diene substrates in hDA reactions involving acylnitroso species. The transient acylnitroso were generated via Ru(II)-, Ir(I)-, and Cu(I)-catalyzed oxidations of HAs using aqueous H_2O_2 (Figure 24) [57]. All three catalytic systems facilitated product formation; however, the Ir(I) catalysts consistently demonstrated higher reactivity than their Ru(II) and Cu(I) counterparts. Although Ru(II) complexes exhibited the fastest reaction rates, they provided only modest yields of the desired cycloadducts.

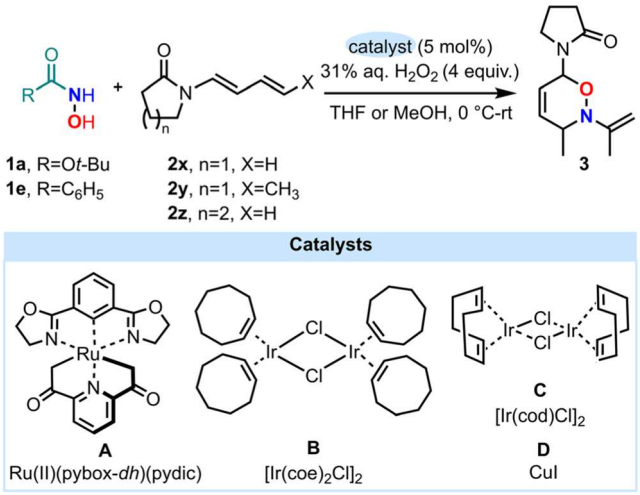

FIGURE 24 | hDA reactions with NOCs generated via Ru(II), Ir(I) and Cu(I)-catalyzed oxidations of HAs by aqueous H_2O_2, with Ndienyl-lactams **2x-z** as a diene source.

A plausible mechanism for the Ir(I)-catalyzed oxidation of HAs by H_2O_2 (Figure 25) involves initial conversion of the dimeric complex $[Ir(coe)_2Cl]_2$ into its monomeric form **28** through coordination with a solvent molecule. Upon addition of hydrogen peroxide, the metal center forms the active Ir(III) peroxo species **29**, which oxidizes the HA to the corresponding acylnitroso intermediate, yielding complex **30**. The resulting acylnitroso species can then participate in a hDA reaction with a diene, either while still coordinated to the metal center or after dissociation [57].

Published in : ChemSusChem (2025), e202501565
DOI: 10.1002/cssc.202501565
Status : Postprint (Author's version)

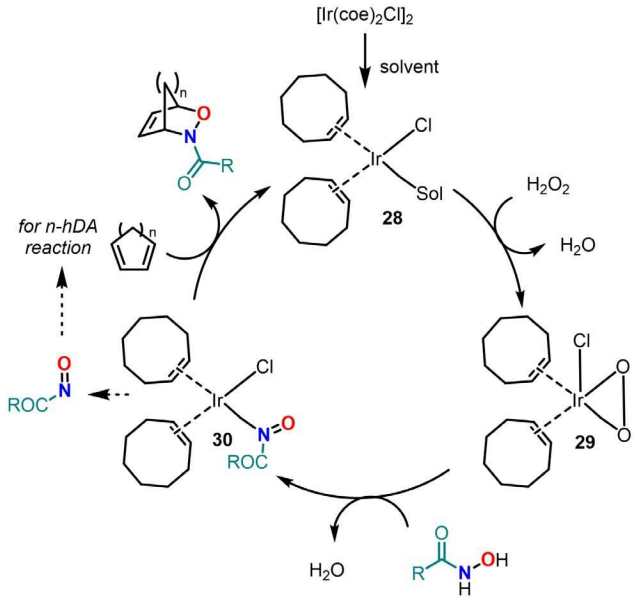

FIGURE 25 | Proposed mechanism for Ir(I)-catalyzed oxidation of HAs by hydrogen peroxide followed by hDA reactions.

2.7 | RHODIUM CATALYSTS

In 2012, Tusun and Lu reported the application of dirhodium(II) caprolactamate [$Rh_2(cap)_4$] in combination with TBHP for the mild oxidation of HAs [71]. This work broadened the known utility of the [$Rh_2(cap)_4$] catalyst, which had previously been used for the oxidation of activated C–H bonds, phenols, and anilines [72, 73].

Initial optimization studies focused on the hDA reaction between Boc-*N*-hydroxylamine **1a** and 1,3-cyclohexadiene **2a** as a model system (Table 14). Using $Rh_2(cap)_4$ (1 mol%) and TBHP (1 equiv., added dropwise) in CH_2Cl_2 at room temperature afforded the desired cycloadduct **3aa** in 87% yield (Table 14, entry 1). Remarkably, the catalyst loading could be reduced to 0.1 mol% without compromising product yield, although this required 2 equivalents of TBHP (Table 14, entry 2). Increasing the amount of TBHP to 4 equivalents further improved the yield (Table 14, entry 3). Additionally, replacing pure TBHP with the more cost-effective T-HYDRO (70 wt% TBHP in water) delivered **3a** in 92% yield, albeit with a longer reaction time required to achieve full conversion (Table 14, entry 4).

Published in : ChemSusChem (2025), e202501565
DOI: 10.1002/cssc.202501565
Status : Postprint (Author's version)

TABLE 14 | Optimization of the conditions for the Rh-catalyzed hDA reaction between Boc-*N*-hydroxylamine **1a** and cyclohexa-1,3-diene **2a**.

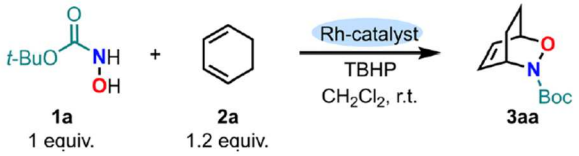

1a 1 equiv. **2a** 1.2 equiv. **3aa**

Entry	Catalyst (mol%)	Oxidant (equiv.)	T (°C)	Time (h)	Yield (%)[a]
1	$Rh_2(cap)_4$ (1)	TBHP (1)	rt	0.25	87
2[b]	$Rh_2(cap)_4$ (0.1)	TBHP (2)	rt	20	84
3	$Rh_2(cap)_4$ (0.1)	TBHP (4)	rt	2	92
4	$Rh_2(cap)_4$ (0.1)	T-HYDRO (4)	rt	38	92
5[c]	$Rh_2(cap)_4$ (0.1)	TBHP (4)	rt	24	/[d]
6	$Rh_2(cap)_4$ (0.1)	None	rt	24	14
7	None	TBHP (4)	rt	56	61
8	$Rh_2(cap)_4$ (0.1)	H_2O_2 (4)	40	78	50
9	$Rh_2(OAc)_4$ (0.1)	TBHP (4)	rt	24	37

[a]Isolated yields.
[b]2 equivalents of TBHP were used.
[c]MeOH as solvent.
[d]A complex with low conversion was obtained.

Attempts to avoid chlorinated solvents by replacing CH_2Cl_2 with methanol proved unsuccessful, yielding only trace amounts of the desired product. Both $Rh_2(cap)_4$ and TBHP were found to be essential for the reaction: omission of either of them led to significantly diminished yields (Table 14, entries 6–7). Furthermore, substituting TBHP with hydrogen peroxide or replacing $Rh_2(cap)_4$ with $Rh_2(OAc)_4$ resulted in slow kinetics and incomplete conversion of the HA (Table 14, entries 8–9).

The optimized conditions, $Rh_2(cap)_4$ (0.1 mol%), TBHP (4 equiv.), and CH_2Cl_2 as the solvent, were then applied to a broader substrate scope of dienes. The results were generally superior to those previously reported using Ru(II) complexes (Table 15) [47, 48, 64–66]. Of particular note, the highly functionalized cyclic diene **2b**′ was successfully used as a trapping agent. The addition of 2 equivalents of $NaHCO_3$ prevented hydrolysis of the silyl ether. Subsequent treatment of **3ab**′ with HF effected desilylation, followed by β-elimination of the amino group to furnish the corresponding *O*-nitroso-aldol product [71].

Published in : ChemSusChem (2025), e202501565
DOI: 10.1002/cssc.202501565
Status : Postprint (Author's version)

TABLE 15 | Scope of the products obtained from the hDA reaction between Boc-*N*-hydroxylamine and a library of 1,3-dienes in the optimized conditions. The reported yields are the isolated yields.

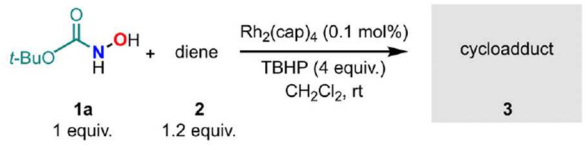

Entry	Diene	Cycloadduct	Time (h)	Yield (%)
1	**2a**	**3aa**	2	92
2	**2b**	**3ab**	14	92
3	**2c**	**3ac**	10	57
4	**2d**	**3ad-I** + **3ad-II**	8	81 **3ad-I**/**3ad-II** 1:2
5	**2f**	**3af-I** + **3af-II**	12	65 **3af-I**/**3af-II** 1:1
6	**2g**	**3ag**	24	61
7	**2h**	**3ah**	14	68
8	**2s**	**3as**	6	96
9	**2a'**	**3aa'**	24	68
10	**2b'**	**3ab'**	14	47[a]

[a]2 equivalents of $NaHCO_3$ were used.

Regarding the mechanism of the oxidative process, although it remains not fully elucidated, two plausible pathways have been proposed. The first involves the well-established generation of *t*-butylperoxy radicals from TBHP in the presence of dirhodium caprolactamate. These radicals are capable of abstracting a proton from the HA, thereby generating an acyl nitroxyl radical.

Published in : ChemSusChem (2025), e202501565
DOI: 10.1002/cssc.202501565
Status : Postprint (Author's version)

This intermediate is then further oxidized to form the corresponding acylnitroso compound. Alternatively, the acyl nitroxyl radical may undergo dismutation to produce the acylnitroso species directly [71].

2.8 | BIOCATALYSIS

Enzyme-catalyzed reactions are particularly attractive due to their high efficiency under mild conditions. Horseradish peroxidase (HRP) is a heme-containing enzyme that catalyzes H_2O_2 or alkyl peroxides dependent oxidations, typically involving single-electron transfer or hydrogen atom abstraction from electron-rich substrates [74, 75]. Upon interaction with H_2O_2, HRP forms higher oxidation state species, namely the ferryloxo complexes known as Compound I (**Cpd I**) and Compound II (**Cpd II**). In the presence of an appropriate electron donor, HRP can enter a catalytic cycle, as illustrated in Figure 26.

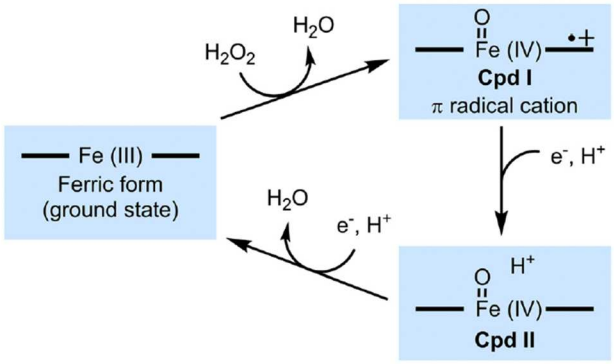

FIGURE 26 | HRP catalytic cycle.

In the context of acylnitroso species generation, several studies investigated the HRP/H_2O_2 system for the oxidation of HAs. One-electron oxidation of HAs or their derivatives leads to the formation of transient nitroxide radicals, which can undergo a variety of decomposition pathways (Figure 27) [76, 77]:

1. Dismutation of the nitroxide radicals, regenerating the parent HA and producing the corresponding NOC species.
2. Hydrolysis of the NOC species to carboxylic acid and HNO.
3. Unimolecular decomposition of the nitroxide radical via C–N bond homolysis, forming an acyl radical (RCO•) and HNO.
4. Unimolecular decomposition of the nitroxide radical to generate the corresponding aldehyde and NO.

Published in : ChemSusChem (2025), e202501565
DOI: 10.1002/cssc.202501565
Status : Postprint (Author's version)

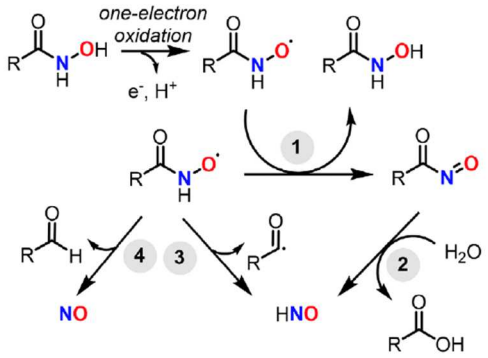

FIGURE 27 | One-electron oxidation of HAs and possible pathways for the decomposition of the formed nitroxide radical.

In 2018, Goldstein et al. reported the use of HRP-derived **Cpd I** and **Cpd II** for the oxidation of HAs, as well as the modulatory effects of transition metal ions on this process [78]. Kinetic studies were conducted on both **Cpd I** and **II** at pH 7.0 and 25°C in the presence of various HAs (Figure 28), including acetohydroxamic acid, suberohydroxamic acid, and suberoylanilide hydroxamic acid (SAHA).

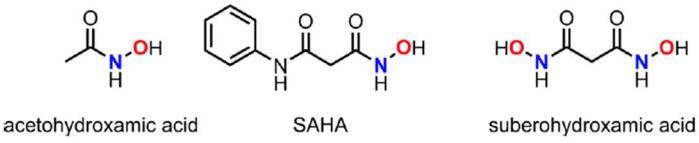

FIGURE 28 | HAs used as examples for the oxidation with Cpd I and Cpd II of HRP.

A reaction mixture containing HRP (5.1–5.2 µM), H_2O_2 (5 µM), and an excess of HA was analyzed. HRP was introduced to H_2O_2 slightly above stoichiometric amounts, ensuring that residual H_2O_2 would not recycle the enzyme and interfere with kinetic analysis. The study focused on two sequential processes: the oxidation of HAs by **Cpd I**, followed by further oxidation mediated by **Cpd II**. The reduction rates of **Cpd I** to **Cpd II**, and subsequently **Cpd II** to the resting-state enzyme, was monitored. Both steps exhibited first-order kinetics, with observed rate constants displaying a linear dependence on HA concentration. Notably, HRP alone did not react with HAs in the absence of H_2O_2, confirming the necessity of peroxide for initiating the oxidative process. Reaction monitoring revealed the transient accumulation of a short-lived intermediate, likely corresponding to the acylnitroso species, which subsequently decayed via a first-order process once H_2O_2 was consumed. The duration of this transient phase depended on the specific rate constant associated with each HA.

Given that HAs are known chelating agents of transition metals, the formation and stability of acylnitroso species were further examined in the presence of transition metal salts, including $Cu(ClO_4)_2$, $NiSO_4$, $FeCl_3$, and $ZnSO_4$. The decomposition of the transient species was monitored indirectly via the detection of nitroxyl (HNO), a known product of such breakdown pathways. Among the tested metal ions, Fe(III) formed the most stable hydroxamato complexes, followed by Cu(II), with Ni(II) and Zn(II) showing relatively weaker interactions.

Published in : ChemSusChem (2025), e202501565
DOI: 10.1002/cssc.202501565
Status : Postprint (Author's version)

In general, the presence of metal complexes facilitated the decomposition of acylnitroso intermediates without significantly altering the overall yield of HNO or the extent of HA oxidation. These observations suggest that, under oxidative stress, HAs serve as a source of HNO, and that this process is not inhibited, but in fact accelerated, by various transition metal ions [78].

2.9 | METAL-FREE CATALYSIS

A representative example of metal-free oxidation of HAs to their corresponding NOC species using H_2O_2 is the work of Lagercrantz and Larsson, published in 1994 [79]. In their study, a mixture of benzohydroxamic acid, H_2O_2, and dimethyl sulfoxide (DMSO) was irradiated with UV light, enabling two photochemical processes: (1) oxidation of the HA to the acylnitroso compound and (2) formation of methyl radicals via the reaction of DMSO with H_2O_2. The acylnitroso species is proposed to form via acyl aminoxyl radicals, following a pathway similar to that of *tert*-butylhydroxylamine, which forms the radical *tert*-BuN(O•)H in the presence of H_2O_2 (Figure 29). H_2O_2 readily cleaves to generate •OH radicals, which abstract a hydrogen atom from the HA to form radical **31e**. This radical can then participate in a Fenton-like radical process, ultimately yielding the NOC species.

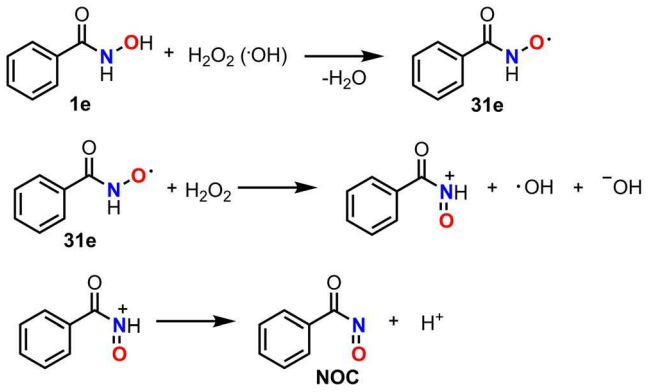

FIGURE 29 | NOC compound formation from HA via acyl aminoxyl radicals.

The formation of the acylnitroso compound was confirmed through its effective trapping of short-lived methyl radicals, producing detectable acyl aminoxyl radicals that persisted for several hours under UV irradiation but rapidly disappeared in the absence of light [79].

In 2018, Saito and coworkers reported a complementary strategy wherein *tetra-n*-butylammonium iodide (TBAI) served as a precatalyst, and either TBHP or H_2O_2 were used as the terminal oxidant for generating acylnitroso species [80]. The selection of iodine-based catalysts was motivated by their favorable characteristics, including low toxicity, mild reactivity, and ease of manipulation. Initial investigations used the hDA reaction between HA **1e** and 1,3-cyclohexadiene **2a** as a model system (Table 16). Various solvents and combinations of iodine(I) precatalysts and oxidants were tested. Dichloromethane was identified as the optimal solvent, yielding adduct **3ea** in higher yields compared to more polar solvents such as ethyl acetate, acetonitrile, or polar protic solvents like DMF and methanol, which did not afford the desired product. Whether trifluoroacetic acid (TFA) was added or

Published in : ChemSusChem (2025), e202501565
DOI: 10.1002/cssc.202501565
Status : Postprint (Author's version)

not, λ^3-iodane catalysts derived from iodobenzene and m-chloroperbenzoic acid (m-CPBA) led to poor yields (<10%, Table 16, entries 1–2). In contrast, iodide salt/ TBHP combinations offered significantly better performance, with the TBAI (5 mol%)/TBHP (1.5 equiv.) system affording **3ea** in 98% yield (Table 16, entry 5). Reducing the amount of TBAI led to diminished yields (Table 16, entry 7), and no reaction was observed in the absence of TBAI (Table 16, entry 8), suggesting the formation of an active iodine species in situ. Replacing TBHP with H_2O_2 also produced **3ea** in good yield (81%, Table 16, entry 10). However, in situ-generated TBA periodate (from TBAB and sodium periodate) was less effective than the other catalytic systems.

TABLE 16 | Optimization of the conditions using the metal-free hDA reaction between HA **1e** and 1,3-cyclohexadiene as model reaction. CH_2Cl_2 was used as solvent.

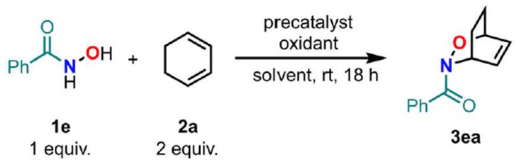

Precatalyst	Oxidants	Solvents
PhI	*m*CPBA	**CH_2Cl_2**
NaI	TBHP	AcOEt
Et_4NI	**30% H_2O_2**	MeCN
TBAI	$Na_2CO_3 \cdot H_2O_2$	DMF
TBAB	$NaIO_4$	MeOH

Entry	Precatalyst (mol%)	Oxidant (equiv.)	3ea yield (%)[a]
1	PhI (5)	*m*-CPBA (1.5)	9
2[b]	PhI (5)	*m*-CPBA (1.5)	0
3	NaI (5)	TBHP (1.5)	38
4	Et_4NI (5)	TBHP (1.5)	74
5	TBAI (5)	TBHP (1.5)	98
6	TBAI (10)	TBHP (1.5)	60
7	TBAI (2)	TBHP (1.5)	64
8	None	TBHP (1.5)	0
9	None	30% H_2O_2 (1.5)	0
10	TBAI (5)	30% H_2O_2 (1.5)	81
11	TBAI (5)	$Na_2CO_3 \cdot H_2O_2$ (1.5)	43
12	TBAB (150)	$NaIO_4$ (1.5)	21
13	TBAB (5)	$NaIO_4$ (1.5)	70

[a]Isolated yields.
[b]CF_3CO_2H (1.5 equiv.) as additive.

After optimizing the reaction conditions, a library of HA was examined as precursors for NOC compounds under these conditions, and their hDA reactions with both cyclic and acyclic dienes were explored (Figure 30). The cycloadducts were obtained in moderate to excellent yields (36%–98%) across all tested cases, except for sorbic acid, which did not undergo the hDA reaction. Notably, in the reaction of **1e** with acyclic dienes, benzoyl anhydride was detected as a side product. Given that benzoyl anhydride can form via dimerization of benzoylnitroso compounds, these findings support the generation of acylnitroso intermediates from **1e** under the proposed catalytic conditions.

Published in : ChemSusChem (2025), e202501565
DOI: 10.1002/cssc.202501565
Status : Postprint (Author's version)

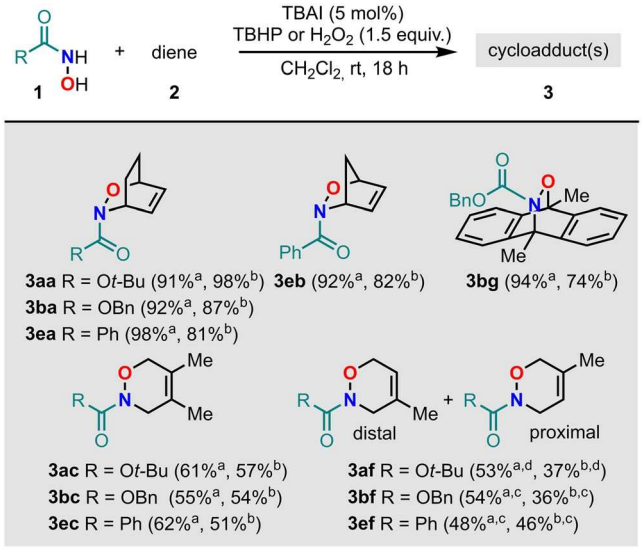

FIGURE 30 | Scope of the products from the hDA reaction between HAs and dienes. The reported yields are the isolated yields. [a] TBHP as oxidant. [b] H_2O_2 as oxidant. [c] distal/proximal 2:1. [d] distal/proximal 1:1.

The same oxidative strategy was also applicable to ene reactions, as demonstrated with HAs **1a** and **1b** reacting with the acyclic alkene **13a** and the cyclic alkene **13d** (Figure 31). However, 1octene failed to produce the corresponding adduct, likely due to the low reactivity typically associated with monosubstituted alkenes.

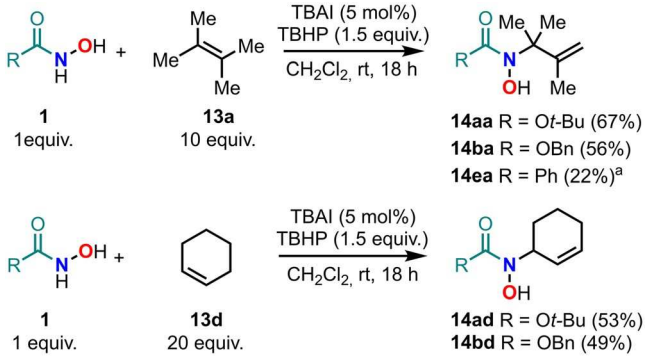

FIGURE 31 | Scope of the products obtained from the ene reaction between HAs and cyclohexene or 2,3-dimethylbut-2-ene.

Further mechanistic studies indicated that, among the iodine species generated from TBAI and TBHP, namely hypoiodite (an unstable intermediate) and triiodide, it is the hypoiodite species that is likely responsible for the observed oxidation [80].

In 2023, the Maegawa group developed an efficient method for converting HAs into carboxylic acids via NOC intermediates [81]. Through systematic optimization, they identified TBAI as the most effective iodine-based precatalyst, and H_2O_2 as the optimal oxidant, outperforming alternatives such

Published in : ChemSusChem (2025), e202501565
DOI: 10.1002/cssc.202501565
Status : Postprint (Author's version)

as oxone and *tert*-butyl hydroperoxide. The optimized reaction conditions comprised HA (1.0 equiv.), TBAI (0.1 equiv.), and H_2O_2 (2.0 equiv.) in a 2:1 mixture of THF and water.

Three control experiments provided valuable mechanistic insights into the reactivity of HA (Figure 32). The addition of TEMPO significantly reduced the product yield (from 98% to 47%), suggesting the involvement of radical species in the reaction pathway. Subjecting *O*-methyl HA to the standard reaction conditions resulted in its complete recovery, indicating its inability to participate in the transformation. In contrast, *N*-methyl HA underwent successful conversion, yielding both *p*-methoxybenzoic acid and *N*-methyl O-*p*-methoxybenzoyl HA, thus demonstrating its role in the reaction.

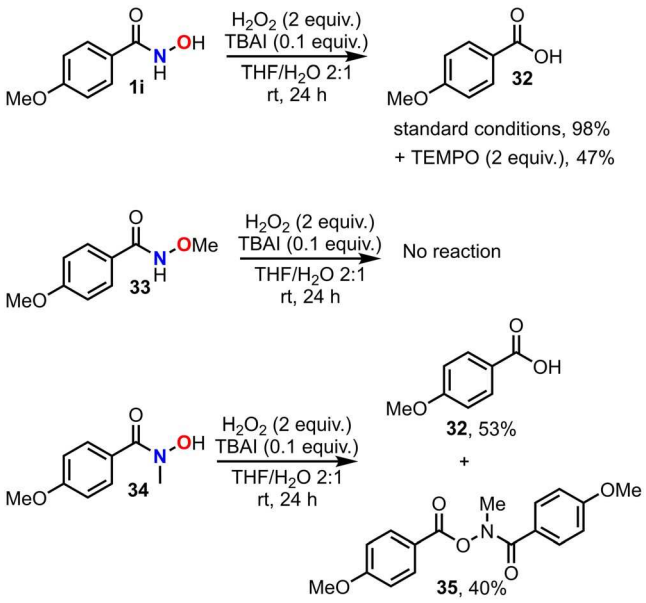

FIGURE 32 | Control experiments for the H_2O_2/TBAI oxidation of HAs.

A plausible mechanism was proposed to explain the observed reactivity. In the first pathway (Figure 33, pathway I), the reaction proceeds via radical intermediates. H_2O_2, decomposed in the presence of TBAI, generates hydroxyl radicals (•OH), which abstract a hydrogen atom from the HA, cleaving the O–H bond and forming an acyl aminoxyl radical. This radical species is then oxidized to the corresponding NOC intermediate, which undergoes hydrolysis to yield the carboxylic acid.

An alternative, nonradical pathway (Figure 33, pathway II) involves the generation of hypervalent iodine species, specifically IO^- and IO_2^-, through the oxidation of iodide (I^-) by H_2O_2.

These species are proposed to directly oxidize the HA to the NOC intermediate.

This dual-pathway model explains the inactivity of HA **33**, which bears a methyl substituent on the oxygen atom and thus cannot form the key acylnitroso species necessary for the transformation. Conversely, the oxoammonium intermediate **36**, formed during oxidation of compound **34**, reacts with either water or the HA to yield the final products.

Published in : ChemSusChem (2025), e202501565
DOI: 10.1002/cssc.202501565
Status : Postprint (Author's version)

Although radical involvement is strongly supported by experimental evidence, the contribution of the second, nonradical pathway cannot be definitively excluded [81].

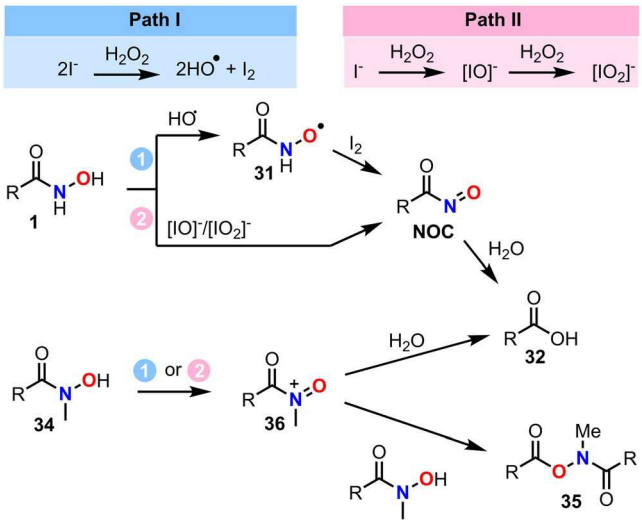

FIGURE 33 | Plausible mechanism for the TBAI/H_2O_2-catalyzed conversion of HAs to carboxylic acids via NOC intermediates.

3 | Catalytic Oxidations toward Nitrosocarbonyl Derivatives Using Molecular Oxygen

The use of molecular oxygen and reactive oxygen species (ROS) as oxidants represents a compelling approach for the generation of NOC species under sustainable and atom-economic conditions. These oxidative strategies capitalize on the low toxicity and environmental compatibility of oxygen, often requiring only catalytic amounts of transition metals or photoactive species to initiate radical or electron-transfer processes. In these systems, oxidation can proceed via in situ generation of ROS such as superoxide (O_2^{-}•), singlet oxygen ($^1O_2$), or hydroxyl radicals (•OH), which play key roles in the activation of HAs or related precursors.

This section reviews the recent advances in aerobic and ROS-driven NOC formation, organized by catalytic system, including copper(I), copper(II), photoredox catalysis, and enzymatic approaches, highlighting mechanistic features, synthetic applications, and emerging trends in green oxidation chemistry.

3.1 | COPPER (I) CATALYSTS

In 2011, de Alaniz and coworkers introduced a method using readily available copper(I) chloride and atmospheric air (1 atm) as a mild, cost-effective, and environmentally benign oxidant for the

Published in : ChemSusChem (2025), e202501565
DOI: 10.1002/cssc.202501565
Status : Postprint (Author's version)

conversion of HC into NOC species (Figure 34) [82]. Notably, these conditions significantly reduced undesired side reactions and prevented decomposition of the hydroxylamine-ene product via oxidation, disproportionation, or elimination pathways. The addition of a catalytic amount of pyridine was found to substantially enhance both the efficiency and selectivity of the transformation.

The reaction conditions were initially optimized for the intramolecular functionalization of allylic and homoallylic HC, proceeding via a type I ene mechanism according to the Oppolzer–Snieckus classification, and yielding 2-oxazolidinone and 1,3-oxazin-2-one scaffolds (Figure 34) [83]. The olefin geometry was shown to be a key factor for reactivity; substrates bearing a Z-alkene were unreactive under these conditions due to geometric constraints preventing cyclization.

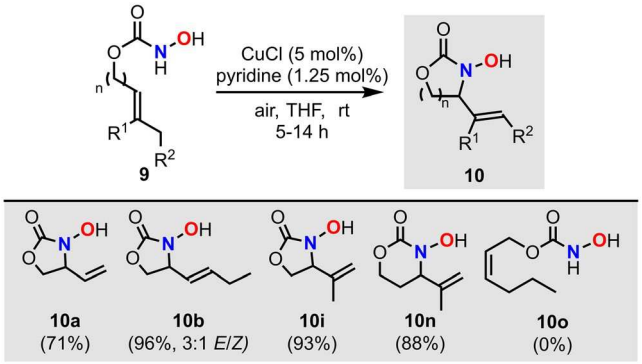

FIGURE 34 | NOC ene reaction catalyzed by a copper(I) chloride catalyst with pyridine as additive and air as oxidant.

The methodology was subsequently extended to intermolecular ene reactions (Table 17) demonstrating compatibility with a range of orthogonally protected HC, including with Boc, Cbz, Fmoc, and Troc groups. These protecting groups can be selectively removed in downstream steps to access free hydroxylamines. The reaction tolerates alkenes of different nature, with electron-rich olefins affording the highest yields. Nevertheless, substrates bearing electron-withdrawing substituents, as well as alkenes with free hydroxyl groups, also participated effectively. Geranyl acetate (**13n**) serves as a representative example of a substrate with electronically differentiated alkenes: the 6,7-double bond engages preferentially in the reaction, as the allylic acetate moiety deactivates the 2,3-double bond.

Published in : ChemSusChem (2025), e202501565
DOI: 10.1002/cssc.202501565
Status : Postprint (Author's version)

TABLE 17 | Intermolecular NOC ene reaction with different alkenes catalyzed by a Cu(I) chloride catalyst with pyridine as additive and air as oxidant.

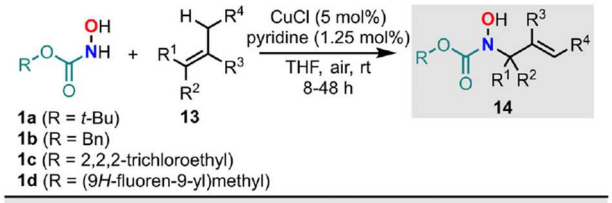

1a (R = *t*-Bu)
1b (R = Bn)
1c (R = 2,2,2-trichloroethyl)
1d (R = (9*H*-fluoren-9-yl)methyl)

13 **14**

Alkenes	Yield (%) with 1b	Alkenes	Yield (%) with 1b
13a	**14ba**, 98	13k-m	**14bk** (R^5 = H), 85 **14bl** (R^5 = Ac), 77 **14bm** (R^5 = TBS), 88
13d	**14bd**, 71	13n	**14bn**, 87 (9:1 select.)
13h	**14bh**, 42, 3:1 (*E*/*Z*)		
13i	**14bi**, 73, 3:1 (*E*/*Z*)		
13j	***twix*-14bj** / ***twin*-14bj** 66 (6:1 twix/twin)	13o-r	**14bo** (R^6 = OMe), 73 **14bp** (R^6 = NH_2), 72 **14bq** (R^6 = OH), 37 **14br** (R^6 = NHPh), 78

Importantly, asymmetric intermolecular ene reactions were also achieved under these mild conditions (Figure 35). Using Oppolzer's sultam as a chiral auxiliary to generate a tiglic acid-derivative (**37**), the corresponding (*R*)-methylene isoxazolidinone (**38**) was obtained with excellent enantioselectivity (98.5:1.5 *er*). Additionally, the chiral auxiliary was quantitatively recovered from the reaction mixture [82].

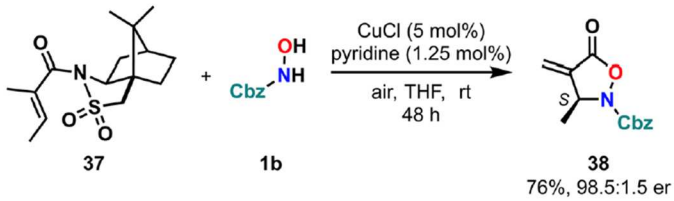

37 **1b** **38**
76%, 98.5:1.5 er

FIGURE 35 | Asymmetric acylnitroso-ene reaction.

Building on their previous findings, the same group further expanded the scope of *N*-substituted hydroxylamines, enabling access to a broader range of NOC derivatives, including acylnitroso, nitrosoformate, nitrosoformamide, iminonitroso, arylnitroso, and P-nitrosophosphine oxide species (Figure 36) [29].

Published in : ChemSusChem (2025), e202501565
DOI: 10.1002/cssc.202501565
Status : Postprint (Author's version)

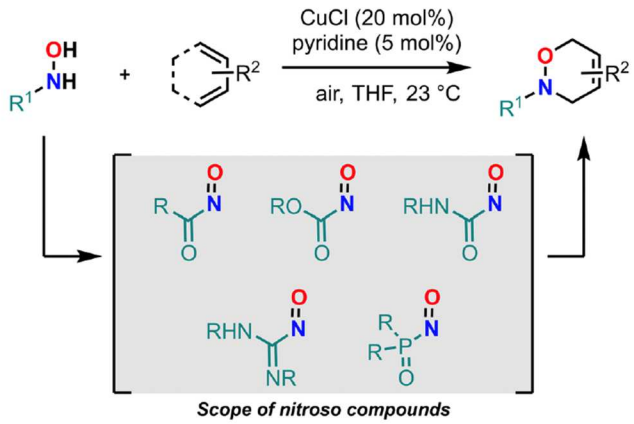

FIGURE 36 | Cu(I)-catalyzed aerobic oxidation of *N*-substituted hydroxylamines.

By increasing the catalyst loading to 20 mol% CuCl and 5 mol% pyridine (from 5 mol% and 1.25 mol%, respectively), transient nitroso compounds were efficiently generated in situ and trapped via hDA reactions. This strategy facilitated the synthesis of a structurally diverse array of *N*-substituted oxazines in moderate to high yields (Table 18).

TABLE 18 | hDA reaction between a library of NOC compounds and 1,3-cyclohexadiene using Cu(I) catalyst and pyridine as additive under aerobic conditions (Nppoc = 3′-Nitrophenylpropyloxycarbonyl).[a]

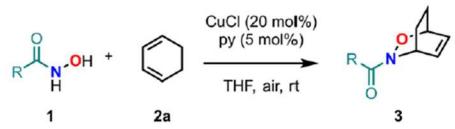

1 2a 3

acynitroso substrates

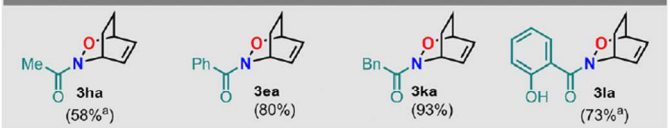

nitrosoformate ester substrates						nitrosoformamide substrates		
Cpd	R^1	Yield (%)	Cpd	R^2	Yield (%)	Cpd	R^3	Yield (%)
3aa	Boc	96	3ma	OMe	97	3ra	H	89
3nca	Troc	87	3na	OTBS	85	3sa	Ph	94
3da	Fmoc	99	3oa	CF_3	97	3ta	Bn	99
3qa	Nppoc	96	3pa	vinyl	94	3ua	pyridin-2-ylmethyl	77

[a]$T = 50°C$

A general trend emerged regarding the influence of the electronic nature of substituents on the nitrogen atom of the NOC. Typically, NOCs bearing electron-withdrawing groups displayed reduced reactivity and afforded lower product yields. For instance, catalytic oxidation of *N*-hydroxyacetamide in the presence of 1,3-cyclohexadiene yielded only 58% of product **3ha**, requiring elevated temperatures and resulting in partial decomposition of the NOC intermediate. In contrast,

Published in : ChemSusChem (2025), e202501565
DOI: 10.1002/cssc.202501565
Status : Postprint (Author's version)

hydroxylamines featuring orthogonal, carbamate-based protecting groups such as Cbz, Boc, Troc, Fmoc, and Nppoc, along with Cbz derivatives bearing *p*-substituents, delivered high product yields, ranging from 85% to 99%. Notably, this protocol enabled the efficient synthesis of a hydroxyurea cycloaddition adduct (**3ra**) in significantly higher yield (89%) compared to the previously reported stoichiometric Dess–Martin periodinane oxidation (39%) [84, 85].

Three key features highlight the strength of this protocol:

1. Excellent solvent compatibility, including reagent-grade MeOH, EtOH, *i*-PrOH, EtOAc, 2-MeTHF, and toluene;

2. Broad substrate scope (aryl hydroxylamines, *N*-hydroxyphosphinamides, and *N*-hydroxyphosphoramidates);

3. Versatility with a wide range of dienes for NOC trapping (Table 19), from species less reactive than 1,3-cyclohexadiene to more complex frameworks such as ergosterol, highlighting the functional group tolerance of the reaction conditions.

TABLE 19 | hDA reaction between *N*-Cbz-hydroxylamine and various dienes by using a Cu(I) catalyst and pyridine as additive under aerobic conditions.

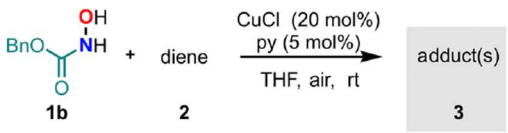

1b **2** **3**

Diene	Yield (%)	Diene	Yield (%)
 **2b**	94	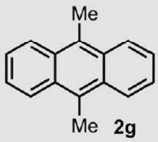 **2g**	96
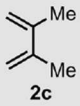 **2c**	71 ene product (17)	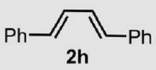 **2h**	80
 **2f**	43, distal/proximal 2:1 ene product (36)	ergosterol **39**	99 16:1 regioisomers
		ergosteryl acetate **40**	86 35:1 regioisomers

However, this method demonstrated only moderate regioselectivity with 2-substituted dienes. For example, the reaction with isoprene (**2f**) yielded a distal/proximal product ratio of 2:1.

Ene reaction outcomes using 2,3-dimethylbutadiene and isoprene suggest a preference for acyclic dienes adopting the *s-trans* conformation, whereas cyclic dienes constrained in an *s-cis* geometry predominantly furnish hDA cycloadducts. This hypothesis was supported by studies involving prenyl alcohol-derived HC **9i** and various dienes (Figure 37), where cyclic dienes failed to deliver ene adducts, while 2,3-dimethylbutadiene predominantly afforded the intramolecular ene product [29].

Published in : ChemSusChem (2025), e202501565
DOI: 10.1002/cssc.202501565
Status : Postprint (Author's version)

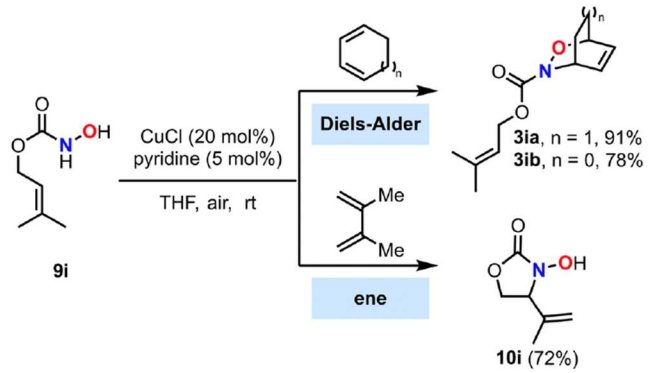

FIGURE 37 | Competing hDA and ene reactions as a function of the nature of the diene partner.

The protocol developed by de Alaniz group [82] was further applied by Gioia in the regio- and stereoselective synthesis of parthenolide analogs for biological evaluation against *Mycobacterium tuberculosis* [86]. These analogs were synthesized via nitroso-ene reaction using hydroxyureas and HC, obtaining the desired products in yields ranging from 25% to 91% (Figure 38). Parthenolide (**41**) underwent successful functionalization with a wide variety of substrates, spanning from polar alkyl to more lipophilic aryl substituents. The nitroso-ene reaction followed Markovnikov's rule, with the NOC enophile preferentially adding to the less-substituted carbon of the alkene. The authors proposed a mechanistic pathway involving an unstable aziridinium intermediate (**44**), which undergoes hydrogen abstraction from the more substituted, sterically less hindered position, resulting in high regioselectivity (Figure 39). Furthermore, the nitroso species was found to preferentially attack the less-hindered *Re*-face of the alkene, delivering high stereoselectivity [86].

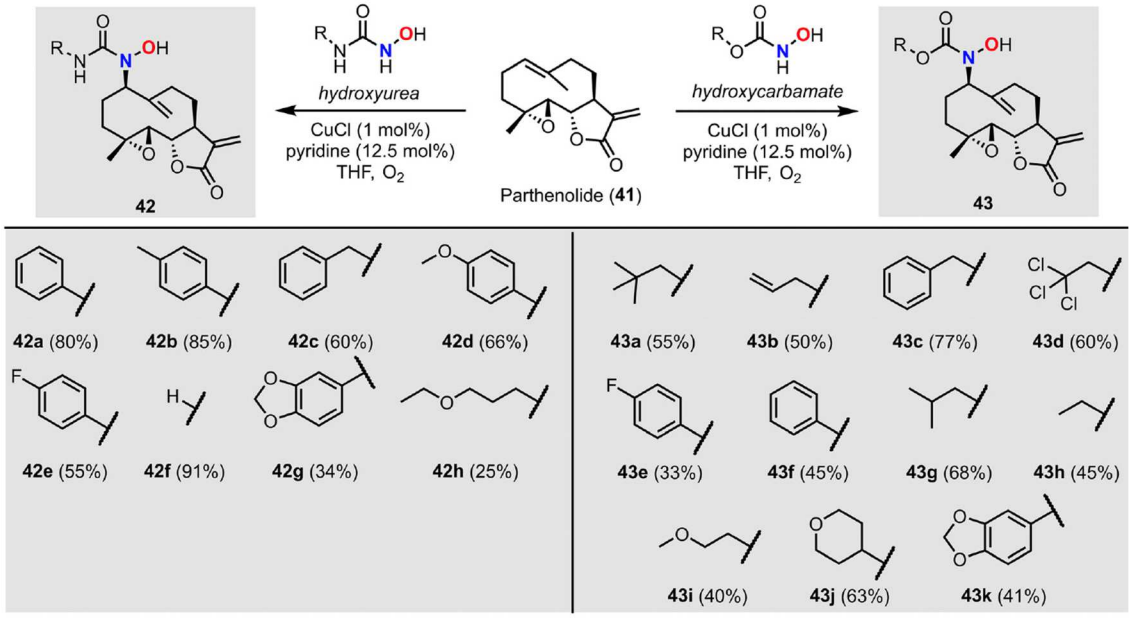

FIGURE 38 | Synthesis of parthenolide derivatives via nitroso-ene reactions with hydroxyureas and HCs.

Published in : ChemSusChem (2025), e202501565
DOI: 10.1002/cssc.202501565
Status : Postprint (Author's version)

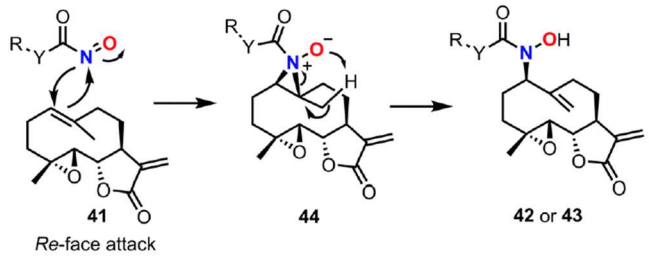

FIGURE 39 | Proposed mechanism to explain regio- and stereoselectivity observed upon the synthesis of Parthenolide derivatives.

To further understand and control regioselectivity in hDA reactions involving unsymmetrical dienes, de Alaniz and coworkers extended their Cu-catalyzed aerobic oxidation strategy to study the [4 + 2] cycloaddition of in situ generated NOCs with 2-substituted 1,3-butadienes [87]. To avoid competing ene-type pathways, 2-aryl-1,3-butadiene **2c**′ was selected as a model diene for investigating solvent and ligand effects (Table 20). In all cases, the distal regioisomer was consistently favored, while solvent and ligand choice had only modest influence on yield and minor effects on selectivity.

TABLE 20 | Optimization of the conditions using the hDA reaction between 2-aryl-1,3-butadiene 2c′ and acylnitroso species produced from the Cu-catalyzed aerobic oxidation of Cbz-*N*-hydroxylamine 1b as model reaction.

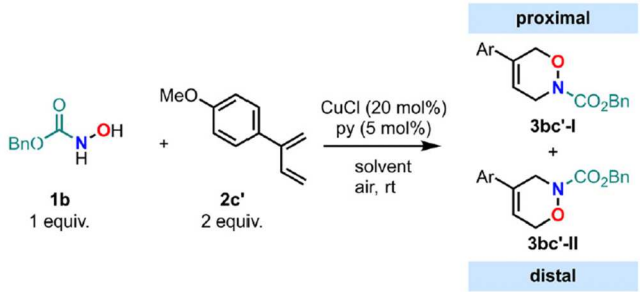

Entry	Solvent	Ligand	Yield (%)[a]	Proximal/distal ratio[a]
1	Toluene	Pyridine	61	1:14
2	MeOH	Pyridine	61	1:15
3	2-MeTHF	Pyridine	71	1:15
4	THF	Pyridine	85	1:15
5	THF	Ethyl oxazoline	78	1:15
6	THF	Ethyl nicotinate	58	1:14
7	THF	Bipyridyl	60	1:15

[a]The reported yields are the overall yields and the regioselectivity was determined by HSQC and ^{15}N HMBC.

Published in : ChemSusChem (2025), e202501565
DOI: 10.1002/cssc.202501565
Status : Postprint (Author's version)

A broader evaluation of HC with varied electronic and steric profiles further supported the generality of the observed regioselectivity. The results aligned with Houk's model, which predicts preferential distal isomer formation when the electron density at the 2-position of the diene is increased (Figure 40) [13]. Enhanced interaction between the diene's HOMO and the LUMO of the nitroso dienophile was proposed to account for this trend. Dienes containing electron-donating aryl groups at the 2-position showed significantly improved distal selectivity (up to 15:1), while those with electron-withdrawing groups yielded lower ratios (up to 4:1). Notably, dienes with *o*- and *p*-methoxyaryl substituents displayed different outcomes: the *o*-methoxy diene yielded product **3bg'** with a 4:1 distal/proximal ratio, whereas the *p*-methoxy analog provided **3bc'** with a higher selectivity of 15:1. This discrepancy was attributed to allylic steric hindrance in the *ortho* isomer, which may force the aryl ring out of conjugation, reducing electron density at the diene.

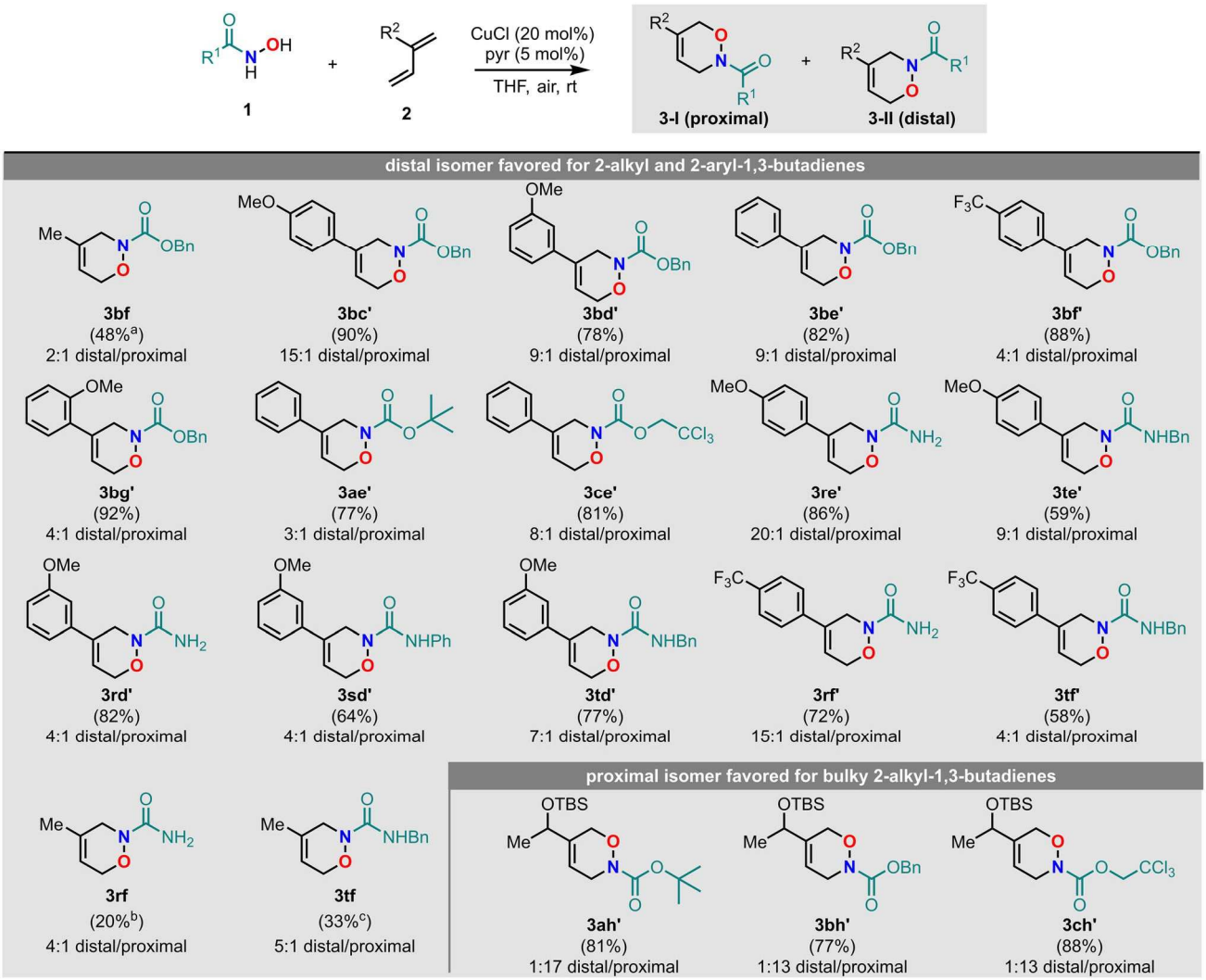

FIGURE 40 | Scope of the products obtained from the hDA reaction between 2-substituted 1,3-butadienes and HC. The reported yields are the overall yields. The ene adduct was isolated in [a] 38% yield, [b] 10% yield, [c] 12% yield.

Published in : ChemSusChem (2025), e202501565
DOI: 10.1002/cssc.202501565
Status : Postprint (Author's version)

Conversely, with bulky substituents at the 2-position (e.g., **3ah**′, **3bh**′, and **3ch**′), the regioselectivity was reversed, favoring the proximal isomer due to unfavorable interactions between the bulky group of the diene and the NOC in the preferred *endo* transition state. While an *exo* transition state could hypothetically allow distal product formation, it is disfavored by the so-called *exo* lone pair effect. The steric profile of the NOC species itself also impacted regioselectivity: reactions of 2-phenyl-1,3butadiene with Cbz- or Troc-protected hydroxylamines produced distal isomers in 9:1 and 8:1 ratios, respectively. However, use of the bulkier Boc group reduced selectivity to 3:1 (**3ae**′). In summary, these findings confirmed Houk′s model and demonstrate that regiocontrol in hDA reactions can be finely tuned through strategic variation of both diene and nitroso compound steric and electronic properties [87].

In 2014, Luo and coworkers reported a mild Cu(I)-catalyzed aerobic oxidation of HC to generate NOC species, which were then used as electrophilic nitrogen sources for the enantioselective α-amination of β-ketocarbonyl derivatives (Figure 41) [88]. Enantioselectivity was achieved through the formation of enamine intermediates using chiral primary amine catalysts. However, using *β*-ketocarbonyls as substrates poses challenges due to the stability of the corresponding enamines *via* intramolecular hydrogen bonding, which can hinder catalytic turnover. Furthermore, these enamines are susceptible to degradation under aerobic conditions.

Initial studies focused on the reaction between acetoacetate **11a** and HC **1b**. Using chiral amine catalyst **46**, CuCl (10 mol%), TfOH, and *m*-nitrobenzoic acid (20 mol%) in acetonitrile under an air atmosphere, the α-amination product **12ba** was obtained in 97% yield with >20:1 regioselectivity and 96% *ee* (Table 21).

Published in : ChemSusChem (2025), e202501565
DOI: 10.1002/cssc.202501565
Status : Postprint (Author's version)

TABLE 21 | Optimization of the conditions using the aerobic asymmetric α-amination of acetoacetate **11a** with HC **1b** using a chiral amine catalyst as model reaction.

Entry	Variation from standard conditions	Yield (%)[a]	12ba/45ba	*ee* (%)[b]
1	None (chiral amine **46**)	97	>20:1	96
2	Chiral amine **47**	61	5:1	65
3	Chiral amine **48**	52	3:1	83
4	No *m*-NO_2PhCO_2H	62	6:1	94
5	No CuCl	nr	/	/
6	Ar atmosphere	trace	/	/
7	MnO_2 oxidant (5 equiv.)	26	nd	60
8	$CuCl_2$	nr	/	/
9	CuO	40	3:1	58
10	CuCN	nr	/	/
11	CuI	nr	/	/
12	CH_2Cl_2 solvent	78	5:1	95
13	THF solvent	52	4:1	55
14	Et_2O solvent	65	8:1	86
15	Toluene solvent	69	3:1	65
16	MeOH solvent	85	nd	35

[a]Isolated yields.
[b]Determined by HPLC on a chiral stationary phase; nd = not determined. nr = no reaction.

Both CuCl and air were essential for the reaction (Table 21, entries 5–6), while alternative oxidants (e.g., MnO_2) or other copper sources led to inferior results (entries 7–11). The presence of *m*-nitrobenzoic acid proved critical, as its omission led to reduced yields (62%) and lower regioselectivity (6:1) (entry 4). Acetonitrile emerged as the optimal solvent (entries 1 and 12–16).

The reaction scope was then expanded under optimized conditions to various β-ketocarbonyls and HCs (Figure 42).

Published in : ChemSusChem (2025), e202501565
DOI: 10.1002/cssc.202501565
Status : Postprint (Author's version)

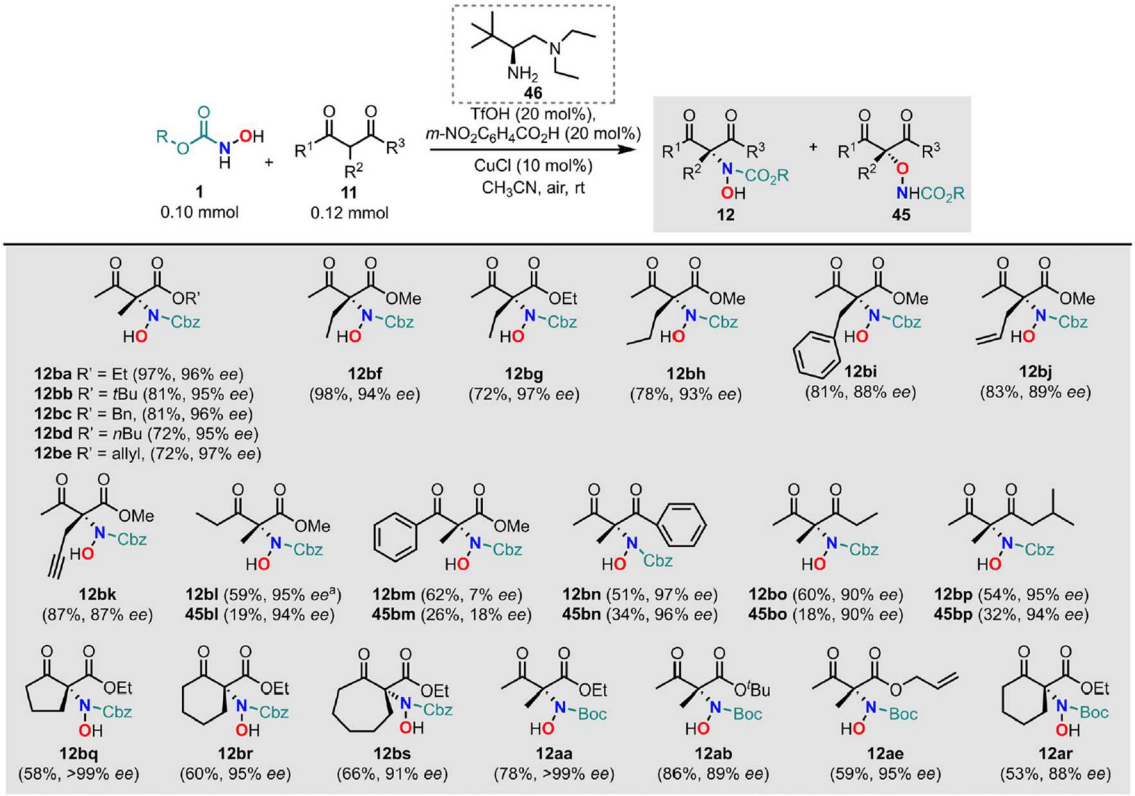

FIGURE 42 | Scope of the products obtained from the aerobic asymmetric α-amination of β-ketocarbonyls using Cbz- or Boc-HC. The reported yields are isolated yields. [a] CuCl (5 mol%).

A range of acetoacetates bearing different ester moieties at the R^3 position, including bulky *tert*-butyl, benzyl, and allyl groups, provided the desired *N*-adducts in high yields and excellent enantioselectivities (**12ba**-**12be**). Likewise, α-substituents at the R^2 position were well tolerated (**12bf**-**12bk**), with high *N/O* regioselectivity and minimal aminoxylation side products. In contrast, modifications at the R^1 position significantly influenced the outcome. For example, ethyl ketone led to the formation of the major *N*-adduct **12bl** and the minor *O*-adduct **45bl**, both with excellent enantioselectivities. However, a lower reaction rate was observed, suggesting potential hindrance to enamine catalysis by large aliphatic ketones.

On the other hand, phenyl ketones gave sluggish rates and, despite the formation of both *N*- and *O*-adducts (**12bm** and **45bm**), both showed low enantioselectivity, possibly due to an unselective enol-based process instead of enamine catalysis.

This oxidative α-amination protocol also proved effective for acyclic 1,3-diketones and cyclic β-ketoesters, yielding the desired *N*-adducts (**12bn**-**12bs**) as the major, if not exclusive, products. Comparable enantioselectivities with slightly reduced yields were observed when *tert*-butyl HC was used instead of the benzyl analog.

Importantly, unlike α-hydroxylaminations of carbonyl compounds using stable nitrosobenzene derivatives, which form difficult to cleave *N*-aryl bonds, the amination products derived from NOC species undergo smooth reductive N–O bond cleavage. For example, selective hydrogenolysis of the

Published in : ChemSusChem (2025), e202501565
DOI: 10.1002/cssc.202501565
Status : Postprint (Author's version)

Boc-protected compound **12bb** using H_2/Ni Raney gave the corresponding free amine, leaving the ketone moiety unaffected (Figure 43) [88].

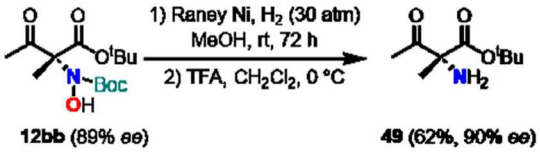

FIGURE 43 |Reductive N-O cleavage to express free amine group.

The remarkable chemoselectivity and enantioselectivity observed in primary amine-catalyzed *N*-nitroso-aldol reactions involving aerobically generated NOCs led Luo and coworkers to conduct a detailed computational study to uncover the mechanistic origins of these effects [89]. Notably, the *N*-selectivity observed in their system was unexpected, as previous efforts using chiral Lewis acids had predominantly yielded *O*-selective products, with the use of (chiral) ligands further enhancing this trend.

In the proposed reaction mechanism (Figure 44), the transformation begins with the formation of an enamine intermediate from the β-ketocarbonyl substrate and the chiral primary amine catalyst (**46**-TfOH). This enamine then undergoes α-amination via an in situ generated NOC to form an imine intermediate, which is subsequently hydrolyzed to regenerate the catalyst and release the final product. Three key factors were investigated to understand this mechanism: (1) the geometry of the enamine intermediate, which was hypothesized to play a crucial role in determining both regio- and enantioselectivity; (2) the bidentate nature of NOCs, which could account for the observed *N*-selectivity; and (3) the specific interactions between the enamine and NOC species to rationalize the enantiocontrol.

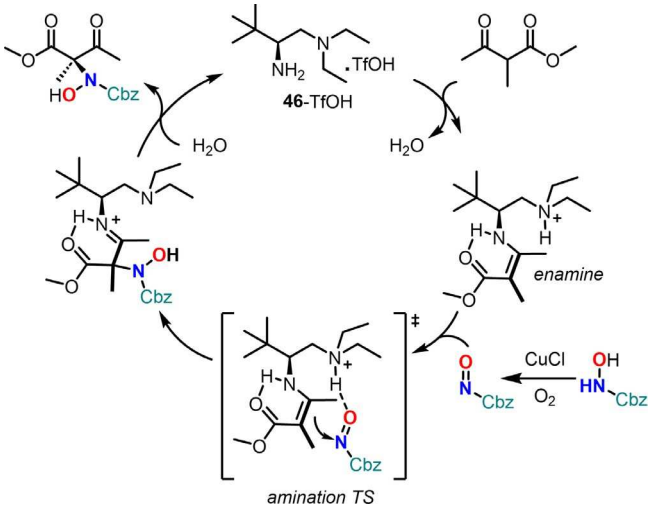

FIGURE 44 |Proposed mechanism for aerobic amination.

Regarding the enamine geometry, several conformational isomers are possible, arising from *E/Z* configurations and *cis/trans* orientations (Figure 45).

Published in : ChemSusChem (2025), e202501565
DOI: 10.1002/cssc.202501565
Status : Postprint (Author's version)

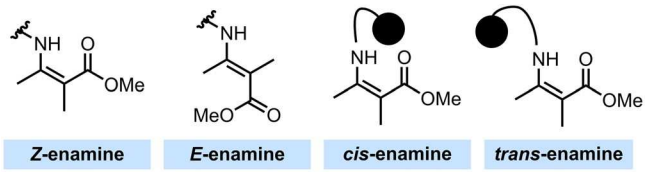

FIGURE 45 |Possible configurations of the enamine intermediate.

Computational analysis identified the *Z-s-trans*-isomer as the most stable conformation (Figure 46). This finding was further validated by single-crystal X-ray crystallography and NMR spectroscopy. The enhanced stability of this isomer can be attributed to three factors (Figure 46): (1) an intramolecular hydrogen bond between the enamine nitrogen and the protonated catalyst (N^+-H group), (2) an additional H^-bonding interaction between the enamine N-H group and the adjacent carbonyl oxygen, and (3) minimized steric repulsion between the *tert*-butyl group on the catalyst and the methyl substituent on the substrate, which favors the *s-trans* configuration over the *s-cis*.

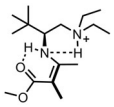

FIGURE 46 | Structure of stable *Z-s*-trans-enamine isomer.

To further investigate the origins of regioselectivity, the researchers examined the potential for bidentate hydrogen bonding between NOCs and the enamine intermediate. Transition state (TS) comparisons were made for the reaction between the most stable enamine (*Z-s-trans*) and NOC Cbz-NO, analyzing the competing pathways leading to *O*- and *N*-regioisomeric products (Figure 47).

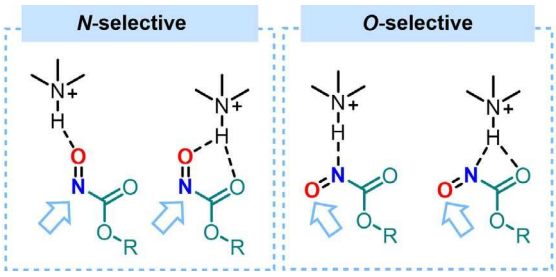

FIGURE 47 | Different modes of H-bonding interactions with the NOC group in the *O*- and *N*-selective transition states.

This study revealed that the formation of the *N*-regioisomer was associated with the most stable TS, driven by a bidentate hydrogen$^-$bonding interaction between the tertiary amine and the nitroso moiety, as well as a favorable π-interaction between the enamine α-methyl group and the electrophilic

Published in : ChemSusChem (2025), e202501565
DOI: 10.1002/cssc.202501565
Status : Postprint (Author's version)

benzyl substituent (Figure 48). In contrast, the formation of the *O*-regioisomer proceeded through a higher-energy TS ($\Delta G^{\neq}$ = 2.8 kcal mol^{-1}). As a result, the computed *N/O* selectivity ratio exceeded 99:1, in excellent agreement with experimental observations.

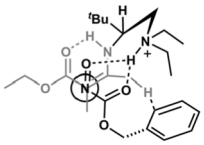

FIGURE 48| *N*-selective transitions state.

The calculations also offered insight into the origins of enantioselectivity, demonstrating a preference for *Si* face addition on both coexisting (*E*)- and (*Z*)-enamine intermediates. This preference follows a Curtin–Hammett-type model, where the TSs are governed by bidentate hydrogen bonding interactions between the enamine and the NOCs. This chelation-based model may have broader implications for other transformations involving NOCs, particularly in systems where hydrogen bonding or metal coordination interactions play a critical role [89].

Building on these insights, Luo's group further investigated the copper-catalyzed aerobic oxidative α-amination of β-ketocarbonyls using nanoelectrospray ionization mass spectrometry (nESI-MS) [90]. This technique was used to monitor and identify key intermediates during the model reaction between ethyl 2methyl-3-oxobutanoate (**11a**) and benzyl HC (**1b**), in the presence of air, CuCl (10 mol%), (S)-*N*1,*N*1-diethyl-3,3-di-methylbutane-1,2-diamine trifluoromethanesulfonic acid salt (**46**·TfOH, 20 mol%), and *m*-nitrobenzoic acid (20 mol%) in acetonitrile (Figure 49). Consistent with prior mechanistic hypotheses [88], nESI-MS data confirmed the formation of the enamine intermediate **50** (Figure 50), though it remained at low concentration throughout the reaction. In contrast, the concentration of the imine intermediate **51** gradually increased over time, suggesting rapid conversion from enamine to imine.

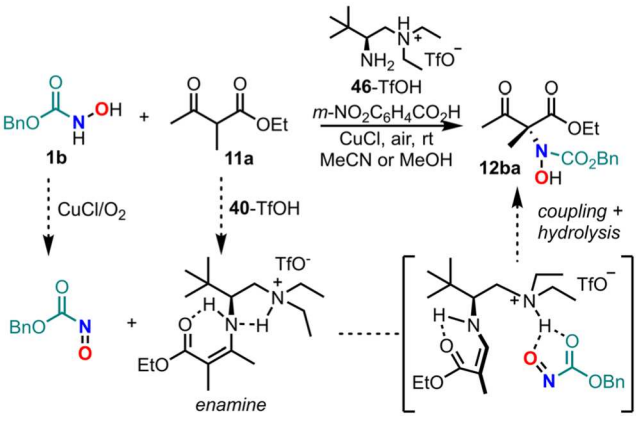

FIGURE 49 | Proposed catalytic cycle for the Cu(I)/diamine-catalyzed *N*-selective asymmetric nitroso-aldol reaction.

Published in : ChemSusChem (2025), e202501565
DOI: 10.1002/cssc.202501565
Status : Postprint (Author's version)

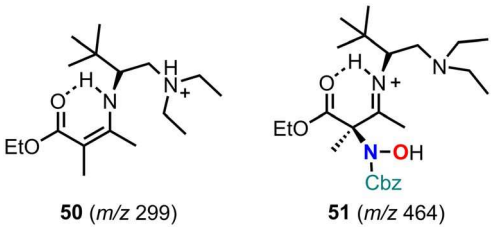

FIGURE 50 | Species detected by nESI-MS supporting enamine catalysis pathway.

Interestingly, switching the solvent from acetonitrile to methanol led to a pronounced drop in enantioselectivity (from 96% *ee* to 35% *ee*), highlighting the solvent's influence on the reaction pathway.

Mass spectrometric analysis revealed that in acetonitrile, the dominant species was the nonhydrolyzed imine ion **51**, with only minimal signals corresponding to the product **12ba**. However, in methanol, **12ba** appeared with higher intensity, along with two new ions, **52** and **53** (Figure 51). These observations suggested a different mechanism: while the enamine pathway with a slower hydrolysis step predominates in acetonitrile, methanol favors an alternative enol-based catalytic pathway (Figure 51) that bypasses hydrolysis entirely. The solvent's lower copper-binding ability relative to the β-ketoester allowed easier enolate formation, thus hindering iminium/enamine formation. The reduced enantioselectivity in methanol was attributed to the longer spatial separation between the chiral ligand and the reactive carbon center in the enolate pathway, compared to the more rigid and directed enamine route.

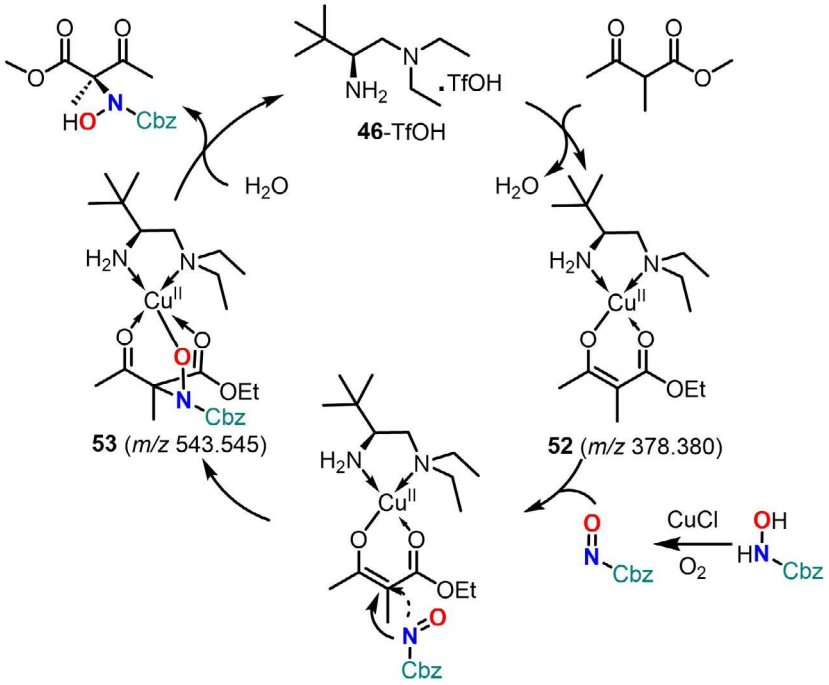

FIGURE 51 | Competing enol catalytic cycle for the nitroso-aldol reaction with methanol as solvent.

Published in : ChemSusChem (2025), e202501565
DOI: 10.1002/cssc.202501565
Status : Postprint (Author's version)

To further support this mechanistic hypothesis, Luo's team used additional techniques including electron paramagnetic resonance (EPR) and UV/Vis spectroscopy to detect Cu(I) and Cu(II) species. Drawing on these results, as well as established pathways for copper-mediated aerobic oxidation, the authors proposed a novel autocatalytic cycle for NOC formation (Figure 52). The cycle begins with the interaction of the Cu(I) complex with molecular oxygen to generate an active binuclear complex (step 1). This complex then reacts with HC to form the CbzNHO· radical and a [(L)Cu(II)OH] species (step 2). Subsequent ligand exchange between [(L)Cu(II)OH] and another equivalent of HC yields the [(L)Cu(II)ONHCbz] complex (step 3). Finally, a hydrogen atom transfer occurs from the oxygen of the CbzNHO· radical to [(L)Cu(II)ONHCbz], resulting in the release of the active NOC species (step 4). Notably, the stability of the [(L)Cu(II)ONHCbz] complex disfavored direct radical binding to copper, thus favoring a bimolecular hydrogen atom transfer pathway in which both the Cu(II) species and the N-centered radical cooperatively facilitate the key transformation [90].

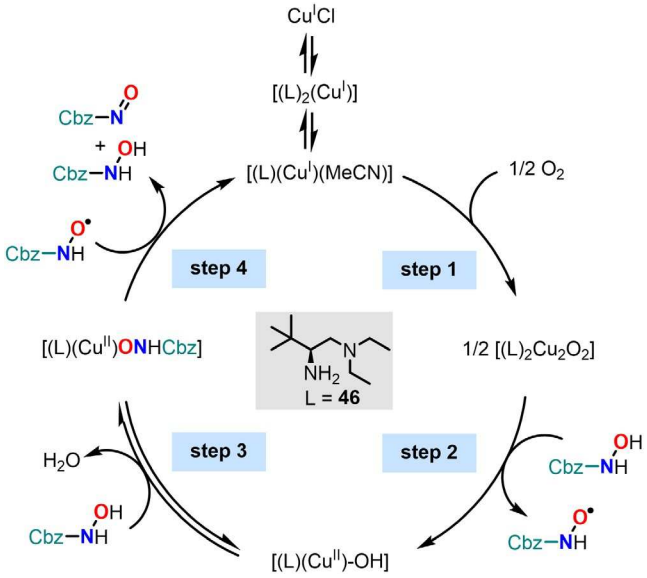

FIGURE 52 | Proposed catalytic cycle for the Cu(I)/diamine-catalyzed aerobic oxidation of a *N*-hydroxylamine for further *N*-selective asymmetric nitroso-aldol reaction.

In the context of enamine-catalyzed α-functionalization of β-ketocarbonyl compounds, the Luo group made an unexpected observation: when α-unsubstituted β-ketoesters were subjected to their standard reaction conditions, the major product was not the anticipated α-amination product **12bt**, but rather a single *N*, *O*-ketal compound, **54bt** (Figure 53) [91]. This product was obtained in high yield and moderate enantioselectivity. Given the limited literature on the enantioselective synthesis of chiral *N*, *O*-ketals, the group focused on their direct preparation from ketones via primary amine catalysis. In this approach, HC served as dual sources of nitrogen and oxygen under aerobic oxidative conditions.

Improved enantioselectivity was achieved by replacing the previously used *m*-nitrobenzoic acid additive with chiral auxiliaries such as the (*R*)- and (*S*)-forms of *N*-Boc-phenylalanine (**55**) and *N*-Boc-*tert*-leucine (**56**) (Figure 53). All enantiomers of **55** and **56** gave high yields (80%–93%) and

Published in : ChemSusChem (2025), e202501565
DOI: 10.1002/cssc.202501565
Status : Postprint (Author's version)

enantioselectivities (82%–85%), with (*R*)-**56** ultimately selected due to the higher enantiomeric excess it conferred. The reaction was found to be highly sensitive to the concentration of dissolved oxygen. Reaction rate, yield, and enantioselectivity were all improved under pure oxygen or elevated pressure (10 atm), compared to ambient air. Nevertheless, for practical reasons, the authors chose to carry out subsequent reactions under 1 atm of oxygen. Control experiments confirmed that no conversion occurred in the absence of the primary amine catalyst **46**, highlighting the central role of aminocatalysis in this transformation.

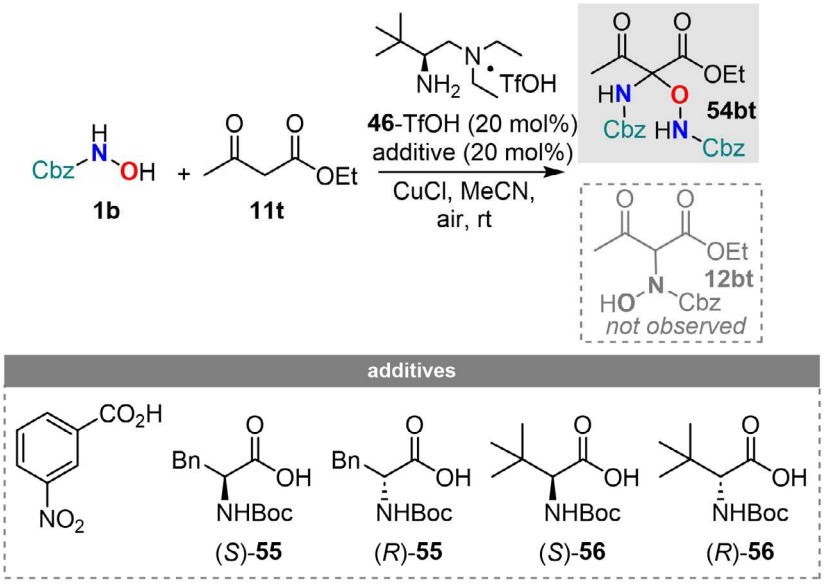

FIGURE 53 | Direct enantioselective synthesis of α-*N*, *O*-ketals from ketones by primary amine catalysis

The optimized conditions for the enantioselective synthesis of *N*, *O*-ketals involved the use of HC (3 equiv.), the *tert*-leucine-derived primary amine catalyst **46** (20 mol%), (*R*)-**56** (20 mol%), and CuCl (15 mol%), under an oxygen atmosphere in acetonitrile at room temperature. The substrate scope of the β-ketoester component was thoroughly explored under these conditions (Figure 54). The transformation displayed excellent tolerance for a range of R^2 substituents, including ethyl, *tert*-butyl, phenyl, and allyl groups, with no observable oxidation of unsaturated moieties. Even β-ketoesters bearing bulky ester groups, such as diphenylmethyl or adamantly, underwent smooth conversion to their corresponding *N*, *O*-ketals (**54b**x**54by**) with high yields and enantioselectivities.

Published in : ChemSusChem (2025), e202501565
DOI: 10.1002/cssc.202501565
Status : Postprint (Author's version)

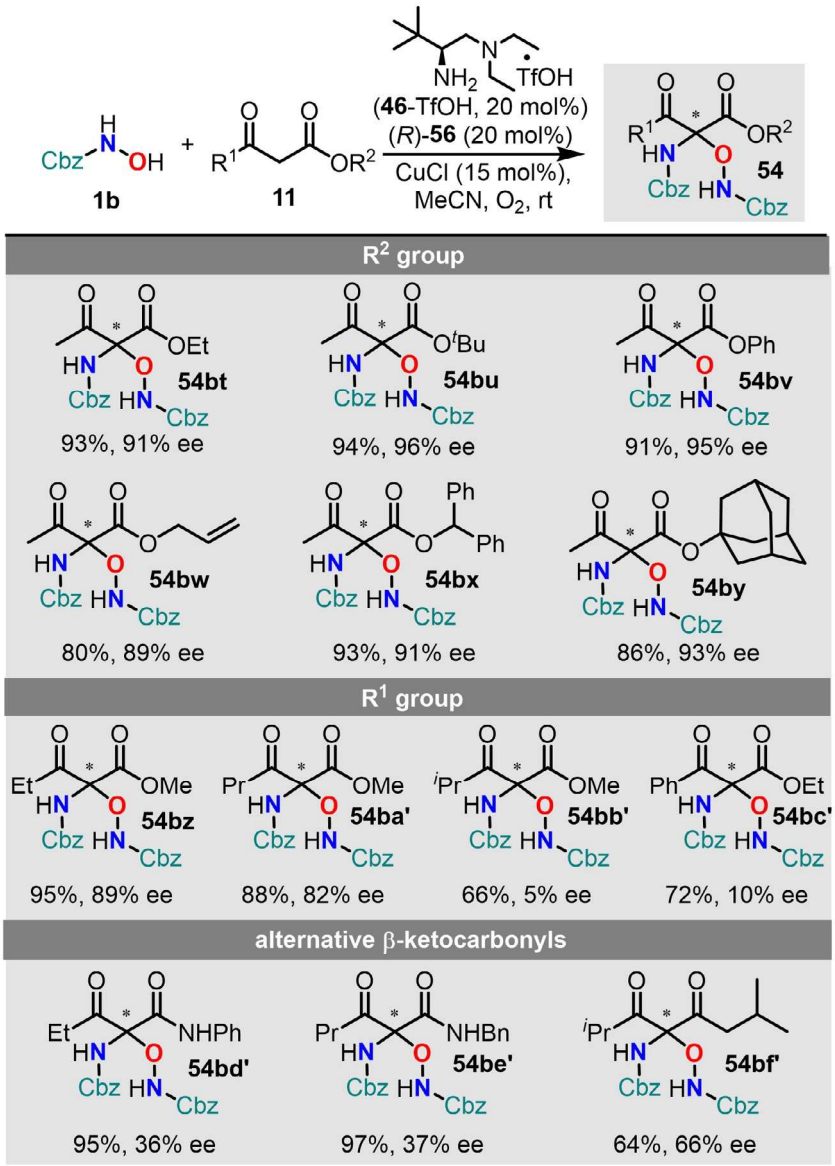

FIGURE 54 | Substrate scope of β-ketocarbonyls for the enantioselective synthesis of *N*, *O*-ketals.

Variation at the R^1 position was also examined. Substrates like methyl propionylacetate and methyl butyrylacetate gave the desired products (**54bz** and **54ba'**) with similarly excellent outcomes. However, β-ketoesters with sterically demanding ketone fragments at R^1, such as methyl isobutyrylacetate and ethyl benzoylacetate, afforded poor enantioselectivity in products **54bb'** and **54bc'**. This suggests that the bulky substrates likely favored an enol-type pathway, bypassing the enamine intermediate, consistent with prior reports. Importantly, the optimized conditions were also effective for other β-ketocarbonyls, such as β-ketoamides and 1,3-diketones, supporting a general α,α-bis-functionalization.

Efforts to extend this methodology to simpler carbonyl compounds revealed notable substrate-dependent reactivity (Figure 55). Six-membered cyclic ketones underwent smooth conversion, affording the corresponding *N*, *O*-ketal adducts in good yields and enantioselectivities. In contrast,

Published in : ChemSusChem (2025), e202501565
DOI: 10.1002/cssc.202501565
Status : Postprint (Author's version)

other cyclic ketones, such as cyclopentanone and cycloheptanone, and linear ketones like 3-pentanone failed to react under the standard conditions. Similarly, simple aldehydes did not participate in the transformation, most likely due to their susceptibility to oxidative degradation (Figure 55). Notably, the ketalization protocol proved amenable to gram-scale synthesis, without compromising yield or enantioselectivity.

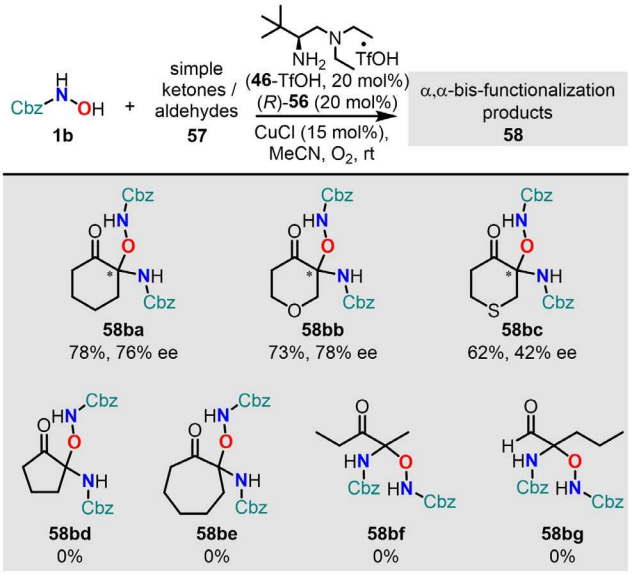

FIGURE 55 | Scope of simple carbonyls for the enantioselective synthesis of N, O-ketals.

A plausible mechanistic pathway was proposed to account for the formation of the *N*, *O*-ketal product (Figure 56). The reaction begins with activation of the β-ketoester **11u** by the chiral primary amine catalyst **46**-TfOH, generating the enamine intermediate **59**. This enamine subsequently reacts with an in situ generated NOC, yielding intermediate **60**. Due to the strong acidity of the α-proton in intermediate **60**, water is eliminated, leading to the formation of a highly electrophilic diimine intermediate **61**. This intermediate then undergoes nucleophilic addition by a second equivalent of HC **1b** to afford intermediate **62**, which is hydrolyzed to release the final product **54bu** and regenerate the amine catalyst.

Published in : ChemSusChem (2025), e202501565
DOI: 10.1002/cssc.202501565
Status : Postprint (Author's version)

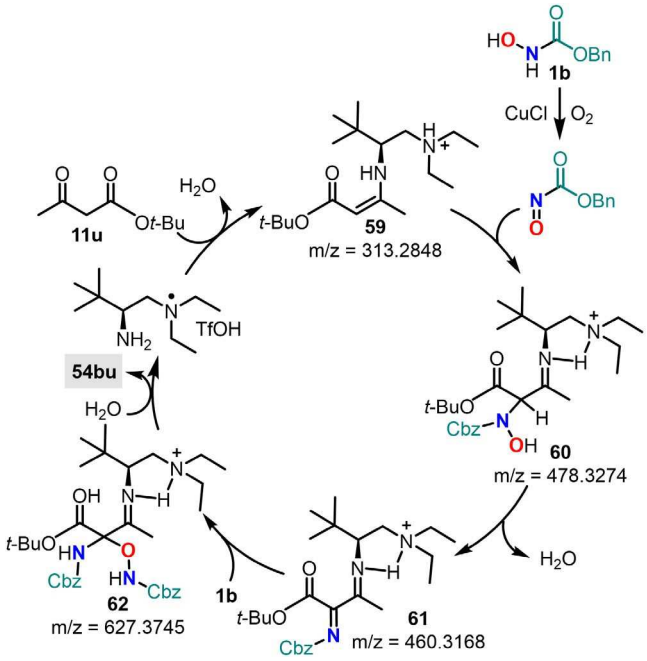

FIGURE 56 | Proposed mechanism for the enamine−iminium−diiminium cycle.

HRMS analysis of the reaction mixture confirmed the presence of key intermediates **59**, **60**, **61**, and **62**, supporting the validity of the proposed mechanism. The stereoselectivity of the reaction is attributed to the conformational and electronic properties of the diimine intermediate **61**. The chiral acidic additive (*R*)-**56** is proposed to play a dual role: promoting stereocontrol through its function as a counterion, and facilitating in the enamine-iminium-diiminium catalytic cycle [91].

In 2015, Baidya et al. introduced a mild one-pot method for the αamination of ketones [92]. Their approach involved a modified Mukaiyama aldol reaction between silyl enol ethers and NOCs, offering distinct advantages over conventional aminating electrophiles such as azodicarboxylates or nitrosoarenes, where N–N or N–Ph bond cleavage to release the free amine can be challenging. In contrast, their method achieves a cascade C–N bond formation accompanied by N–O bond cleavage in a single step (Figure 57) [92]. This strategy exploits the oxophilic nature of silicon, which allows coordination of the silyl enol ether with the oxygen atom of the NOC, leaving the nitrogen center available for a highly *N*-selective aldol-type reaction. During this process, the silyl group transfers from the oxygen of the silyl enol ether to the oxygen of the resulting nitroso-aldol intermediate. This rearrangement facilitates cleavage of the relatively weak N⁻O bond, ultimately furnishing α-amino ketones.

Published in : ChemSusChem (2025), e202501565
DOI: 10.1002/cssc.202501565
Status : Postprint (Author's version)

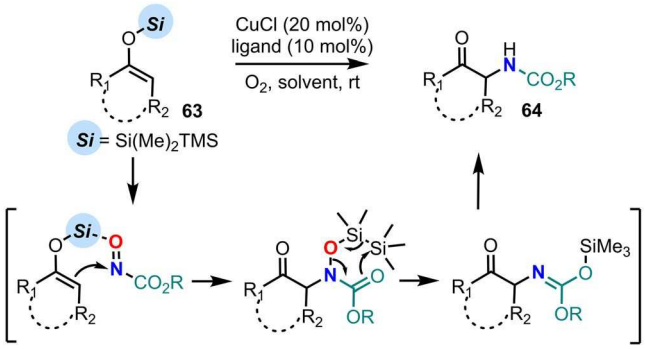

FIGURE 57 | Selective C–N bond formation via nitroso Mukaiyama aldol reaction.

Reaction conditions were optimized using silyl enol ether **63a** as a model substrate, along with a copper-mediated mild aerobic oxidation to generate the NOC in situ from Cbz-N-hydroxylamine **1b** (Table 22). The use of CuCl (20 mol%) and pyridine (10 mol%) under an O_2 atmosphere at room temperature afforded product **64ba** in a high yield of 81% (Table 22, entry 1). X-ray analysis of the crystallized product confirmed the excellent *N*-selectivity and successful N–O bond cleavage.

TABLE 22 | Optimization of the conditions for the Baidya's modified Mukaiyama aldol reaction between silyl enol ether **63a** and Cbz-*N*-hydroxylamine **1b**.

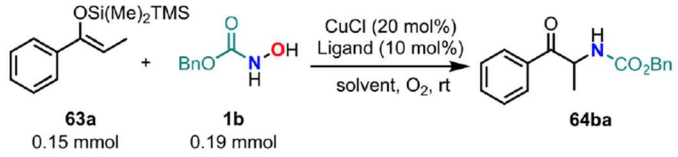

63a 0.15 mmol | **1b** 0.19 mmol | **64ba**

Entry	Solvent	Ligand	Yield (%)[a]
1	THF	Pyridine	81
2	CH_3CN	Pyridine	98
3	CH_3CN	2,2′-Bipyridine	96
4	CH_3CN	2-Ethyl-2-oxazoline	83
5[b]	CH_3CN	Pyridine	66
6[c]	CH_3CN	Pyridine	N.R.

[a]Isolated yields.
[b]Addition of 10 mol% $Cu(OTf)_2$.
[c]MnO_2 as oxidant instead of $CuCl/O_2$.

To prevent condensation between the in situ generated NOCs and excess HC **1b**, the latter was added slowly. Replacing THF with acetonitrile as the solvent (Table 22, entry 2) further improved the yield, increasing it to 98%. Other amine ligands also proved effective: 2,2′-bipyridine and 2-ethyl-2-oxazoline afforded yields of 96% and 83%, respectively (Table 22, entries 3–4). However, the addition of $Cu(OTf)_2$ as a secondary catalyst (Table 22, entry 5) resulted in a lower yield and significant desilylation of **1a**. When MnO_2 was used as the oxidant to generate the NOCs in situ, no reaction was observed (Table 22, entry 6).

Published in : ChemSusChem (2025), e202501565
DOI: 10.1002/cssc.202501565
Status : Postprint (Author's version)

The versatility of this one-pot, *N*-selective nitrosocarbonyl Mukaiyama aldol cascade was demonstrated through the synthesis of a wide array of α-amino ketones (Figure 58). A broad range of silyl enol ethers (cyclic and acyclic, electron-rich and electron-poor, as well as unsubstituted or sterically hindered) were found to be compatible with this methodology. Notably, a double nitroso-aldol reaction was successfully carried out, affording compound **64bm** in 95% yield.

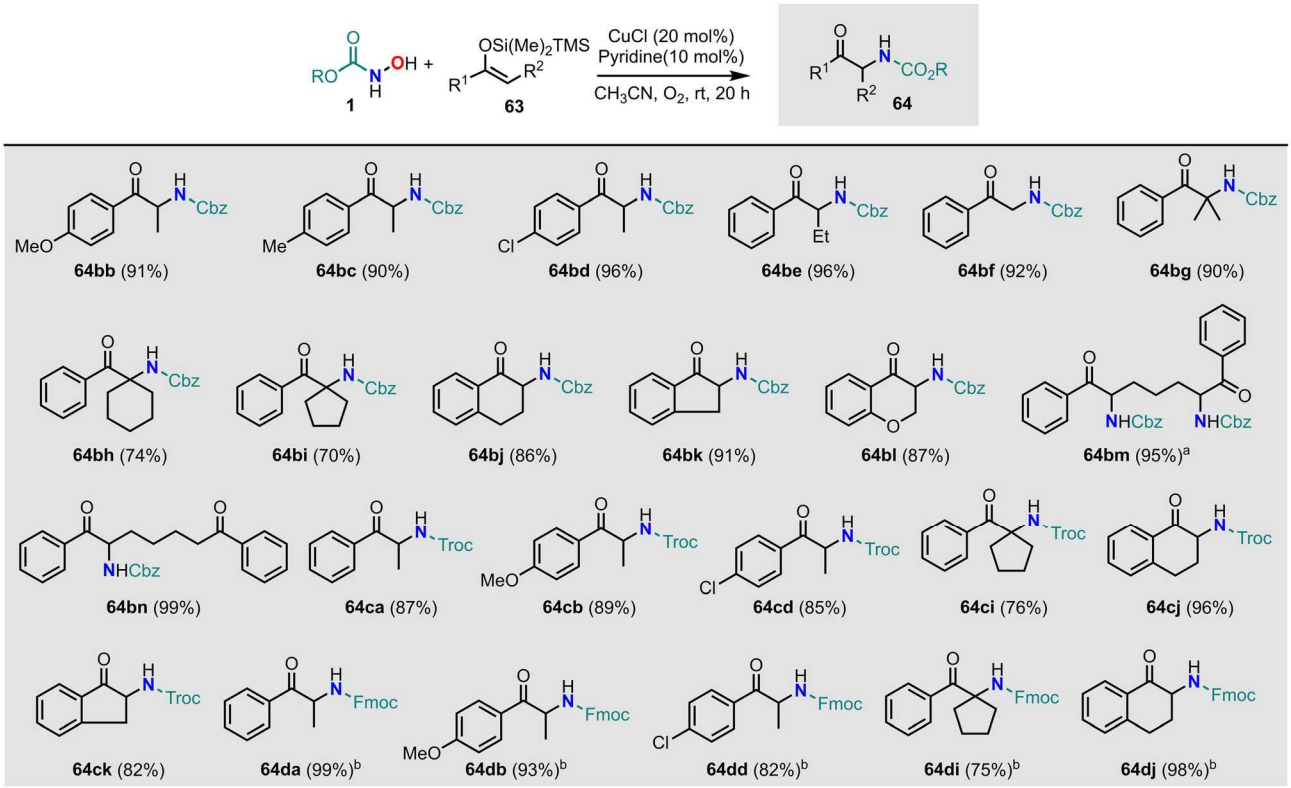

FIGURE 58 | Scope of the products obtained from the Mukaiyama aldol reaction between different cyclic and acyclic silyl enol ethers and various HAs. Reported isolated yields. [a] 36 h of reaction. [b] 1 mL THF was used as cosolvent.

Furthermore, the reaction was not limited to Cbz-protected HAs; it also proceeded efficiently with other easily removable protecting groups such as Troc-NHOH and Fmoc-NHOH. Although the reaction with Boc-NHOH was feasible, it exhibited slower kinetics, likely due to increased steric hindrance.

To demonstrate the practicality of this transformation, the authors scaled up the reaction to the gram scale, achieving the isolation of compound **64ba** in 97% yield.

Additionally, the diastereoselectivity of the process was proved through the reaction of silyl enol ether **63a** with a chiral NOC compound derived from (-)-menthol (**1v**), which yielded the desired product **64va** in 82% yield and with a high diastereomeric ratio of 19:1 (Figure 59).

Published in : ChemSusChem (2025), e202501565
DOI: 10.1002/cssc.202501565
Status : Postprint (Author's version)

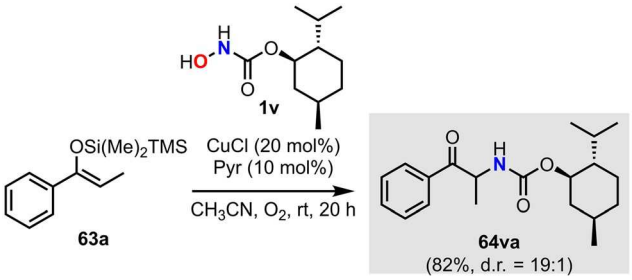

FIGURE 59 | Diastereoselective Mukaiyama aldol reaction between **63a** and a (-)-menthol derived chiral NOC compound **1v**.

To further validate the proposed mechanism involving N–O bond cleavage, the reaction was tested with TMS- and TBS-substituted silyl enol ethers under the optimized conditions. While excellent *N*-selectivity was observed in both cases, with yields ranging from 59% to 91%, N–O bond cleavage did not occur (Figure 60). This result suggests the inability of these intermediates to undergo the necessary rearrangement via a six-membered cyclic transition state. These facts highlight the essential role of the disilane backbone in facilitating the NOC aldol cascade [92].

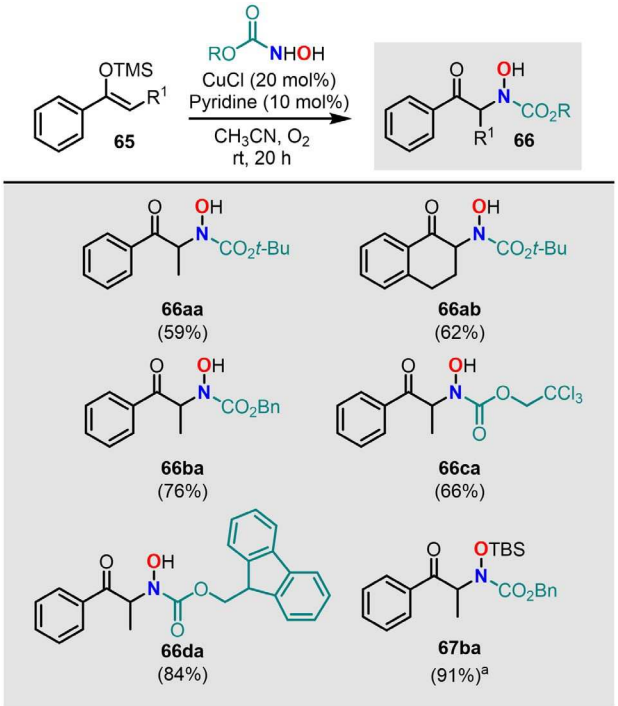

FIGURE 60 | Scope obtained from the Mukaiyama aldol reaction between TMS-substituted silyl enol ethers and various HAs. Isolated yields. [a] Reaction conducted with the TBS-substituted silyl enol ether.

For the asymmetric formation of C⁻N bonds via NOC aldol reactions, two principal strategies are conceivable. The first involves the use of activated nucleophiles, such as β-ketoesters and aldehydes bearing stereodirecting groups, in combination with known chiral Lewis acids or chiral organocatalysts.

Published in : ChemSusChem (2025), e202501565
DOI: 10.1002/cssc.202501565
Status : Postprint (Author's version)

The second strategy introduces chirality through the NOC intermediate (enophile), thus potentially broadening the scope of asymmetric transformations. This approach enables the use of nonactivated substrates, including ketones and carboxylic acid derivatives, and facilitates highly *N*-selective NOC hetero-ene reactions: an advantage over traditional aldol-type processes, which often struggle with competing *O*- versus *N*-regioselectivity.

The latter approach was pioneered by the de Alaniz group, who investigated asymmetric α-amination using a TMS-enol ether derived from cyclohexanone (**68a**) and a HA derived from Oppolzer's sultam (**1w**) as model substrates (Table 23) [93]. Under aerobic conditions, using CuCl (10 mol%) as the catalyst and pyridine (10 mol%) as an additive in THF at room temperature, the desired product **69wa** was obtained in 70% yield with a diastereomeric ratio (*dr*) > 95:5 (Table 23, entry 1). The product was isolated and characterized after a hydrolytic workup.

Reducing the catalyst loading to 5 mol% or replacing THF with 1,2-dichloroethane led to lower yields (Table 23, entries 2–3).

TABLE 23 | Conditions optimization for the α-amination of the TMS-enol ether derived from cyclohexanone **68a** with a HA derived from Oppolzer's sultam **1w**.

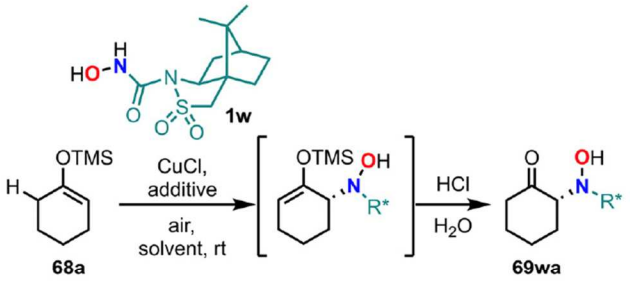

Entry	CuCl (mol%)	Additive[a]	Solvent	Yield (%)[b]	*dr*[b]
1	10	Pyridine	THF	70	>95:5
2	5	Pyridine	THF	65	>95:5
3	5	Pyridine	DCE	57	>95:5
4	5	EtOx	THF	70	>95:5
5	10	EtOx	THF	99	>95:5

[a]Equimolar to CuCl.
[b]Isolated yields and *dr* were calculated by ^{1}H NMR.

However, replacing pyridine with 2-ethyloxazoline (EtOx) significantly improved the reaction outcome (Table 23, entry 4). Under the optimized conditions (CuCl (10 mol%) and EtOx (10 mol%)) the product was obtained in quantitative yield with a *dr* > 95:5 (Table 23, entry 5). Notably, no formation of the competing *O*-regioisomer was detected.

The substrate scope was then explored using various silyl enol ethers in conjunction with HA **1w** (Figure 61). Both cyclic aliphatic *E*-silyl enol ethers and acyclic silyl enol ethers, regardless of *E/Z* geometry,

Published in : ChemSusChem (2025), e202501565
DOI: 10.1002/cssc.202501565
Status : Postprint (Author's version)

performed well in terms of yield and diastereoselectivity. Interestingly, for acyclic silyl enol ethers, the reactions led to mixtures enriched in the same major diastereomer irrespective of the starting geometry (*E* or *Z*). This phenomenon was exemplified in reactions involving silyl enol ethers derived from 3-pentanone.

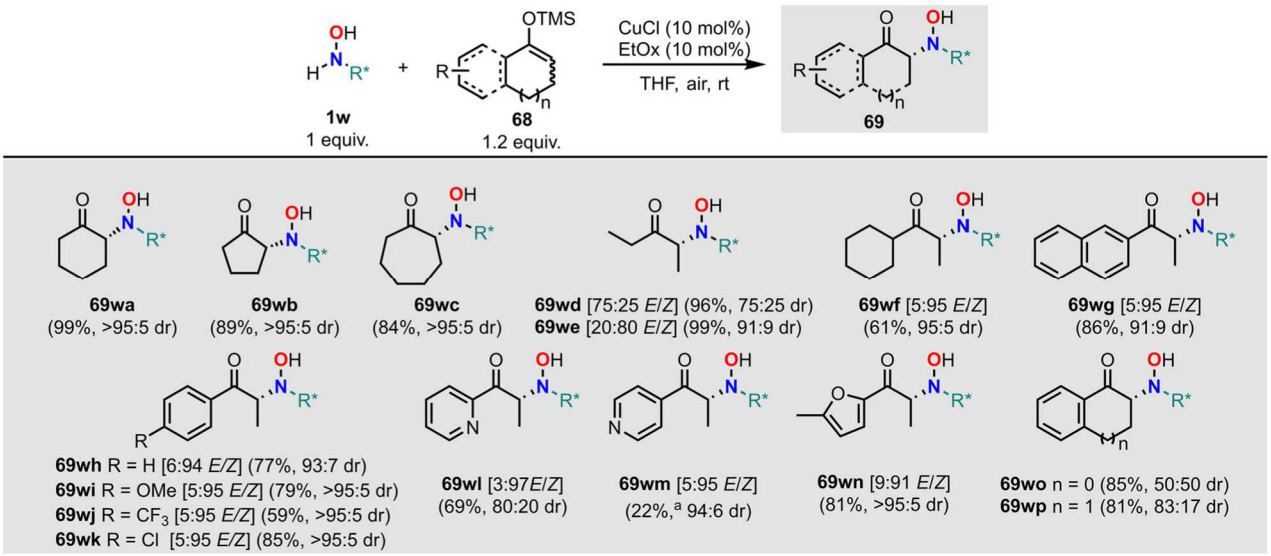

FIGURE 61 | Scope of the products obtained from the asymmetric NOC ene reaction between different silyl enol ethers and HA **1b**. The *dr* were calculated by ^{1}H NMR. [a] Lower yield due to product instability.

The methodology was further extended to include heteroaromatic silyl enol ethers (**69wl**-**69wn**) and cyclic aromatic *E*-silyl enol ethers (**69wo**-**69wp**), all delivering satisfactory results. Encouraged by these findings, the mild reaction conditions were also applied to silyl ketene thioacetals (Figure 62), thereby enabling the synthesis of non-natural amino acids and their hydroxylamino analogs, including D-Ala, D-Leu, D-Trp, D-Phe, and D-Val, with high diastereoselectivities.

Published in : ChemSusChem (2025), e202501565
DOI: 10.1002/cssc.202501565
Status : Postprint (Author's version)

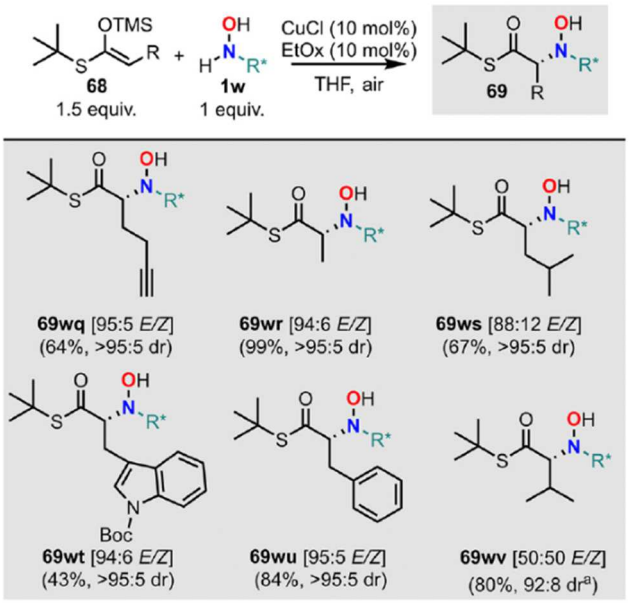

FIGURE 62 | Scope obtained from the asymmetric NOC ene reaction between silyl ketene thioacetals and HA **1w**. The *dr* were calculated by ^{1}H NMR. [a] 2 equivalents of the silyl ketene thioacetal were used.

A predictive model for the asymmetric NOC ene reaction was then developed. In reactions involving silyl enol ethers, the process follows enophilic regioselectivity at the *twix* position (Figure 63, top square for *twix*, *twin*, and *lone* position reference). For *E*-enolate substrates containing allylic hydrogens (68wa68wd), *twix* selectivity is achieved via the prototropic pathway. This is due to the NOC adopting a *Re*-face skewed approach toward the nucleophile, which minimizes steric interactions (path a, Figure 63). In contrast, for *Z*-enolate substrates (68we-68wf), the *twix* position corresponds to the oxygen atom bearing the TMS group, favoring the silatropic pathway (path b, Figure 63).

Similarly, substrates lacking allylic hydrogens (**68wg**-**68wv**) preferentially undergo the *twix*-selective silatropic pathway (path c, Figure 63). In these cases, the NOC maintains the same *Re*-face skew trajectory to minimize steric hindrance, resulting in products with consistent absolute stereochemistry.

The relatively lower diastereoselectivities observed for **68wo** and **68wp** are attributed to increased steric interactions of the *twin*-selective silatropic pathway, where the NOC approaches the nucleophile with reduced facial bias (path d, Figure 63) [93].

Published in : ChemSusChem (2025), e202501565
DOI: 10.1002/cssc.202501565
Status : Postprint (Author's version)

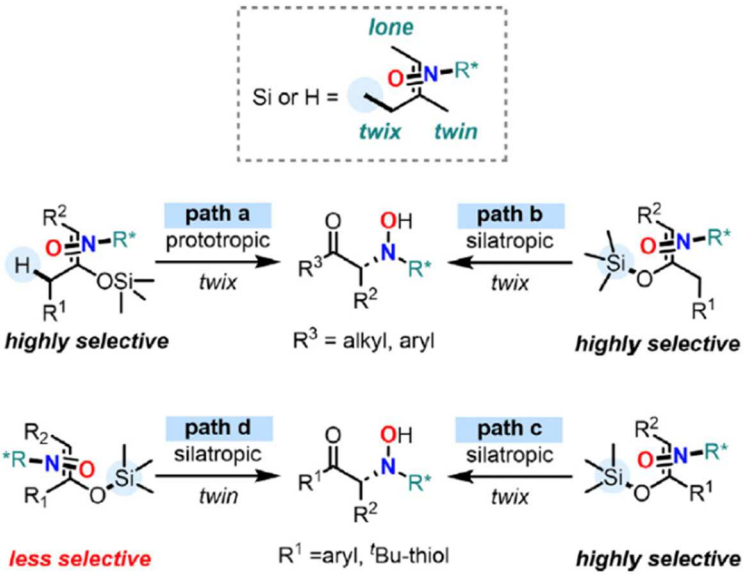

FIGURE 63 | Mechanism and predictive model for the asymmetric NOC ene reaction.

To demonstrate the practical utility of this methodology and the dispensability of the auxiliary, selected products were subjected to post-functionalization (Figure 64). For example, the diastereoselective reduction of **69wa** with sodium borohydride afforded the chiral oxazolidinone **70**. Such functional groups are widely used as ligands in asymmetric catalysis and are frequently found in bioactive molecules [93].

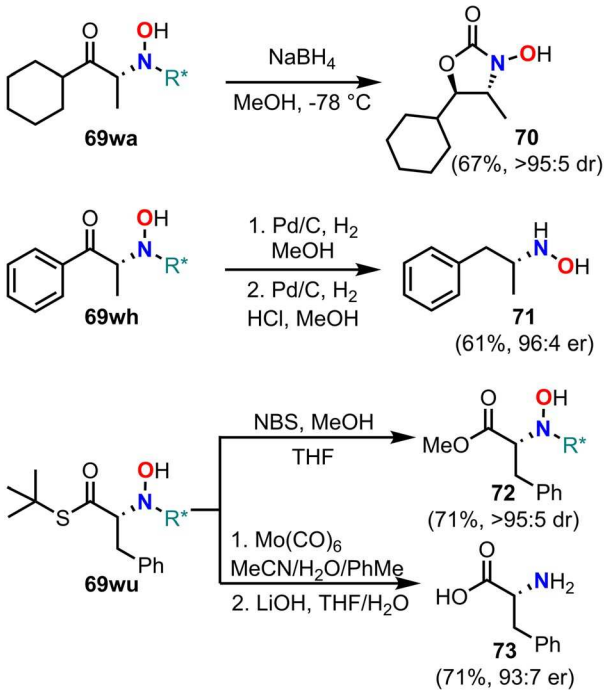

FIGURE 64 | Transformations of the obtained α-amino carbonyls.

Published in : ChemSusChem (2025), e202501565
DOI: 10.1002/cssc.202501565
Status : Postprint (Author's version)

The use of chiral NOCs in asymmetric synthesis was further exemplified in hDA reactions. Building on the foundational work by Read de Alaniz [29], Kan and coworkers reported the preparation of a key intermediate for the total synthesis of the antibiotic Pactamycin (Figure 65) [94]. This was achieved through a regio- and face-selective hDA reaction between acylnitroso compound **1w** (bearing a camphorsultam chiral auxiliary) and chiral cyclopentadiene **74** (Figure 65). This reaction was critical for the installation of the correct stereocenters in the final product and enabled an improved yield of key intermediate **76**, increasing from 10% to 20% [94, 95].

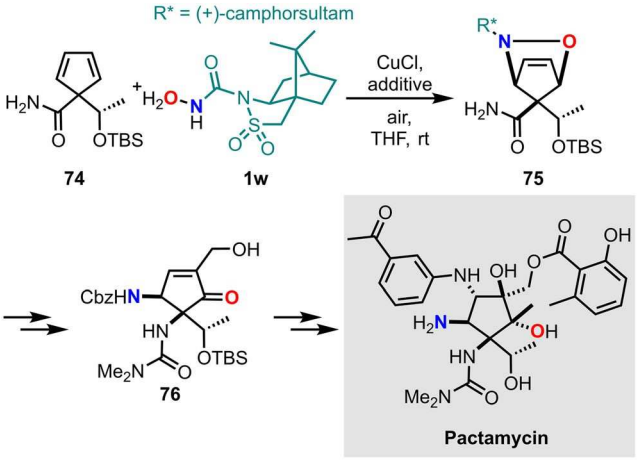

FIGURE 65 |Preparation of key intermediate **76** for the synthesis of Pactamycin.

Notably, product **75** was obtained as the sole diastereomer from the cycloaddition. The high stereoselectivity of the reaction was rationalized and supported by DFT calculations, which involved a systematic search for transition state structures that differentiate the diastereotopic faces of **74** [94]. These insights laid the foundation for subsequent theoretical studies by Liu and Houk on π-facial stereoselectivity in acylnitroso cycloadditions to 5,5-unsymmetrically substituted cyclopentadienes [96].

The synthetic potential of Cu(I)-catalyzed aerobic oxidation of HCs was further demonstrated by Xu and Zhang, who introduced a synergistic Rh/Cu catalytic system (Figure 66) [97]. This system enabled hydroxyamination of aryl C–H bonds using commercially available HC and molecular oxygen as the oxidant at room temperature. Previously, Rh(III) complexes had been shown to be effective catalysts for atom- and step-economical C–C and C–heteroatom bond formation via C–H functionalization [98], using electrophilic partners such as imines [99], aldehydes [100], and isocyanates [101]. Expanding on these works, NOCs compounds were successfully used in Rh(III)-catalyzed C–H bond functionalization, offering a sustainable route to benzo[c]isoxazole derivatives (**78aa**-**78as**, Figure 66): important scaffolds in several bioactive natural products [102].

Published in : ChemSusChem (2025), e202501565
DOI: 10.1002/cssc.202501565
Status : Postprint (Author's version)

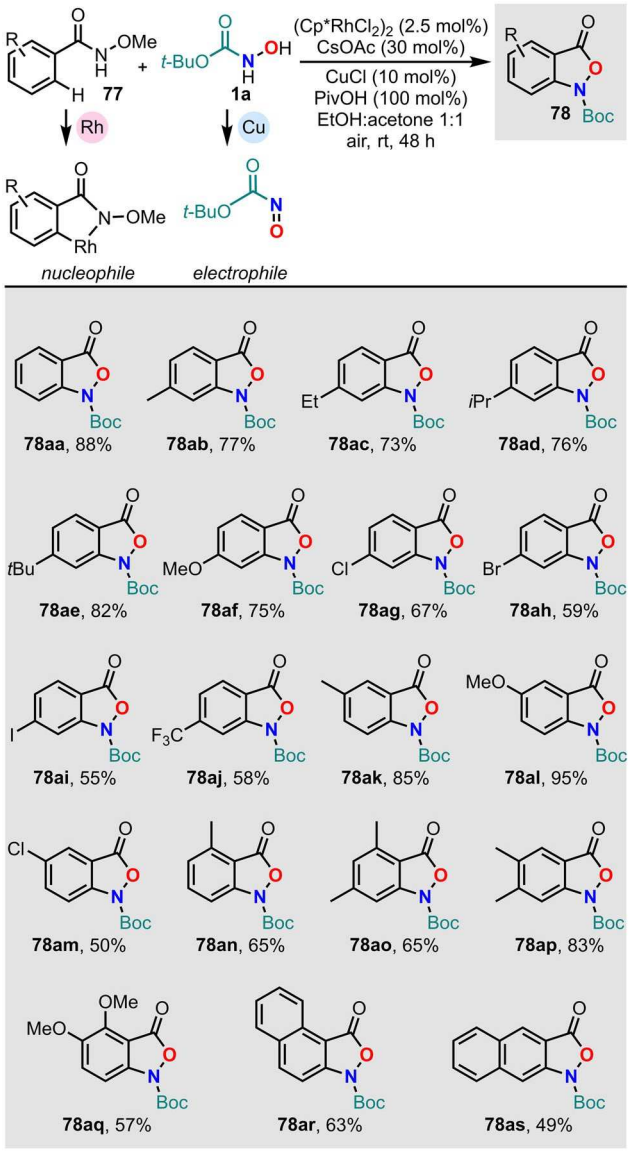

FIGURE 66 | Synthesis of benzo[c]isoxazol-3(1H)-ones. Isolated yields are reported.

Among the Cu(I) salts tested, CuCl proved to be the most effective, with no product formation observed in its absence. Solvent screening identified a 1:1 mixture of ethanol and acetone as optimal. Among the acids evaluated as additives, pivalic acid (PivOH) was as effective as acetic acid. Under these optimized conditions, a broad range of substrates was investigated to explore the reaction scope (Figure 66). The Rh/Cu-catalyzed system efficiently delivered benzo[*c*]-isoxazol-3(1*H*)-ones in good to excellent yields, demonstrating broad functional group tolerance on the aryl moieties of benzamides, including methoxy, chloro, bromo, iodo, and trifluoromethyl groups, regardless of their position (*para*, *meta*, or *ortho*).

The proposed reaction mechanism (Figure 67) begins with the reversible C–H bond cleavage of substrate **77a**, forming a five-membered rhodacycle intermediate **79**. The in situ–generated NOCs

Published in : ChemSusChem (2025), e202501565
DOI: 10.1002/cssc.202501565
Status : Postprint (Author's version)

(from the copper-catalyzed aerobic oxidation of *N*-Bochydroxylamine **1a**) then coordinates with **79** to form intermediate **80**. This species undergoes nucleophilic addition to yield a seven-membered rhodacycle **81**. Subsequent protonolysis leads to the hydroxyamination intermediate **82**, which undergoes a final metal- or acid-catalyzed nucleophilic substitution, affording the final product **78aa** along with the release of *O*-methylhydroxylamine [97].

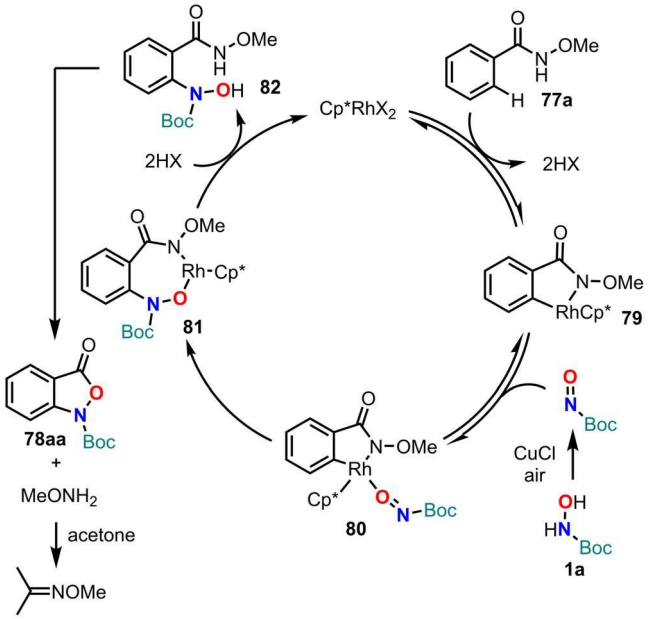

FIGURE 67 | Proposed mechanism for the synergistic Rh/Cu-catalyzed formation of benzo[*c*]-isoxazol-3(1H)-ones.

3.2 | COPPER (II) CATALYSTS

Whiting explored the use of Cu(II) catalysis to oxidize HAs and hydrazides, generating acyl-nitroso and azo dienophiles, respectively [103]. A comprehensive screening of copper(II) salts (including $CuCl_2$, $CuBr_2$, and CuI_2), catalyst loadings, ligand systems (such as tetramethylthiourea, 2-ethyl-2-oxazoline, and various combinations), and solvents led to the identification of optimal conditions: $CuCl_2$ (10 mol%), 2-ethyl-2-oxazoline (20 mol%), methanol as solvent, at room temperature under an air atmosphere (Figure 68).

Published in : ChemSusChem (2025), e202501565
DOI: 10.1002/cssc.202501565
Status : Postprint (Author's version)

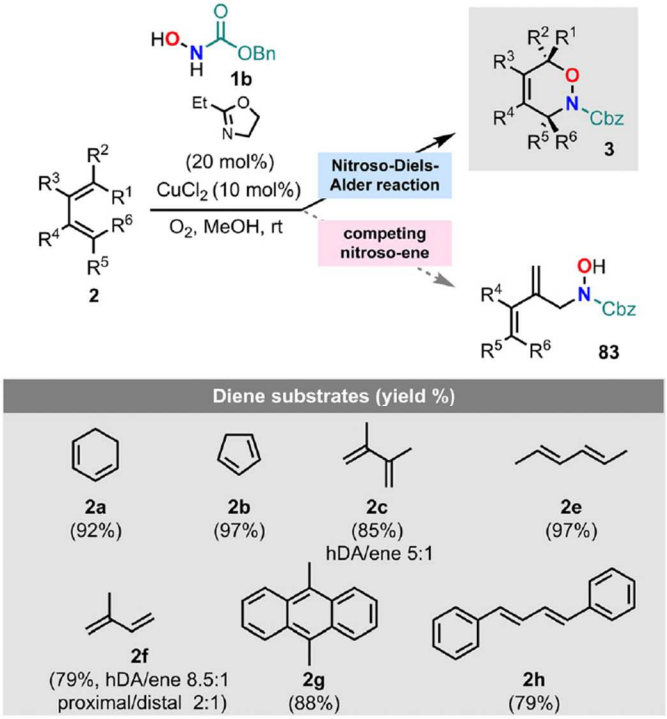

FIGURE 68 | Intermolecular hDA reaction between HCs and different dienes catalyzed by $CuCl_2$ with 2-ethyl-2-oxazoline ligand in aerobic conditions.

A wide range of dienes was used as trapping agents for the in situ generated NOCs, affording excellent yields via intermolecular hDA reactions (Figure 68). Although chemoselectivity was not perfect, dienes prone to competing ene reactions still provided high overall yields, with the [4 + 2] cycloaddition pathway remaining predominant. A solvent effect was observed, although the mechanistic pathway remained unclear. Methanol was ultimately selected as the most favorable solvent based on both the reaction rate and the ratio of Diels–Alder to ene adducts.

The methodology was successfully extended to intramolecular hDA reactions and to acyl hydrazide substrates (Figure 69) [103].

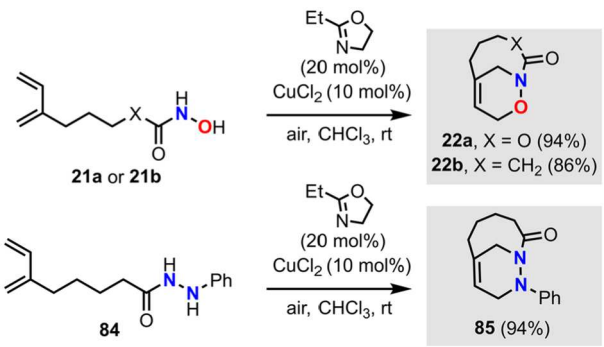

FIGURE 69 | Intramolecular hDA reaction between HCs or hydrazides and dienes catalyzed by $CuCl_2$ with 2-ethyl-2-oxazoline ligand in aerobic conditions.

Published in : ChemSusChem (2025), e202501565
DOI: 10.1002/cssc.202501565
Status : Postprint (Author's version)

To gain deeper insight into the reactivity of the acylnitroso species, the authors conducted both experimental and theoretical investigations [104]. A small library of HAs was reacted with cyclohexa-1,3-diene or 2,3-dimethylbuta-1,3-diene under three different conditions: (a) a reference reaction using $NaIO_4$ as oxidant, (b) aerobic oxidation using $CuCl_2$ (10 mol%) and 2-ethyl-2oxazoline (20 mol%) in methanol at room temperature, and (c) aerobic oxidation under refluxing toluene to promote nitroso species formation.

Under the first set of conditions (a), all 20 expected products were obtained after 4 h (Figure 70). In contrast, under Cu(II)-catalyzed aerobic oxidation, only six HAs yielded cycloadducts. However, the yields obtained under conditions (b) with copper catalysis (90%–99% (Figure 70)) were substantially higher than those observed with $NaIO_4$ (13%–51%). Ene adducts **83sc** and **83xc** were observed from the copper-catalyzed oxidation of HAs **1s** and **1x** with 2,3-dimethyl-1,3-butadiene, with hDA/ene product ratios of 9:1 and 6:1, respectively. This suggests a higher selectivity of the NOC derived from **1x** compared to that from **1s**. The fact that ene products were not observed under other conditions indicates a role for copper in enabling this competing pathway.

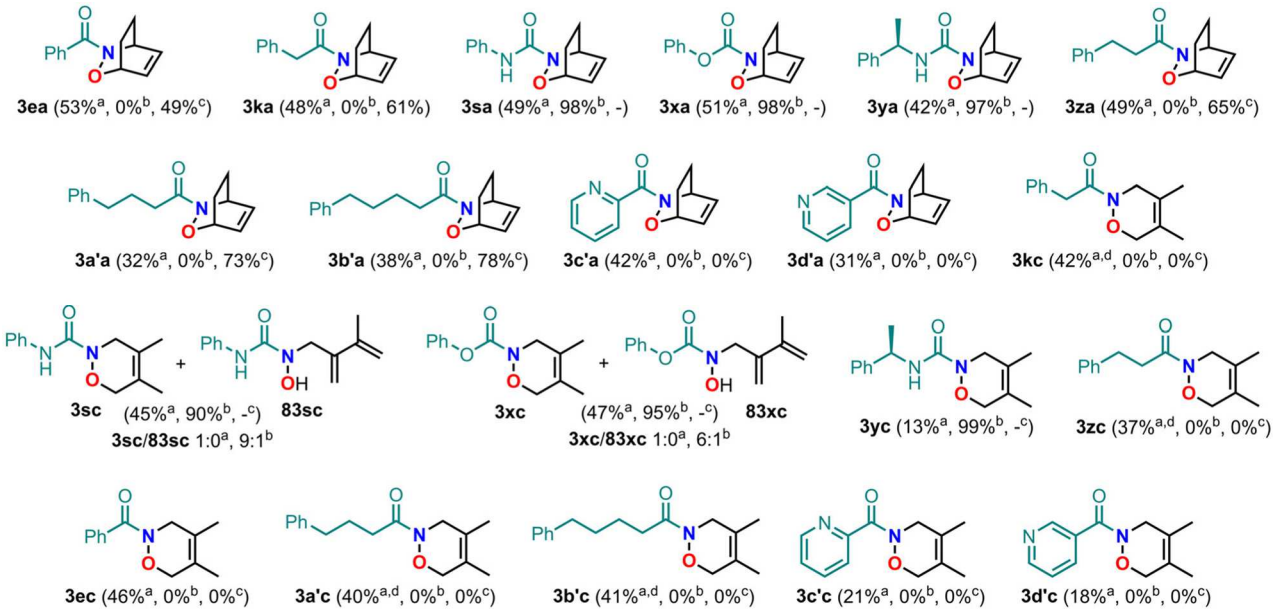

FIGURE 70 | Products obtained from the hDA reaction between HAs and cyclohexa-1,3-diene or 2,3-dimethylbuta-1,3-diene using three different procedures (a,b, and c). The reported yields are the isolated yields. [a] HA (0.83 mmol), diene (2 equiv.), $NaIO_4$ (0.83 mmol), MeOH, rt, 2–4 h; [b] HA (0.63 mmol), diene (2 equiv.), $CuCl_2$ (0.06 mmol), 2-ethyl-2-oxazoline (0.12 mmol), MeOH, rt, 2–6 h; [c] HA (1.4 mmol), diene (2 equiv.), $CuCl_2$ (0.14 mmol), 2- ethyl-2-oxazoline (0.28 mmol), toluene, heated under reflux, 4–20 h.

Interestingly, the chiral HA **1y** did not produce ene products under the same copper-catalyzed conditions. Instead, it afforded cycloadducts **3ya** and **3yc**. This discrepancy may be attributed to the presence of multiple reactive conformations of **1y**, with no single dominant geometry capable of enforcing facial selectivity.

Published in : ChemSusChem (2025), e202501565
DOI: 10.1002/cssc.202501565
Status : Postprint (Author's version)

Under the high-temperature conditions of method (c), cycloadducts formed readily from 1,3-cyclohexadiene, but not from 2,3-dimethylbutadiene, suggesting that the cyclic diene is better suited to these conditions. No cycloadducts were obtained from HAs containing pyridyl substituents, likely due to chelation of the pyridyl or amine group to the copper catalyst, which inhibits the oxidation step. These observations indicate that the Cu(II) system is only effective for HAs containing a heteroatom linker between the aryl and carbonyl groups.

Among the tested substrates, phenyl HC and 1-hydroxy-3phenylurea yielded cycloadducts in high yields with both 1,3-cyclohexadiene and 2,3-dimethyl-1,3-butadiene under room temperature copper catalysis. These promising results prompted further exploration of six additional dienes (Figure 71), with generally high product yields. One exception was the adduct **3sg**, derived from dimethylanthracene, which may undergo retrocycloaddition (cycloreversion).

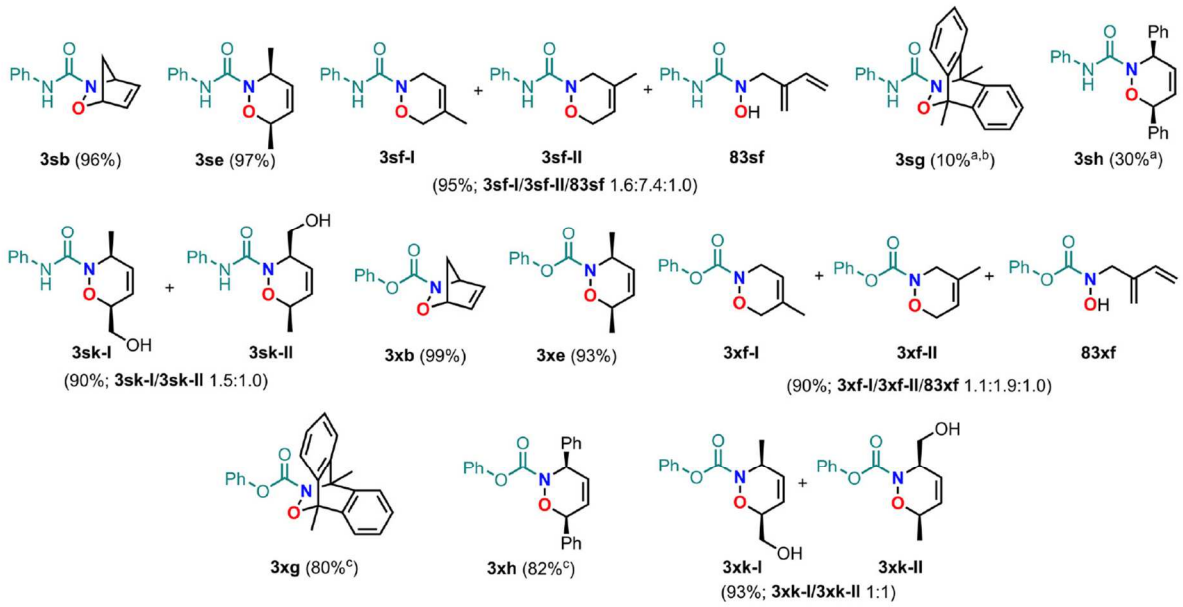

FIGURE 71 | Scope of the products obtained from the hDA reaction between phenyl HC or 1-hydroxy-3-phenylurea and various dienes using the copper-oxazoline/air catalytic system in methanol. The procedure is the same as in Figure 70. The reported yields are the isolated yields. [a] After 48 h. [b] Yield not accurate due to cycloreversion of the cycloadduct. [c] After 24 h.

To rationalize the experimental observations, DFT calculations (B3LYP/6-31G* level of theory, gas phase) were performed to analyze the conformations and chemoselectivity of the hDA cycloadducts. Energetic comparisons of conformers A-D (Figure 72), along with rotational energy barriers between the *anti* and *syn* forms (A and B), helped explain the presence of multiple conformers detected in the ^{1}H NMR spectra of several products.

Published in : ChemSusChem (2025), e202501565
DOI: 10.1002/cssc.202501565
Status : Postprint (Author's version)

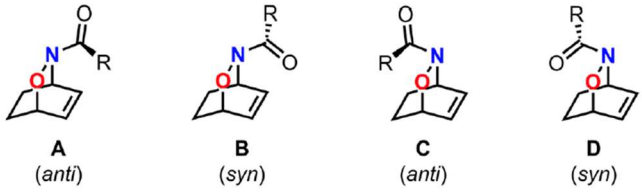

FIGURE 72 | Conformers **A-D** for hDA cycloadducts.

Theoretical investigations revealed three key conclusions:

1. The hDA pathway is favored over the ene pathway. *Endo* transition states are energetically preferred compared to *exo* and ene transition states. For reactions involving 2,3-dimethylbutadiene or 2-methylbutadiene, ene transition states exhibit significantly higher activation barriers. The observed ene products in the copper-catalyzed reactions suggest that the copper complex may enable these otherwise disfavored pathways.

2. For cyclic dienes, the computed activation parameters for the hDA reaction ($\Delta G^{\neq}$ = 2.4⁻2.8 kcal·mol^{-1}) and the computed reaction parameters ($\Delta G^{\#}$ = 30 kcal·mol^{-1}) indicated that the hDA process was both kinetically and thermodynamically favored.

3. For acyclic dienes, the energy barrier for isomerization from the *s-trans* to the reactive s-cis conformation is generally higher than the hDA transition-state energy. This explains the slowness of reactions with substrates like 1,4diphenylbutadiene. In cases involving highly reactive acylnitroso intermediates, the slow conformational interconversion of the diene can lead to competition between productive hDA cycloaddition and decomposition of the NOC, resulting in variable yields.

In a subsequent study, Read de Alaniz and collaborators demonstrated that the α-amination of α-alkyl-β-ketoesters could be achieved under mild conditions by using highly reactive nitrosoformate intermediates as the electrophilic nitrogen source (Figure 73) [55]. They developed a straightforward protocol enabling the simultaneous enolization of β-ketoesters and the aerobic oxidation of N-substituted hydroxylamines, thereby generating enolate equivalents and NOCs, respectively [55].

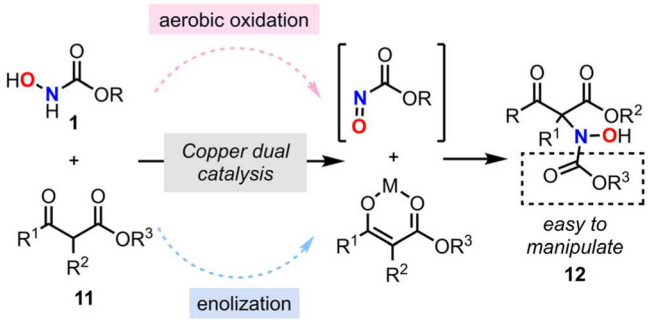

FIGURE 73 | α-amination of carbonyl compounds via *N*-selective nitrosoformate aldol reaction.

Published in : ChemSusChem (2025), e202501565
DOI: 10.1002/cssc.202501565
Status : Postprint (Author's version)

Reaction conditions were optimized using ethyl β-ketoester **11a** and Cbz-*N*-hydroxylamine **1b** as model substrates. Under optimized conditions, the desired product **12ba** was obtained in 86% yield with a 3:1 *N/O* selectivity ratio, using CuCl/$Cu(OTf)_2$ as catalysts (10 mol% each), and pyridine as an additive in THF (Table 24, entry 1). Replacing THF with MeOH significantly improved *N*-selectivity to 11:1 (Table 24, entry 2), and the removal of pyridine further increased it to 14:1 (Table 24, entry 3). In contrast, the use of polar solvents other than MeOH or the omission of either CuCl or $Cu(OTf)_2$ resulted in diminished efficiency and/or selectivity (Table 24, entries 4–7). The optimal conditions were thus identified as 5 mol% each of CuCl and $Cu(OTf)_2$ in MeOH at room temperature. The catalytic system's chelating Lewis acid properties were crucial for dual activation of the nitrosoformate electrophile and the β-ketoester nucleophile, enabling efficient α-amination.

TABLE 24 | Optimization of the conditions for the *α*-amination of ethyl *β*-keto ester using Cbz-*N*-hydroxylamine.

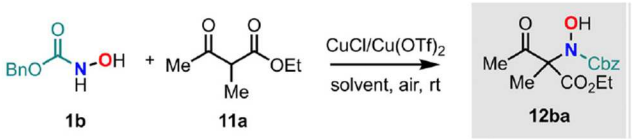

Entry	CuCl/$Cu(OTf)_2$ (mol%:mol%)	Additive (mol%)	Solvent	Yield (%)[a]	N/O ratio[b]
1	10:10	Pyridine (1.25)	THF	86	3:1
2	10:10	Pyridine (1.25)	MeOH	91	11:1
3	10:10	None	MeOH	94	14:1
4	10:10	None	EtOH	90	4:1
5	10:10	None	*i*PrOH	80	2:1
6	10:0	None	MeOH	94	9:1
7	0:10	None	MeOH	74	14:1
8	5:5	None	MeOH	97	14:1

[a]Isolated yields of the *N*- and *O*-products mixture.
[b]Determined by ^{1}H NMR.

With optimized conditions in hand, the scope of the reaction was extended to a diverse library of β-ketoesters and hydroxylamines (Figure 74).

Published in : ChemSusChem (2025), e202501565
DOI: 10.1002/cssc.202501565
Status : Postprint (Author's version)

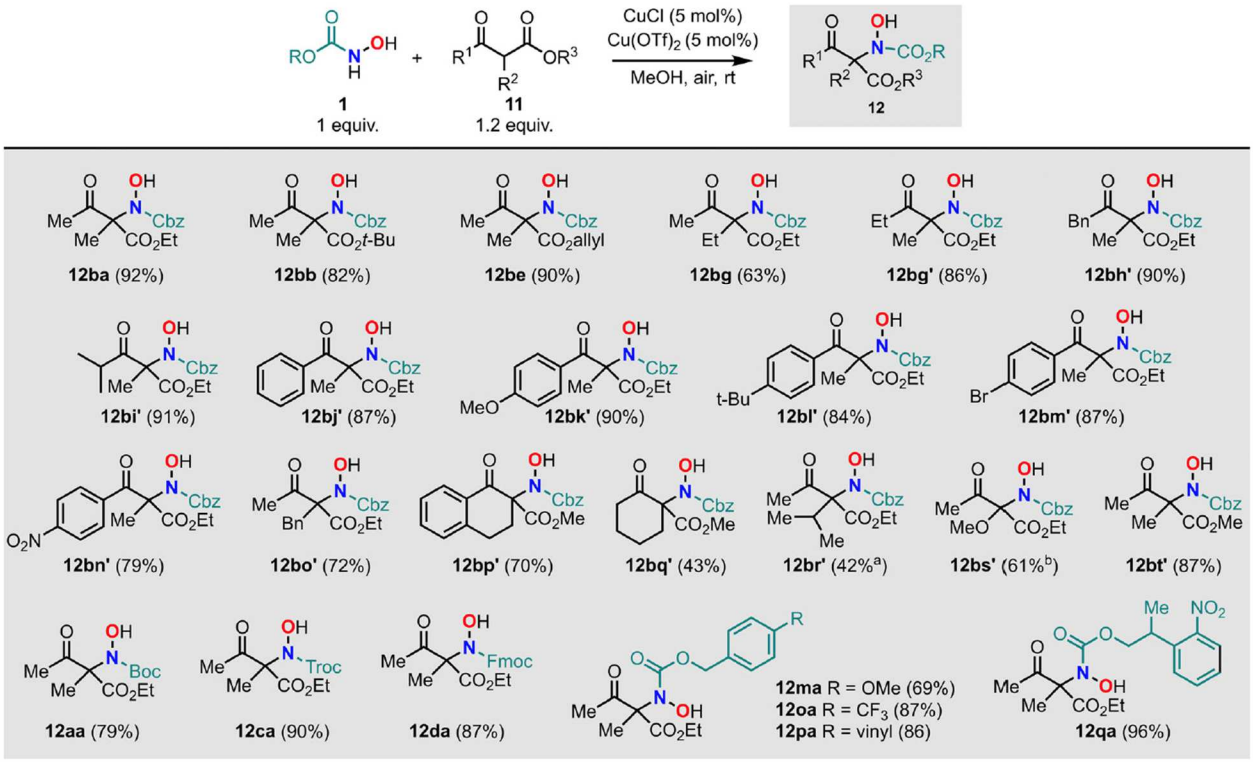

FIGURE 74 | Scope of the products obtained from the *α*-amination of different *β*-ketoesters using various hydroxylamines. The reported yields are the isolated yields of the N-regioisomer. [a] Reaction conducted with 20 mol% of each catalyst. [b] Unsubstituted *β*-ketoester (R^2=H) was used as starting reagent.

β-Ketoesters bearing alkyl, benzyl, or aryl substituents at R^1 consistently afforded the hydroxyamination products in excellent yields. The electronic properties of aryl substituents at R^1 had negligible impact on the reaction outcome (**12bj'**-**12bn'**). At the α-position (R^2), variations in steric bulk were tolerated to a degree (**12bg**, **12bo'**-**12bs'**), although increased steric hindrance led to slower reaction rates and reduced *N*-selectivity (**12bp'**-**12br'**). For example, cyclic β-ketoesters yielded products **12bp'** and **12pq'** in lower yields, with a significant increase in the formation of the *O*-regioisomer, which constituted 25% and 40% of the product mixture, respectively. Interestingly, when using an unsubstituted carbonyl compound (R^2 = H), the reaction unexpectedly proceeded via N–O bond heterolysis, yielding an α-imino β-ketoester intermediate that was trapped by methanol to form product **12bs'**.

Similar to the β-ketoester scope, the method also tolerated a broad range of *N*-substituents on hydroxylamines. Substrates bearing orthogonal protecting groups such as Cbz, Boc, Fmoc, Troc, and Nppoc delivered products in yields exceeding 79%. In all cases, minor amounts of the *O*-selective adduct were observed but could be separated via column chromatography. This transformation, feeding upon the high *N*-electrophilic nature of nitrosoformate intermediates as, is synthetically valuable for the synthesis of α-amino acid derivatives. To demonstrate the versatility of the α-amination products, further functionalization was performed, including deprotection of the amino group, N–N bond cleavage, and formation of *N*-oxazolidinones (Figure 75) [55, 105].

Published in : ChemSusChem (2025), e202501565
DOI: 10.1002/cssc.202501565
Status : Postprint (Author's version)

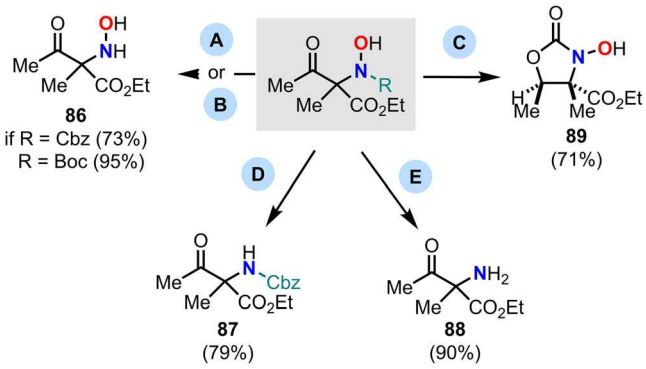

FIGURE 75 | Further transformations of the α-amination adducts. Conditions: A (R = Cbz): Pd/C, MeOH, H2; B (R= Boc): TFA, CH2Cl2; C (R= Cbz): Zn, HCl, reflux; D (R = Cbz): 1. Zn, HCl, reflux 2. Pd/C, H2; E (R= Troc): NaBH4, MeOH.

Building on their research into copper-catalyzed *N*-selective nitroso-aldol reactions, Read de Alaniz's group next investigated the possibility of reversing the *N/O* regioselectivity, directing the reaction instead toward *O*-selectivity (Figure 76) [106].

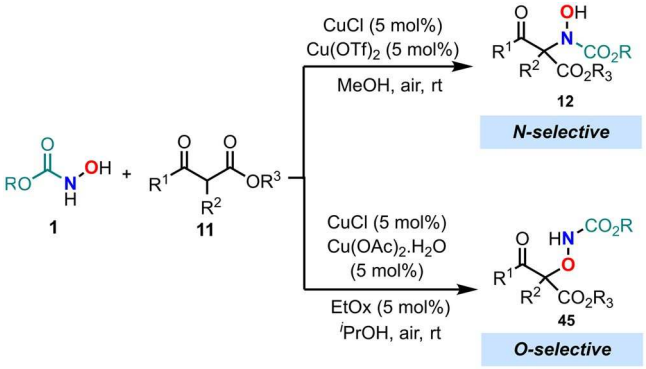

FIGURE 76 | Regioselectivity control on the NOC aldol reaction.

In their previously studied reaction between β-ketoester **11a** and *N*-Boc-hydroxylamine **1a**, the use of CuCl and Cu(OTf)$_2$ (each at 5 mol%) under aerobic conditions in methanol afforded a mixture of *O*- and *N*-regioisomers in 96% overall yield, with an *O/N* ratio of 1:4 (Table 25, entry 1). Substituting MeOH with more sterically hindered alcohols such as ethanol and isopropanol progressively improved *O*-selectivity, yielding *O/N* ratios of 1:1 and 2:1, respectively (Table 25, entries 2–3). Further enhancement in *O*-selectivity was achieved by replacing $Cu(OTf)_2$ with either $CuCl_2$ or $Cu(OAc)_2{\cdot}H_2O$ as the Cu(II) source, increasing the *O/N* ratio to 3:1 without compromising the overall yield (Table 25, entries 4–5).

The introduction of 2-ethyl-2-oxazoline (EtOx) as a ligand (5 mol%) in conjunction with $Cu(OAc)_2{\cdot}H_2O$ led to a marked increase in *O*-selectivity. Under these conditions, the reaction proceeded with a high yield of 94% and an *O/N* ratio of 10:1 (Table 25, entry 8). Notably, omission of the Cu(I) catalyst resulted in a very slow reaction (Table 25, entry 9), while the removal of the Cu(II) catalyst led to decreased

Published in : ChemSusChem (2025), e202501565
DOI: 10.1002/cssc.202501565
Status : Postprint (Author's version)

yield and selectivity (Table 25, entry 10). These observations support a dual catalytic mechanism, wherein both Cu(I) and Cu(II) species are essential for efficient and selective transformation.

TABLE 25 | Optimization of the conditions using the aerobic Cu-catalyzed aminooxylation of *β*-ketoester **1** using *N*-Boc-hydroxylamine **2** as model reaction.

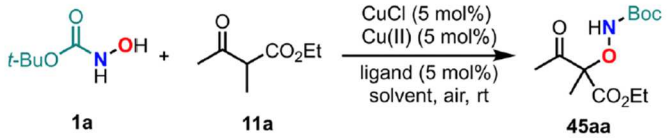

1a 11a 45aa

Entry	Cu(II) catalyst	Solvent	Yield (%)[a]	*O/N* ratio[a]	Entry
1[b]	$Cu(OTf)_2$	MeOH	96	1:4	1[b]
2[b]	$Cu(OTf)_2$	EtOH	82	1:1	2[b]
3[b]	$Cu(OTf)_2$	*i*PrOH	83	2:1	3[b]
4[b]	$CuCl_2$	*i*PrOH	90	3:1	4[b]
5[b]	$Cu(OAc)_2.H_2O$	*i*PrOH	97	3:1	5[b]
6[c]	$Cu(OTf)_2$	*i*PrOH	93	1.5:1	6[c]
7[c]	$CuCl_2$	*i*PrOH	75	6:1	7[c]
8[c]	$Cu(OAc)_2.H_2O$	*i*PrOH	94	10:1	8[c]
9[c,d]	$Cu(OAc)_2.H_2O$	*i*PrOH	90	20:1	9[c,d]
10[c]	None	*i*PrOH	53	5:1	10[c]

[a]Isolated yields of the *O*- and *N*-products mixture and the *O/N* ratios were determined by ^{1}H NMR.
[b]No EtOx ligand.
[c]EtOx as ligand.
[d]No CuCl.

With optimal conditions established for the *O*-selective NOC aldol reaction, the scope of the methodology was evaluated using a series of acyclic and cyclic β-ketoesters. The resulting aminooxylation products were obtained in excellent yields ranging from 57% to 97%, with *O/N* ratios spanning from 2:1 to greater than 20:1 (Figure 77).

Published in : ChemSusChem (2025), e202501565
DOI: 10.1002/cssc.202501565
Status : Postprint (Author's version)

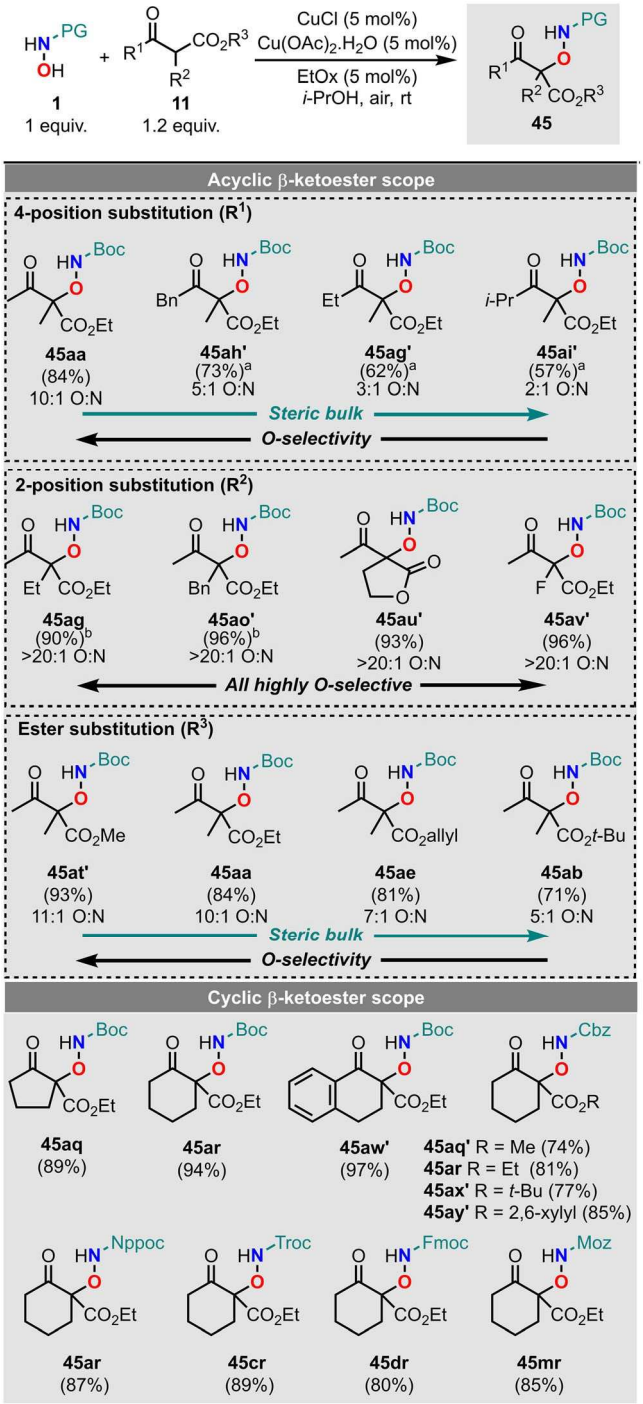

FIGURE 77 | Acyclic and cyclic β-ketoesters scope of the coppercatalyzed *O*-nitrosocarbonyl aldol reaction.

Regioselectivity was observed to decrease with increasing steric hindrance at the R^1 position of the β-ketoester, whereas the opposite trend was noted for R^2 substitution. This was exemplified by the complete *O*-selectivity observed for products **45ag**, **45ao'**, **45au'**, and **45av'**. In contrast, increasing steric bulk at the R^3 position negatively impacted regioselectivity, as reflected in the product distributions of **45aa**, **45ab**, **45ae**, and **45at'**.

Published in : ChemSusChem (2025), e202501565
DOI: 10.1002/cssc.202501565
Status : Postprint (Author's version)

Reactions involving cyclic β-ketoesters with 5- and 6-membered rings, in combination with various HCs bearing protecting groups such as Cbz, Fmoc, Troc, Nppoc, and Moz, consistently afforded high yields of the *O*-regioisomer. These results highlight the broad substrate compatibility of this transformation. Asymmetric induction was achieved by replacing EtOx with (R, R)-PhBox as the ligand (Figure 78). Notably, steric effects also influenced enantioselectivity: bulkier ester substituents at the R^3 position led to increased levels of enantioinduction.

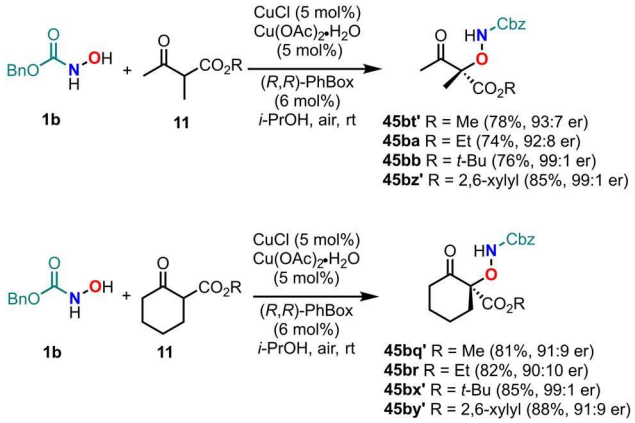

FIGURE 78 | Asymmetric copper-catalyzed *O*-nitrosocarbonyl aldol reaction.

The ambivalent reactivity of the NOC species in the aldol reaction was found to be strongly influenced by both steric and electronic properties of the Cu(II) Lewis acid catalyst. Weakly coordinating counterions, such as OTf^- and BF_4^-, promoted nonselective outcomes, whereas strongly associating counterions, including CO_3^{2-} and AcO^-, favored *O*-selectivity. Furthermore, the *O/N* ratio could be tuned by varying the amount of EtOx ligand, with complete *O*-selectivity achieved at 40 mol% EtOx [106].

A tentative mechanistic proposal suggests that the nitrosoformate species approaches the catalyst/β-ketoester complex via a square-pyramidal or octahedral geometry, with the counterion occupying an axial position. This spatial arrangement is proposed to block coordination of the nitroso species to the Lewis acid, thereby directing the electrophilic attack toward the β-ketoester (Figure 79). The observed preference for *O*-selectivity is attributed to the minimization of steric clashes between the protecting group of the nitroso compound and the metal-bound β-ketoester complex. This mechanistic rationale also supports the use of *N*-Boc-protected hydroxylamines to promote *O*-selective pathways and explains the influence of steric hindrance at the R1 and R3 positions on the regiochemical outcome [106].

Published in : ChemSusChem (2025), e202501565
DOI: 10.1002/cssc.202501565
Status : Postprint (Author's version)

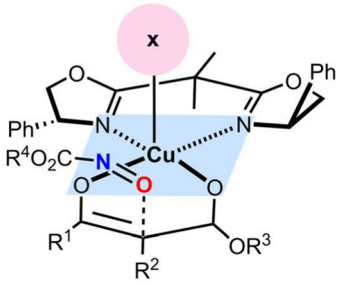

FIGURE 79 | Proposed model for the *O*-nitrosocarbonyl aldol reaction. X = counterion.

Building on the work of Read de Alaniz [106], Maji and Yamamoto reported the asymmetric synthesis of tertiary α-hydroxy phosphonic acid derivatives under aerobic oxidation conditions [107]. These compounds are of considerable interest as they serve as bioisosteric and isopolar analogs of natural motifs, mimicking α-hydroxy carboxylic acids and metabolically relevant phosphate esters [108, 109].

The oxidative coupling of β-ketophosphonate **90a** with N-Boc hydroxylamine (**1a**) was accomplished using $Cu(OTf)_2$ (10 mol%), PhBox (12 mol%), CuCl (10 mol%), and atmospheric air (1 atm) as the terminal oxidant (Figure 80). The reaction furnished the α-oxidation product **91aa** in 94% yield with 97% ee after 12 h, displaying complete *O*-selectivity. Both Cu(I) and Cu(II) catalysts were found to be essential, as the omission of either led to significantly reduced yields and prolonged reaction times. Slight improvements were observed under similar conditions using dry air or an O_2 atmosphere (1 atm), affording 97% yield and 97% *ee*. This performance is comparable to previous oxidative conditions using MnO_2, which required an excess (~5 equiv.) of the oxidant [36].

The substrate scope was systematically explored (Figure 80), demonstrating that a wide variety of cyclic and acyclic β-ketophosphonates could undergo this transformation to yield α-aminoxy phosphonates in high yields and with excellent enantioselectivities. Substitutions at the R^1 position of acyclic β-ketophosphonates **90g-90j**, including both alkyl and aryl groups, were well tolerated. However, substitution at the R^2 position proved more sensitive with β-ketophosphonate **90l**, containing a propargyl group at R^2, that failed to generate the desired product **90al**. The reaction also proved compatible with other *N*-protected HAs, delivering *O*-nitroso-aldol products **91bh**, **91e′h**, and **91e′d** in yields ranging from 70% to 88% and with excellent enantioselectivities (98% to >99% *ee*). In all cases, the absolute configuration of the α-hydroxylated products was determined to be *R* through chiral HPLC comparison with literature data [36].

Published in : ChemSusChem (2025), e202501565
DOI: 10.1002/cssc.202501565
Status : Postprint (Author's version)

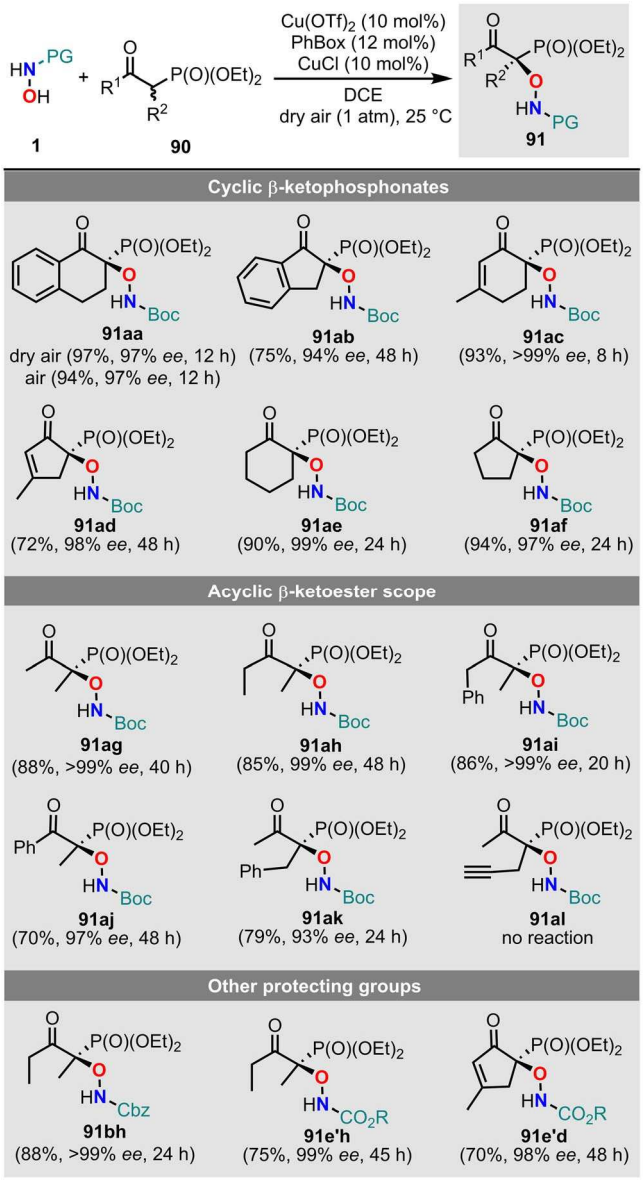

FIGURE 80 | Scope of asymmetric O-nitroso-aldol reaction of β-ketophosphonate **90** with N-protected HA **1** under aerobic oxidation. Conditions: **90** (0.1 mmol), **1** (0.12 mmol), $Cu(OTf)_2$ (0.01 mmol), PhBox ligand (0.012 mmol), CuCl (0.01 mmol) in 2 mL CH_2Cl_2 under dry air (1 atm). The yields are the isolated yields. The ee value was determined using HPLC on chiral stationary phase. R = 4-$BrC_6H_4CH_2$. PG = protecting group.

In 2014, Hashmi and coworkers explored a novel dearomatization strategy of indoles using in situ generated electrophilic nitrosoformate compounds [105]. Despite the inherent challenges, including the tendency of indole systems to undergo rearomatization and the instability of nitrosoformates, this method enabled the synthesis of structurally valuable pyrroloindoline derivatives, which are key motifs in natural product synthesis. Drawing inspiration from the foundational works of Whiting and Read de Alaniz [29, 82, 103], the authors conducted an extensive study on the reaction of tryptamines and tryptophols, acting as enamines to trap nitrosoformates intermediates, followed by the intramolecular

Published in : ChemSusChem (2025), e202501565
DOI: 10.1002/cssc.202501565
Status : Postprint (Author's version)

nucleophilic quench the corresponding iminium intermediate to form dearomatization product **93** (Figure 81).

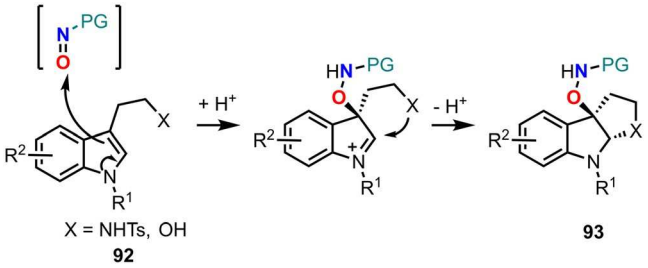

FIGURE 81 | Proposed copper-catalyzed nitrosoformate dearomatization reaction. PG = protecting group.

The reaction conditions were optimized using Cbz-Nhydroxylamine **1b** and tryptamine **92a** as model substrates (Table 26). Using CuCl (10 mol%) in methanol under air at room temperature afforded the desired product **93ba** in 42% yield as a single diastereoisomer (Table 26, entry 1). Substitution of CuCl with $Cu(OTf)_2$ completely suppressed product formation, whereas combining both copper sources significantly increased the yield to 70% (Table 26, entries 2–3). Interestingly, although this dual catalyst system promoted *O*-selectivity, it closely resembled Read de Alaniz's, which favored *N*- selectivity [55]. Further studies confirmed the critical influence of catalyst choice and stoichiometry on the efficiency and selectivity of the reaction.

TABLE 26 | Conditions optimization for the Cu-catalyzed dearomatization reaction with Cbz-*N*-hydroxylamine **1b** and tryptamine 92a as model substrates. Reaction conditions: **92a** (100 µmol), **1b** (110 µmol), catalyst (10 mol%), solvent (1 mL), air, 24 h.

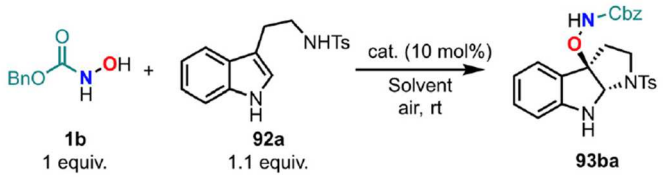

Entry	Catalyst	Solvent	Yield (%)[a]
1	CuCl	MeOH	42
2	$Cu(OTf)_2$	MeOH	0
3	$CuCl/Cu(OTf)_2$	MeOH	70
4	$CuCl/Cu(OAc)_2.H_2O$	MeOH	45
5[b]	$CuCl/Cu(OTf)_2$	MeOH	31
6	$CuCl/Cu(OTf)_2$	CH_2Cl_2	Trace
7	$CuCl/Cu(OTf)_2$	THF	17
8[c]	$CuCl/Cu(OTf)_2$	*i*PrOH	13

[a]Isolated yields.
[b]**92a** (150 µmol), **1b** (100 µmol).
[c]48 h.

Published in : ChemSusChem (2025), e202501565
DOI: 10.1002/cssc.202501565
Status : Postprint (Author's version)

Using the optimized conditions, a library of tryptamines and tryptophols was investigated, affording dearomatized products in yields ranging from 48% to 90% (Figure 82). X-ray crystallographic analysis confirmed the regioselectivity, with *cis*- anellation of the two five-membered rings playing a key role in achieving high diastereoselectivity.

To further explore the synthetic potential of this methodology, the team investigated an intramolecular dearomatization involving a nitrosoformate [4 + 4] dimerization cycloaddition, which produced the dimeric products **95a** and **95b** in 40% and 45% yield, respectively (Figure 83). Additionally, initial efforts toward diastereoselective nitrosoformate dearomatization using enantioenriched tryptophan methyl esters showed potential for chirality transfer, albeit with moderate yields and low diastereomeric ratios (Figure 84) [105].

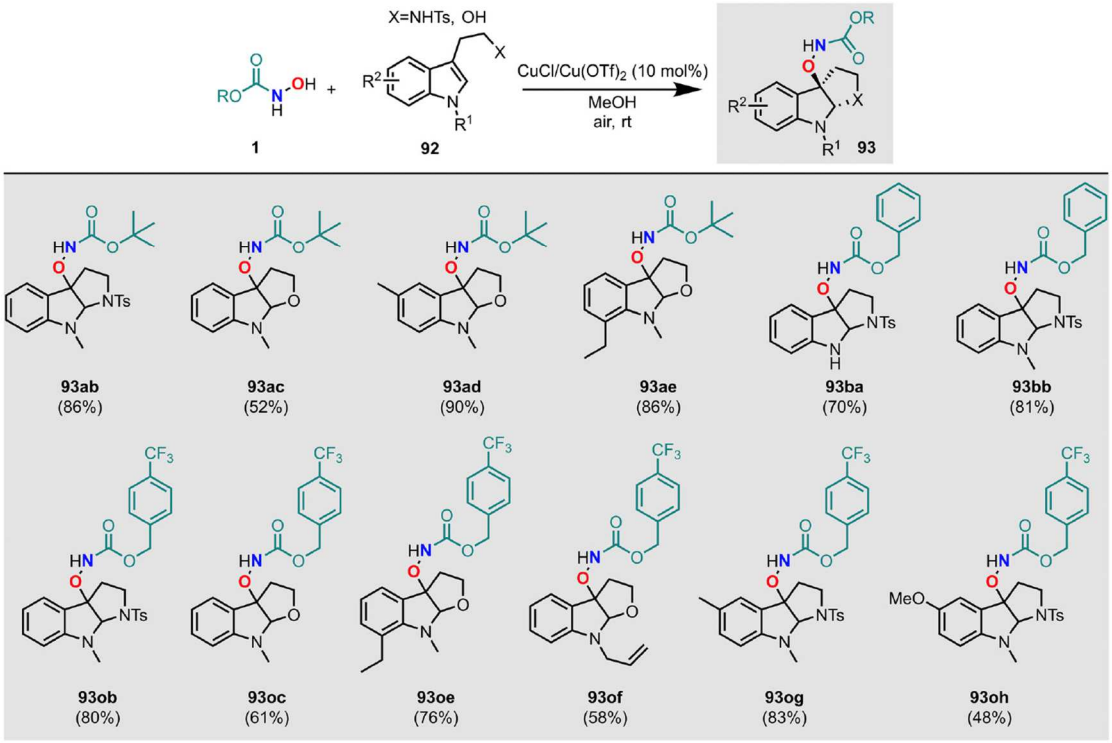

FIGURE 82 | Scope of the products obtained from the aerobic Cu-catalyzed dearomatization of a library of tryptamines and tryptophols using various HCs.

Published in : ChemSusChem (2025), e202501565
DOI: 10.1002/cssc.202501565
Status : Postprint (Author's version)

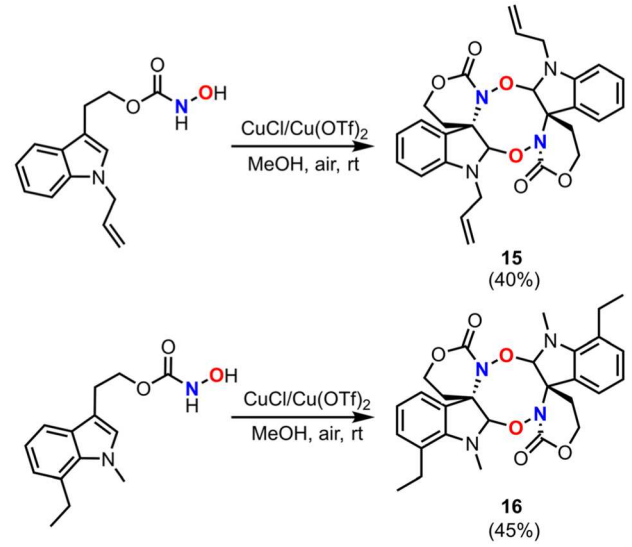

FIGURE 83 | Intramolecular nitrosoformate dearomatization via a [4 + 4] dimerization cycloaddition.

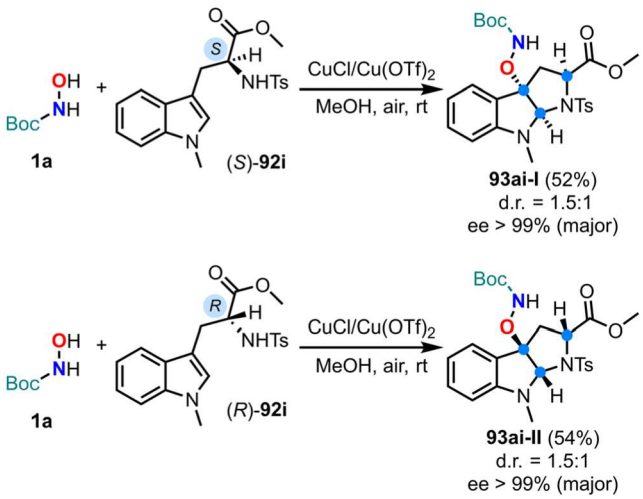

FIGURE 84 | Diastereoselective Cu-catalyzed dearomatization reaction of enantioenriched tryptophan methyl esters using Boc-*N*-hydroxylamine.

3.3 | PHOTOREDOX CATALYSIS

In 2013, Tan and colleagues introduced a simple one-pot method for the acylnitroso-ene reaction, utilizing organic dyes as photoredox catalysts and air as the terminal oxidant [110]. The key advantage of this approach lies in the use of inexpensive organic dyes as viable alternatives to conventional inorganic transition-metal photocatalysts. Furthermore, the reaction is entirely light-controlled, as no product formation occurs in the absence of either the light source or the photocatalyst.

Among the dyes and solvents tested, Rose Bengal (RB) and acetonitrile emerged as the optimal combination. The addition of pyridine as an additive and an increase in reaction temperature to 35°C

Published in : ChemSusChem (2025), e202501565
DOI: 10.1002/cssc.202501565
Status : Postprint (Author's version)

further enhanced the efficiency of the transformation. Various hydroxylamine protecting groups were compatible with this methodology.

The reaction was explored using a range of styrene derivatives bearing electron-withdrawing and electron-donating groups (Figure 85), as well as aliphatic alkenes (Table 27), affording products in yields ranging from 33% to 83% and 44% to 81%, respectively. Notably, the method was successfully scaled to the gram scale, even with a reduced catalyst loading of 1 mol%. Although singlet oxygen ene products were detected when cyclohexene was used, their formation was minimal. Disubstituted trans-4-octene afforded higher yields compared to monosubstituted 1-octene (Table 27, entries 2–3), likely due to the increased reactivity of the more electron-rich disubstituted olefins. Importantly, the acylnitroso enophile preferentially abstracts an allylic hydrogen atom from the geminal alkyl group on the more substituted side of the alkene (Table 27, entry 4).

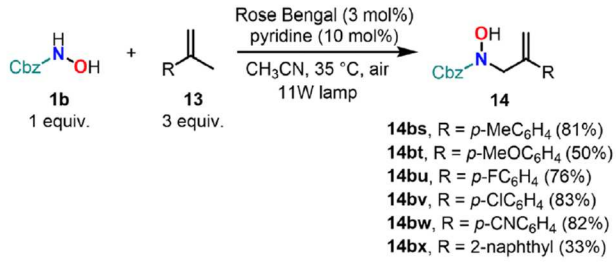

FIGURE 85 | NOC ene reaction of various *N*-protected HCs by irradiation in the presence of RB and pyridine as additive.

TABLE 27 | NOC ene reaction between *N*-Cbz-HC and styrene derivatives by irradiation in the presence of RB and pyridine as additive.

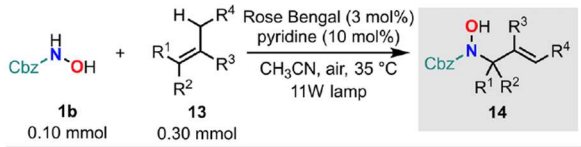

Entry	Alkene	Yield (%) / (*E*/*Z*)
1	**13d**	71
2	**13g**	44 (4:1)
3	**13i**	70 (4:1)
4	**13l**	70
5	**13o**, R = OMe **13p**, R = NH_2 **13q**, R = OH **13y**, R = OBn	77 81 50 59
6	**13z**	68

Published in : ChemSusChem (2025), e202501565
DOI: 10.1002/cssc.202501565
Status : Postprint (Author's version)

The reaction with 1-methyl-1-cyclohexene (**13j**, Figure 86) illustrates the regioselectivity achieved in this process. The preference for allylic hydrogen abstraction from the cis position can be rationalized by considering steric factors: the nitroso enophile approaches along a skewed trajectory in the favored *twix* arrangement, wherein the Cbz group orients toward the less hindered side of the alkene to minimize steric interactions. It is important to note that singlet oxygen, being highly reactive, can react with alkenes yielding peroxides, and thus affect the selectivity of the desired transformation. In this case, additional products (**96a-c**, Figure 86) were formed via the ene reaction of singlet oxygen with the alkene. Selectivity for the acylnitroso-ene reaction was improved by increasing the HA concentration, thereby suppressing side reactions involving singlet oxygen.

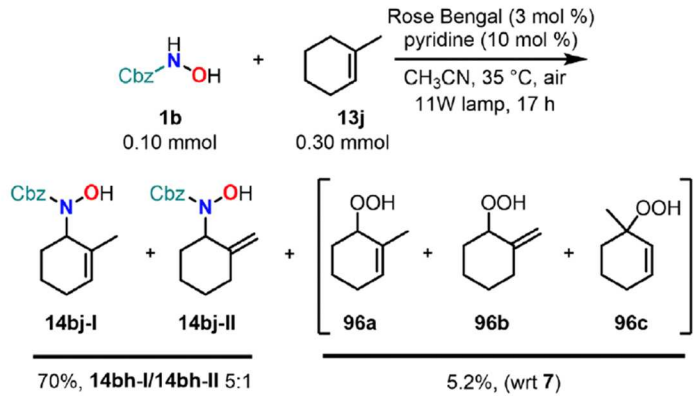

FIGURE 86 | Acylnitroso-ene reaction of benzyl HC (**1b**) with1-methyl-1-cyclohexene (**13j**).

A mechanism was proposed, beginning with visible-light irradiation and the excitation of RB to its excited state (RB*) (Figure 87). Two potential photoinduced sensitization mechanisms were then considered:

1. Single-electron transfer mechanism: RB* oxidizes the HAvia single electron transfer, generating the HA radical cation. The RB radical anion (RB•−) is then reoxidized to the ground state RB by molecular oxygen, completing the photoredox cycle.
2. Energy transfer mechanism: energy transfer from RB* to molecular oxygen produces singlet oxygen, which subsequently oxidizes the HA to the same radical cation intermediate. This intermediate is then deprotonated by the strongly basic superoxide anion.

Published in : ChemSusChem (2025), e202501565
DOI: 10.1002/cssc.202501565
Status : Postprint (Author's version)

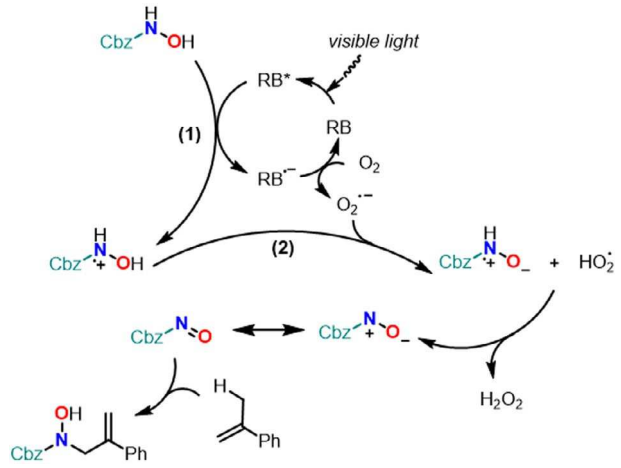

FIGURE 87 | Proposed mechanism for the aerobic photocatalyzed generation of acylnitroso species for ene reactions.

In both cases, hydrogen atom abstraction leads to the formation of the reactive nitroso intermediate, with H_2O_2 generated as a byproduct. The acylnitroso intermediate then undergoes the ene reaction with the alkene, furnishing the final product. The presence of hydrogen peroxide was confirmed by iodometric testing at the conclusion of the reaction. Additionally, to further probe the mechanism, the reaction was performed in both CH_3CN and CD_3CN. Since the lifetime of singlet oxygen is influenced by the solvent, being significantly shorter in protonated solvents compared to their deuterated counterparts, any disparity in yield would suggest the involvement of singlet oxygen. However, as no substantial rate enhancement was observed when using CD_3CN, singlet oxygen was determined not to be a key participant. Therefore, the explanation involving electron transfer appeared to be more suitable [110].

In 2015, Read de Alaniz's research group reported a photoredox oxidation of HA derivatives using commercially available light sources, air as the terminal oxidant, and the readily accessible $Ru(bpy)_3Cl_2{\cdot}6H_2O$ as the catalyst, used at a loading as low as 1 mol%, under ambient temperature conditions (Figure 88) [111]. The addition of pyridine or 2,6-lutidine (2.0 equiv.) was crucial to completely inhibit the [4 + 2] cycloaddition between molecular oxygen and the diene used to trap the in situ generated acylnitroso species. Although other Ru-, Ir-, and Eu-based catalysts were tested, none outperformed $Ru(bpy)_3Cl_2{\cdot}6H_2O$. The nature and amount of the base additive, as well as the choice of solvent, were systematically optimized, establishing the best conditions as $Ru(bpy)_3Cl_2{\cdot}6H_2O$ (1 mol%) and 2,6-lutidine (2 equiv.) in DCE.

Published in : ChemSusChem (2025), e202501565
DOI: 10.1002/cssc.202501565
Status : Postprint (Author's version)

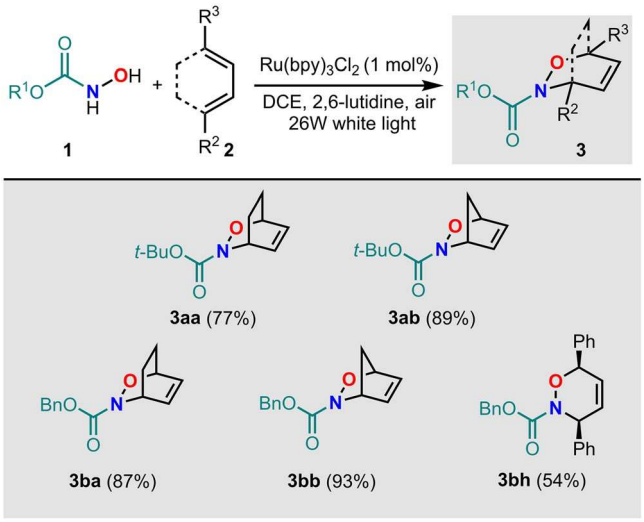

FIGURE 88 | hDA reaction between *N*-protected hydroxylamines and various dienes catalyzed by $Ru(bpy)_3Cl_2$ using light and air as terminal oxidant.

These conditions were applied to the hDA reaction between *N*-protected hydroxylamines and various dienes, as well as to the ene reaction with different alkenes, affording products in yields ranging from 54% to 93% and 34% to 99%, respectively (Figures 88 and 89). Notably, under the optimized conditions, the hDA reaction proceeded without competing formation of endoperoxides or hydroxyenones. Furthermore, application of the same conditions to the ene reaction yielded the desired products without observable decomposition, proving the mildness of the process. The substitution pattern of the olefin was found to significantly impact the efficiency of the ene reaction, with fully substituted alkenes providing higher yields of the corresponding allylic hydroxylamines compared to monosubstituted alkenes.

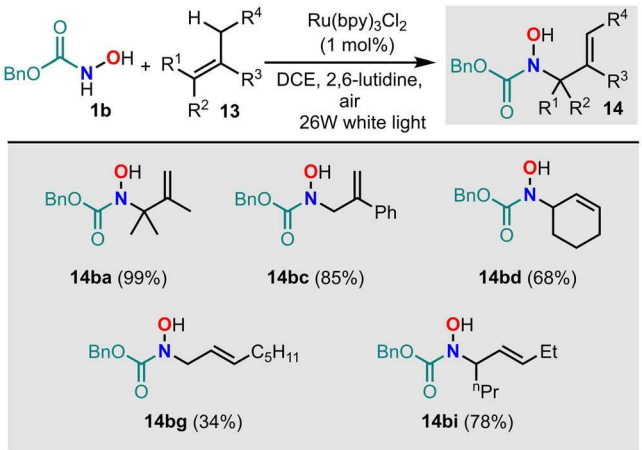

FIGURE 89 | NOC ene reaction between *N*-Cbz-hydroxylamine and different alkenes catalyzed by $Ru(bpy)_3Cl_2$ using light and air as terminal oxidant.

Published in : ChemSusChem (2025), e202501565
DOI: 10.1002/cssc.202501565
Status : Postprint (Author's version)

To distinguish between a photoredox mechanism and one involving singlet oxygen (Figure 90), Stern-Volmer quenching studies were conducted. The fluorescence intensity of the catalyst exhibited a linear dependence on the concentration of the Cbz-protected hydroxylamine, indicating a direct interaction between the excited state of the catalyst and the substrate. This observation suggests that the most probable pathway involves oxidation of the hydroxylamine by the excited state of $Ru(bpy)_3Cl_2{\cdot}6H_2O$ (pathway A, Figure 90).

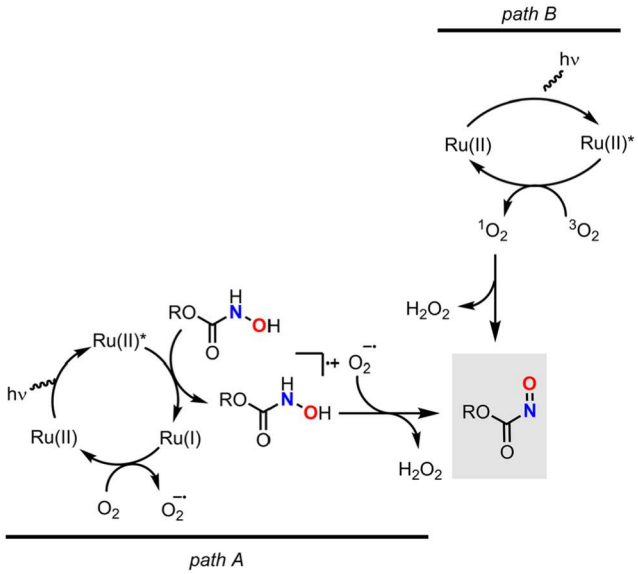

FIGURE 90 | Proposed mechanisms Ru-catalyzed photochemical generation of NOCs. (A) Photoredox catalyzed oxidation. (B) Singlet oxygen-mediated oxidation.

A distinctive advantage of this photoredox methodology is the ability to exert spatiotemporal control over the generation of NOCs. The reaction could be effectively switched on and off in response to light exposure, without any loss of efficiency even after multiple light–dark cycles. Given that NOCs can serve as donors of HNO, this light-controlled process also provides a platform for the in situ generation of HNO under mild conditions [111].

In 2019, Quadrelli and colleagues reported a photoredox catalytic process using the decatungstate anion $[W_{10}O_{32}]^{4-}$ as a catalyst to oxidize HAs, generating NOCs via a hydrogen atom transfer (HAT) mechanism [112]. The decatungstate anion was selected for its exceptional excited-state properties. Upon UV photon absorption, it undergoes a transformation to a highly oxidizing excited state, reaching a redox potential of +2.4 V *vs.* SCE, thus enabling the efficient generation of a potent oxidant using only solar light irradiation.

The formation of the NOC intermediate was investigated using tetrabutylammonium decatungstate (TBADT) as the catalyst, a Xenon lamp simulating solar light (500 W m^{-2} intensity), and dienes as trapping agents (Figure 91). The process required the presence of molecular oxygen, as no product formation was observed when the reaction was conducted under nitrogen. Increasing the amount of photocatalyst or extending the irradiation time did not improve the yield; in fact, prolonged irradiation had a detrimental effect due to decomposition of the reactive intermediates. However, the addition

Published in : ChemSusChem (2025), e202501565
DOI: 10.1002/cssc.202501565
Status : Postprint (Author's version)

of a mild base and the use of an aqueous reaction medium were found to enhance the overall efficiency of the transformation.

Under optimized conditions, a library of HAs derivatives was explored (Figure 91). Reactive dienes, such as cyclopentadiene and 1,3-cyclohexadiene, efficiently trapped the transient NOC, leading to the formation of the corresponding cycloadducts in moderate to good yields. Further investigations into electronic effects revealed that HAs bearing either electron-donating or electron-withdrawing groups failed to deliver the desired products (Figure 92). Instead, side products such as ketone **97** and urea **98** were isolated. These structures are proposed to arise from dimerization and decomposition with rearrangement of the NOC intermediates. Although the desired cycloadducts could not be isolated in these cases, the formation of ketone **97** and urea **98** provided compelling evidence for the generation of the expected NOC intermediates, whose short-lived nature under the reaction conditions limited their effective trapping by the dienes in solution [112].

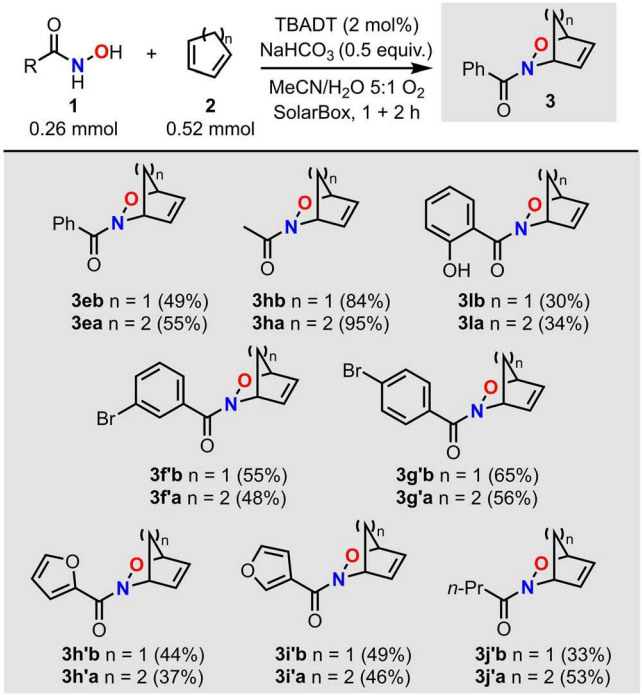

FIGURE 91 | hDA reaction between substituted HAs and cyclopentadiene or 1,3-cyclohexadiene catalyzed by TBADT with solar light irradiation.

Published in : ChemSusChem (2025), e202501565
DOI: 10.1002/cssc.202501565
Status : Postprint (Author's version)

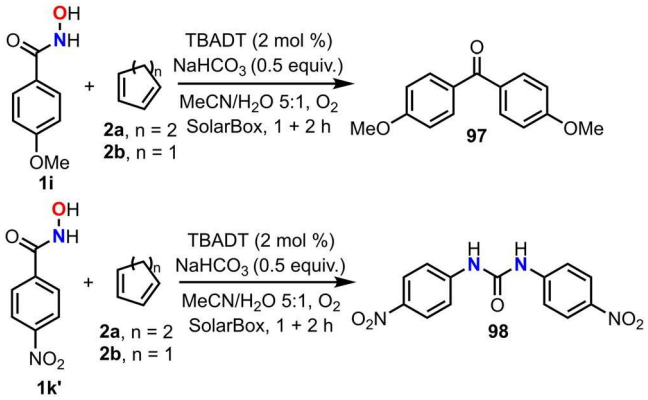

FIGURE 92 | hDA reaction between two substituted benzohydroxamic acids, bearing respectively an electron-donating and an electronwithdrawing group, and cyclopentadiene or 1,3-cyclohexadiene catalyzed by TBADT under visible light irradiation mimicking solar light.

Recently, Ma and Lam reported a light-induced S-N coupling reaction between HAs and sodium sulfinates for the synthesis of acylsulfonamides, valuable motifs in pharmaceuticals and bioactive molecules [113]. The key step involves the in situ photogeneration of a NOC intermediate, triggered by the excitation of the photocatalyst 2,3,5,6-tetra(9H-carbazol-9-yl)benzonitrile (4CzBN) under blue LED irradiation in the presence of oxygen. Mechanistic studies suggest that energy transfer from the excited state of 4CzBN to O_2 generates singlet oxygen, which then oxidizes the HA substrate to the reactive NOC that reacts in turn with the sodium sulfinate to form the S–N bond.
The method exhibits a broad substrate scope, accommodating a range of HAs, HCs, and sodium sulfinates, with yields ranging from 33% to 97%. This demonstrates excellent tolerance toward electron-donating and electron-withdrawing groups, including halides, trifluoromethyl, methoxy, and heterocycles. Overall, this work presents a mild and sustainable photochemical strategy for accessing acylsulfonamides via controlled NOC generation under metal-free conditions.

3.4 | BIOCATALYSIS

The design of enzymatic cascades, resembling miniaturized artificial metabolic pathways, has emerged as an attractive alternative to traditional synthetic organic methods. This approach allows operations under mild conditions and the use of environmentally friendly reagents. Furthermore, the high compatibility between different enzymes enables streamlined reaction setups, improving efficiency and sustainability.

Inspired by copper- and iron-based homogeneous systems described in the literature for NOC chemistry, Deska's group explored the use of redox-active metalloproteins containing either of these two elements as active site motifs to oxidize HCs (Figure 93) [114]. Among the enzymes screened, two systems stood out: the oxygen-activating CotA laccase from *Bacillus licheniformis* and a bi-enzymatic system combining glucose oxidase (GOx) from *Aspergillus niger* with horseradish peroxidase (HRP). Both enzymatic systems demonstrated remarkable robustness and tolerated some water-miscible

Published in : ChemSusChem (2025), e202501565
DOI: 10.1002/cssc.202501565
Status : Postprint (Author's version)

cosolvents, such as dioxane. This solvent tolerance is advantageous for processing HCs or HAs with higher lipophilicity without compromising reactivity or selectivity.

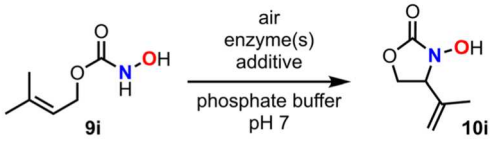

Enzime & additives	Time (h)	Conv. (%)	Yield (%)
laccase CotA (*B. licheniformis*)	7	100	74
peroxidase (horseradish) / glucose oxidase (*A. niger*) D-glucose	2	100	97

FIGURE 93 | Optimal enzymes for the oxidative cyclization of **9i**.

Both systems exhibited good catalytic efficacy. Overall, the HRP/ GOx system delivered higher yields, with maximum turnover numbers reaching 43,500, compared to 12,100 for CotA. In the conversion of **9i** to **10i**, involving the formation of a stereogenic center, no enantioselectivity was observed with peroxidase-catalyzed reactions, resulting in racemic **10i**. Although certain laccases afforded moderate enantiomeric excesses under slightly acidic conditions, these conditions also facilitated product degradation.

In both biocatalytic systems, the reaction outcome strongly depended on the geometry of the starting alkene (Figure 94a). Treatment of the *E*- and *Z*-isomers of 2-hexenyl HCs (E-**9b** and Z-**9b**) under identical conditions led to good yields of oxazolidinone **10b** from the *E*-isomer, while the *Z*-isomer decomposed to the corresponding allylic alcohol, suggesting nitroso intermediate hydrolysis and decarboxylation.

Interestingly, the HRP-mediated oxidation of the benzoate-derived hydroxamic acid **9p** yielded the amidohydroxylated species **99p** as the sole product, alongside unreacted starting material (Figure 94b). Moreover, isotope labeling studies using deuterated and nondeuterated versions of the symmetrical derivative **9i** revealed a strong inverse isotope effect (kH/kD = 0.79) with the HRP/GOx system, but no significant isotope effect with the CotA-catalyzed reaction (Figure 94c). These findings suggest that the two enzymatic systems operate via different mechanisms, with the HRP system involving a hybridization change (sp^2 to sp^3) during the rate-limiting step.

Published in : ChemSusChem (2025), e202501565
DOI: 10.1002/cssc.202501565
Status : Postprint (Author's version)

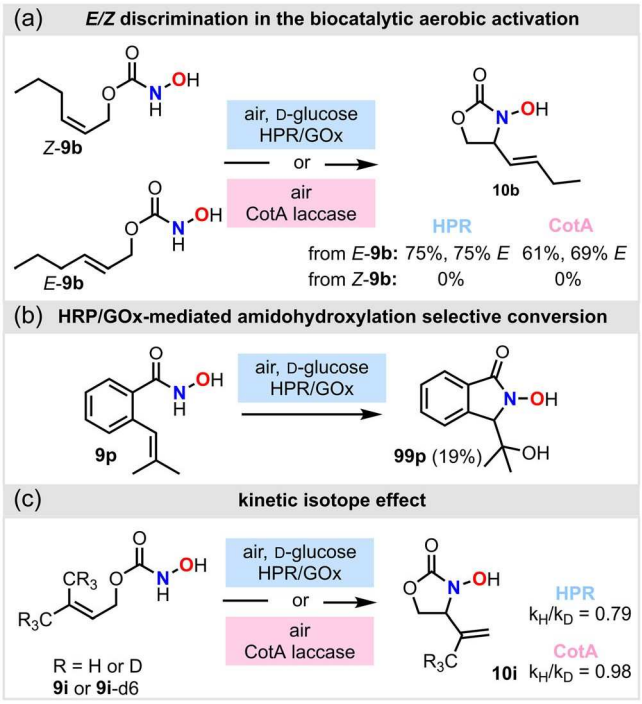

FIGURE 94 | Enzyme-mediated cyclizations that provided hints on the underlying reaction pathways of aqueous nitroso-ene reactions.

Overall, these results point to the involvement of a geometrically rigid intermediate, such as an aziridine *N*-oxide (ANO, Figure 95). Evidence suggests that HRP generates free acylnitroso intermediates, which subsequently cyclize independently of the peroxidase, through an ANO intermediate. In contrast, laccase-catalyzed processes seem to genuinely promote ANO formation, offering a stereochemically defined environment for C–N bond formation and eliminating the secondary isotope effect characteristic of uncatalyzed nitroso-ene reactions [114].

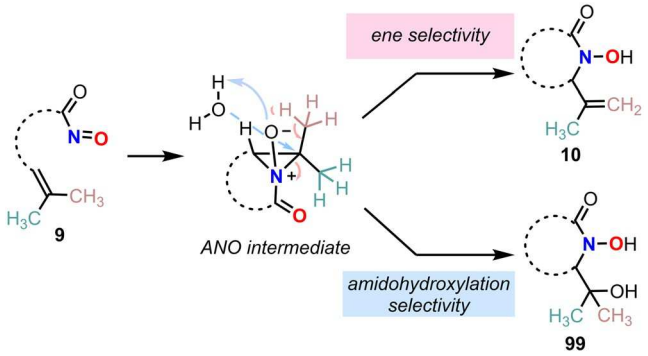

FIGURE 95 | Possible mechanism for the enzyme-mediated cyclization.

Further studies with the HRP/GOx system highlighted the advantages of using commercially available biocatalysts to generate *N*-heterocyclic structures, demonstrating broad substrate tolerance,

Published in : ChemSusChem (2025), e202501565
DOI: 10.1002/cssc.202501565
Status : Postprint (Author's version)

scalability, and recyclability. This method proved compatible with lipase-mediated HA formation, showcasing its versatility in integrating multiple biocatalytic processes (Figure 96).

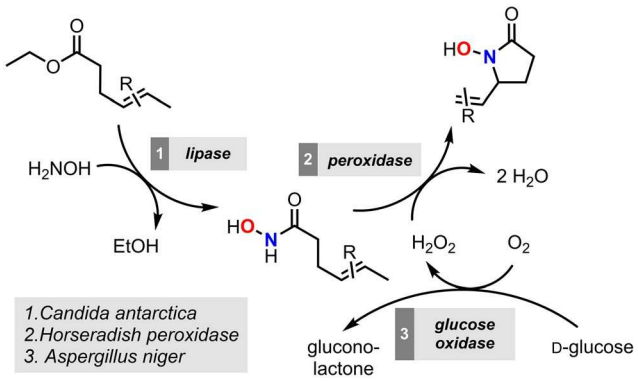

FIGURE 96 | Biocatalytic sequence for the preparation of N-heterocycles using hydroxylamine as nitrogen source.

This method accommodates a range of substitution patterns around the olefin, resulting in products with moderate to excellent yields (Figure 97). For instance, γ-lactams **10a** and **10i** were efficiently prepared using this biocatalytic method. Traditionally, the synthesis of **10i** requires refluxing in benzene [115], whereas the biocatalytic approach achieves it at room temperature in aqueous solution. Moreover, the spirocyclic product **10q**, derived from HA **9q**, was obtained in yields significantly superior to those reported for purely chemical methods [116]. Treatment of the *E*-isomer of HA **9b** led to **10b** in 75% yield with an *E/Z* ratio of 4:1. Overall, yields and *E/Z* selectivities were comparable to those obtained from the corresponding HCs, highlighting the broad applicability of the method. However, the cyclization of heterofunctionalized HAs to generate products **10r-t** was unsuccessful [117].

Published in : ChemSusChem (2025), e202501565
DOI: 10.1002/cssc.202501565
Status : Postprint (Author's version)

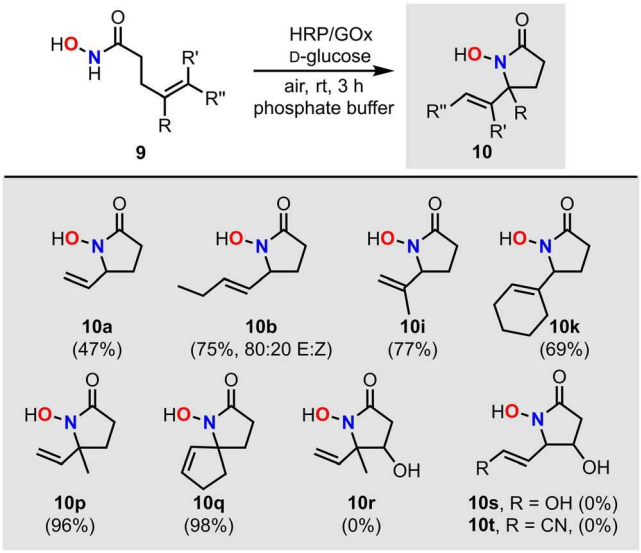

FIGURE 97 | Scope of the biocatalytic intramolecular nitroso-ene reaction of γ,δ-unsaturated HAs.

The method was also extended to intermolecular ene reactions and hDA reactions (Figure 98). In the intermolecular ene reaction (Figure 98a), the addition of the non-ionic PEG-based detergent Brij 35 facilitated phase transfer, allowing coupling products to be synthesized using only a moderate excess of olefin. Cyclic dienes performed poorly and thus were used as cosolvents instead of *n*-heptane.

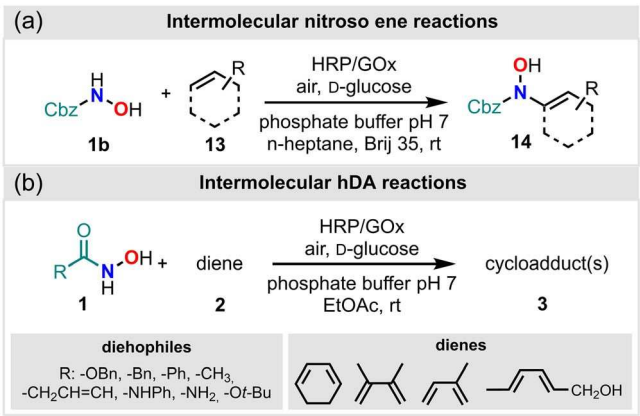

FIGURE 98 | Scope of the biocatalytic intermolecular ene and hDA reactions.

For [4 + 2] cycloadditions (Figure 98b), a biphasic H_2O/EtOAc system proved optimal, as emulsifiers such as Brij 35 were not beneficial. Although other solvents like *n*-heptane and toluene were tested, none surpassed EtOAc. The synthetic scope of the HRP-induced [4 + 2] cycloaddition was explored by modifying both the diene and dienophile partners (Figure 98). Regardless of the hydroxylamine's acylation pattern, bicyclic products were obtained in good to excellent yields. Notably, substrates bearing unsaturated acyl groups on nitrogen outperformed those with saturated groups; for instance, benzamide delivered significantly higher yields than acetamide (85% vs. 18%), and *N*-phenylurea surpassed urea (98% vs. 11%).

Published in : ChemSusChem (2025), e202501565
DOI: 10.1002/cssc.202501565
Status : Postprint (Author's version)

This phenomenon has not been observed in the hDA literature and may be connected to the interaction of the substrate with the enzyme's active site. Studies of HRP-C, the most abundant isoenzyme of HRP, revealed an aromatic binding pocket that explains the enzyme's bias toward recognizing small aromatic molecules and stabilizing the thus formed nitroso intermediates. Intermolecular [4 + 2] cycloadditions might be facilitated by improving the transport of the lipophilic diene substrate to the nitroso intermediate formed in the aqueous layer. Consequently, sorbic alcohol with its significantly increased solubility in water, performed well in the bimolecular nitroso-Diels–Alder reaction [118].

Upscaling and recycling studies were performed for the intramolecular nitroso-ene reaction yielding **10i** (Figure 93) [118]. Upon scaling from milligram to gram scale (starting with 4.0 g of **9i**), reaction time increased from 2 to 24 h, and yield dropped from 97% to 73%. Nevertheless, the biotransformation remained clean, with no significant side-product formation. This reduction in efficiency was attributed to limited oxygen availability at larger scale, which could be addressed in the future by transitioning to reactor setups with better aeration control.

Regarding recyclability, the ene-type biotransformation exhibited high tolerance to ethyl acetate. A biphasic set up was then used, where the ene-substrate was introduced as a solution in the organic cosolvent. Upon completion, the product could be easily removed by separating the phases, and the system could be recharged with fresh ethyl acetate containing a new portion of the ene substrate for subsequent transformations.

Careful adjustment of D-glucose concentration prevented heme peroxidase bleaching by regulating H_2O_2 levels. Full conversion and quantitative yields of **10i** were achieved in early catalytic cycles, though conversion dropped significantly after the fourth cycle, likely due to enzyme denaturation in the presence of organic solvents.

In the case of HRP, the hydrogen bonds in the active site can be disrupted under these conditions, causing the enzyme to unfold and release the iron-containing prosthetic group, which renders the enzyme inactive.

It is important to note that enzymatic reactions are often highly effective in terms of their catalytic turnover. While this is typically true when using native substrates, the application of bioacatalysis in non-natural reactions can be hindered by a reduced number of total turnovers. Contrary to expectations, the HPR-mediated cyclization of **9i** proceeded with great efficacy, achieving a total turnover of over 217,000 (relative to the catalytically active iron porphyrin center) [118].

4 | Conclusions and Perspectives

In this review, we have compiled and analyzed the current literature on the catalytic generation of NOCs from HAs and their derivatives, with a particular focus on methods utilizing oxygen or peroxides as terminal oxidants. A key feature of these processes is the mild reaction conditions required to access the transient NOCs, making them compatible with complex, functionalized molecules and suitable for downstream functionalization strategies. Moreover, ongoing efforts are directed toward the

Published in : ChemSusChem (2025), e202501565
DOI: 10.1002/cssc.202501565
Status : Postprint (Author's version)

development of chiral catalysts capable of enabling enantio- and diastereoselective transformations from these intermediates, with promising early results.

Tables 28 and 29 summarize the optimal oxidation conditions using oxygen- and peroxide-based strategies discussed throughout this review. Additionally, a color-coded sustainability assessment is provided for each study (red = low sustainability, orange = moderate, and green = high). Specifically, the sustainability of the solvent was evaluated according to GSK's solvent sustainability guide [119]. Catalyst sustainability was assessed based on both the metal (or other active species) and its loading. For the metal, factors such as crustal abundance, toxicity, extraction impact, and recyclability were considered to generate a sustainability ranking (Table 30) [120–122]. Regarding catalyst loading, we categorized optimal loadings as <2.5 mol%, moderate loadings as 2.5–5 mol%, and poor loadings as >5 mol%.

TABLE 28 | Summary of conditions using peroxides as oxidant to generate NOCs. Sustainability highlights are presented concerning the solvent, the type and loading of catalyst and the reaction temperature. The color code represents low (red), moderate (orange), and high (green) sustainability.

				Sustainability highlights				
				Catalyst				
	Entry	Conditions	Trapping reaction	Solvent	Metal (or other)	Loading (mol%)	*T* (°C)	Ref.
Fe	1	$FeCl_3$ (5 mol%), $NH_2CH_2CH_2NH_2$ (15 mol%), 30% aq. H_2O_2 (7 equiv.).	hDA	CH_2Cl_2	Fe	5	r.t.	[46]
	2	$[Fe(L)Cl]_2$ (0.1 mol%), H_2O_2 (1.2 equiv.). 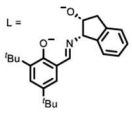	hDA	Acetone	Fe	0.1	r.t.	[47]
Mg	3	$MgCl_2$ (10 mol%), TBHP (1.2 equiv.).	α-amination of α-alkyl-β-ketoesters	MeCN	Mg	10	40°C	[54]
Cu	4	CuCl or $CuCl_2$ (5 mol%), $HOCH_2CH_2NH_2$ (15 mol%), 30% aq. H_2O_2 (7 equiv.).	hDA	CH_2Cl_2	Cu	5	r.t.	[46]
	5	CuI (2 mol%), 31% aq. H_2O_2 (1.1–1.2 equiv.).	ene (N, selective)	MeOH or THF	Cu	2	0 – r.t.	[56]
	6	Cu(pybox-dh) or Cu-pybox-iPr (2 mol%), H_2O_2 (4 equiv.).	ene (N, selective)	MeOH	Cu	2	0 – r.t.	[57]
	7	CuCl (15 mol%), H_2O_2 (5 equiv.).	ene (N, selective) hDA	CH_2Cl_2/ MeCN	Cu	15	r.t.	[58]
V	8	VO(*Oi*-Pr)$_3$ (1 mol%), CHP or TBHP (1 equiv.).	hDA	CH_2Cl_2	V	1	r.t.	[62]
Ru	9	$RuCl_2(PPh_3)_4$ (10 mol%), TBHP (3 equiv.).	hDA	CH_2Cl_2	Ru	10	r.t.	[64]

(Continues)

Published in : ChemSusChem (2025), e202501565
DOI: 10.1002/cssc.202501565
Status : Postprint (Author's version)

TABLE 28 | (Continued)

	Entry	Conditions	Trapping reaction	Sustainability highlights: Catalyst: Solvent	Metal (or other)	Loading (mol%)	T (°C)	Ref.
	10	Ru(salen) (0.1 mol%), TBHP (1 equiv.). 	hDA	CH_2Cl_2	Ru	0.1	r.t.	[48]
	11	Ru(II)(pybox-dh)(pydic) (11 mol%), H_2O_2 (4 equiv.). 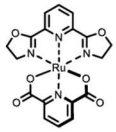	hDA	THF	Ru	11	0 – r.t.	[68]
	12	Ru(II)(pybox-dh)(pydic)* (5 mol%); H_2O_2 (4 equiv.). 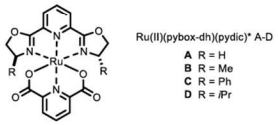	Asymmetric hDA	MeOH	Ru	5	0 – r.t	[69]
	13	[Ru(L)Cl](*p*-cymene) (0.1 mol%), H_2O_2 (1.1 equiv.). 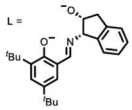	hDA	Acetone	Ru	0.1	r.t.	[46]
	14	Ru(II)(pybox-dh)(pydic) (2 mol%), 31% aq H_2O_2 (1.2 equiv.).	ene (N, selective)	MeOH or THF	Ru	2	0 – r.t	[56]
Ir	15	$[Ir(cod)Cl]_2$ or $[Ir(coe)_2Cl]_2$ (5 mol%), H_2O_2 (4 equiv.).	hDA	MeOH or THF	Ir	5	0 – r.t	[69]
	16	$[Ir(coe)_2Cl]_2$ (2 mol%), H_2O_2 (4 equiv.).	hDA	THF	Ir	2	0 – r.t	[70]
	17	$[Ir(cod)Cl]_2$ or $[Ir(coe)_2Cl]_2$ (5 mol%), 31% aq H_2O_2 (4 equiv.).	ene (N, selective)	MeOH or THF	Ir	5	0 – r.t	[57]
	18	$[Ir(cod)Cl]_2$ or $[Ir(coe)_2Cl]_2$ (2 mol%), 31% aq H_2O_2 (1.1–1.2 equiv.).	ene (N, selective)	MeOH or THF	Ir	2	0 – r.t	[56]
Rh	19	$Rh_2(cap)_4$ (0.1 mol%), TBHP (4 equiv.).	hDA	CH_2Cl_2	Rh	0.1	0 – r.t	[71]
Enzyme	20	HRP/ H_2O_2 1.04:1	no trapping (decomposition to HNO)	H_2O - DMSO (10%–30%)	enzyme	0.1	r.t.	[78]
hν	21	H_2O_2, UV light	methyl radical trapping	DMSO	UV light	–	r.t.	[79]
Metal-free	22	TBAI (5 mol%), TBHP or H_2O_2 (1.5 equiv.).	ene (N, selective) hDA	CH_2Cl_2	TBAI	5	r.t.	[80]
	23	TBAI (10 mol%), H_2O_2 (2 equiv.).	carboxylic acid formation	H_2O/THF (2:1)	TBAI	10	r.t.	[81]

Published in : ChemSusChem (2025), e202501565
DOI: 10.1002/cssc.202501565
Status : Postprint (Author's version)

TABLE 29 | Summary of conditions using oxygen as oxidant to generate NOCs. Sustainability highlights are presented concerning the solvent, the type and loading of catalyst, and the reaction temperature. The color code represents low (red), moderate (orange), and high (green) sustainability.

					Sustainability highlights				
					Catalyst				
	Entry	Nitrosocarbonyl precursor	Conditions	Trapping reaction	Solvent	Metal (or other)	Loading (mol%)	*T* (°C)	Ref.
Cu (I)	1	HA, HC, *N*-hydroxyureas, *N*-hydroxyphosphinic amides	CuCl (20 mol%), pyridine (5 mol%), air.	hDA	THF	Cu	20	r.t.	[29]
	2	HC	CuCl (5 mol%), pyridine (1.25 mol%), air.	ene	THF	Cu	5	r.t.	[82, 86]
	3	HC	CuCl (10 mol%), 46-TfOH (20 mol%), *m*-$NO_2C_6H_4CO_2H$ (20 mol%), air. 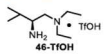 46-TfOH	asymmetric *α*-amination of *α*-alkyl-*β*-ketoesters	MeCN	Cu	10	r.t.	[88]
	4	HC	CuCl (15 mol%), 46-TfOH (20 mol%), (R)−56 (20 mol%), O_2. 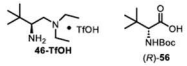 46-TfOH (R)-56	asymmetric *α*,*α*-bisfunctionalization of *α*-unsubstituted *β*-ketocarbonyls, *β*-ketoamides, 1,3-diketones and six-membered cyclic ketones	MeCN	Cu	15	r.t.	[91]
	5	HC	CuCl (20 mol%), pyridine (10 mol%), O_2.	*α*-amination of ketones (N-selective NOC Mukaiyama aldol)	MeCN	Cu	20	r.t.	[92]
	6	HC	CuCl (10 mol%), 2-ethyl-2-oxazoline (10 mol%), air.	*α*-amination of ketones (N-selective NOC Mukaiyama aldol)	THF	Cu	10	r.t.	[93]
	7	HC	CuCl (10 mol%), $(Cp^*RhCl_2)_2$ (2.5 mol%), CsOAc (30 mol%), PivOH (100 mol%), air.	Hydroxyamination of aryl C–H Bonds	EtOH/ Acetone (1:1)	Cu	10	r.t.	[97]
Cu(II)	8	HC	$CuCl_2$ (10 mol%), 2-ethyl-2-oxazoline (20 mol%), air.	hDA	MeOH	Cu	10	r.t.	[103]
	9	HC	CuCl (5 mol%), $Cu(OTf)_2$ (5 mol%), air.	*α*-amination of *α*-alkyl-*β*-ketoesters	MeOH	Cu	10	r.t.	[55]
	10	HC	CuCl (5 mol%), $Cu(OAc)_2$, H_2O (5 mol%), 2-ethyl-2-oxazoline (5 mol%), air. *Replacing 2-ethyl-2-oxazoline with (R, R)-PhBox allows asymmetric induction	*α*-oxygenation of *α*-alkyl-*β*-ketoesters	iPrOH	Cu	10	r.t.	[106]
	11	HC	CuCl (10 mol%), $Cu(OTf)_2$ (10 mol%), air.	indoles dearomatization	MeOH	Cu	20	r.t.	[105]

(Continues)

Published in : ChemSusChem (2025), e202501565
DOI: 10.1002/cssc.202501565
Status : Postprint (Author's version)

TABLE 29 | (Continued)

	Entry	Nitrosocarbonyl precursor	Conditions	Trapping reaction	Sustainability highlights				Ref.
					Catalyst				
					Solvent	Metal (or other)	Loading (mol%)	*T* (°C)	
hν	12	HC	RB (3 mol%), pyridine (10 mol%), air, 11W lamp.	ene	MeCN	RB (light)	3	35	[110]
	13	HC	$Ru(bpy)_3Cl_2$ (1 mol%), 2,6-lutidine (2 equiv.), 26W white light	ene hDA	DCE	Ru - light	1	r.t.	[111]
	14	HC	TBADT (2 mol%), NaHCO3 (0.5 equiv.), O_2, SolarBox	hDA	MeCN/H_2O (5:1)	TBADT - light	2	r.t.	[112]
Enzyme	15	HA, HC, *N*-hydroxyureas	(intramolecular ene) HRP/GOx, D, glucose; phosphate buffer pH 7, air. (intermolecular ene) HRP/GOx, D, glucose; phosphate buffer pH 7, n-heptane, Brij 35, air. (intermolecular n-hDA) HRP/GOx, D, glucose; phosphate buffer pH 7, EtOAc, air.	ene hDA	Phosphate buffer + cosolvent	enzyme	<0.01	r.t.	[114]

TABLE 30 | Sustainability rating for the metals used as catalysts in the presented works. Crustal abundance, toxicity, extraction impact, and recyclability have been considered.

Metal	Crustal abundance	Toxicity	Extraction impact	Recyclability	Sustainability rating
Fe	Very high	Low	Low	Excellent	Excellent
Mg	Very high	Very low	Low	Excellent	Excellent
Cu	Medium-high	Moderate	Medium	Good	Good
V	Medium	High	Medium-high	Moderate	Moderate
Ru	Very low	Moderate	High	Limited	Poor
Rh	Extremely low	Moderate	Very high	Limited	Very poor
Ir	Extremely low	Moderate	Very high	Limited	Very poor

Published in : ChemSusChem (2025), e202501565
DOI: 10.1002/cssc.202501565
Status : Postprint (Author's version)

Similarly, reaction temperature was evaluated: room temperature was considered optimal, moderate temperatures ranged from 0°C to room temperature and from room temperature to 35°C, and temperatures above 35°C or below 0°C were classified as poor.

Recent trends point to four main areas for further advancement in NOC chemistry (Figure 99).

The invaluable ability of flow technology to unlock spatiotemporal control on reactions involving transient species is particularly appealing [123, 124]. Whether NOCs are generated through conventional or photochemical oxidation of precursors, the control on concentration gradients, local stoichiometry, and reaction heat is highly promising for suppressing competitive reactions [111, 112]. Additional synergies include the potential for reaction telescoping [125, 126], process intensification [114, 115], and seamless scalability [127, 128]. More specifically when using oxygen as the terminal oxidizer, the ability to modulate the system pressure in flow setups combined with high mass transfer efficiencies [129] is expected to greatly enhance the process, as extensively illustrated for gas–liquid reactions in flow [123, 124].

The second area of potential improvement encompasses the application of electrochemistry for the generation of NOC derivatives. One of the major advantages of electrochemistry is its potential to operate without the need for stoichiometric terminal oxidants. While early studies in the 1970s [130] led primarily to carboxylic acids (via acylium cation intermediates) rather than NOC products, recent developments have shown that NOC intermediates can indeed be formed and successfully trapped in nitroso-Diels–Alder reactions [131]. Further exploration is warranted to extend this approach to more challenging transformations, such as ene and aldol reactions, both in batch and in flow-based electrochemical setups [132, 133].

A third opportunity for innovation draws on radical pathways for NOCs formation. The generation of amidoxyl radicals [76, 134], suggests an alternative two-step, one-electron-at-a-time mechanism for NOCs generation, rather than a conventional concerted two-electron oxidation. This strategy could open up novel reactivity and reaction design options.

Finally, biocatalysis offers a particularly appealing path forward [135, 136]. Although enzymatic methods do not automatically guarantee a greener or more sustainable process, they offer clear advantages over traditional approaches that often rely on chlorinated solvents and high molecular weight halogenated oxidants. The use of water as a reaction medium and common, low toxicity-reagents can significantly improve environmental compatibility. Moreover, enzymatic transformations often exhibit high catalytic turnover numbers and may pave the way for stereoselective applications, further expanding the synthetic utility of NOC chemistry.

In summary, the catalytic generation of NOCs from HA derivatives has evolved into a rich and diverse field, encompassing metal-based, enzymatic, metal-free, or photocatalytic approaches. Whether using peroxides or molecular oxygen as terminal oxidants, these methods consistently demonstrate the possibility of forming highly reactive intermediates under mild and sustainable conditions. The broad variety of catalysts explored highlights the flexibility and potential of NOC chemistry to adapt to different synthetic needs. As advances continue to push the boundaries of reactivity, selectivity, and environmental responsibility, this area of research promises to provide increasingly powerful tools for

complex molecule construction, opening new opportunities for the development of efficient and selective synthetic methodologies.

Acknowledgments

This work was supported by the "Fonds de la Recherche Scientifique de Belgique (F.R.S.-FNRS)" (Incentive grant for scientific research MIS under grant No F453020F, JCMM), the "Fonds pour la Formation à la Recherche dans l'Industrie et dans l'Agriculture (F.R.I.A.-FNRS)" (PhD fellowship, TT), and the University of Liège (Council for Research and Valorization in Science and Techniques (IPD-STEMA 2022 postdoctoral fellowship, YHT).

Funding

This work was supported by the "Fonds de la Recherche Scientifique de Belgique (F.R.S.-FNRS)" (Incentive grant for scientific research MIS under grant No F453020F, JCMM), the "Fonds pour la Formation à la Recherche dans l'Industrie et dans l'Agriculture (F.R.I.A.-FNRS)" (PhD fellowship, TT) and the University of Liège (Council for Research and Valorization in Science and Techniques (IPD-STEMA 2022 postdoctoral fellowship, YHT).

Conflicts of Interest

The authors declare no conflicts of interest.

Data Availability Statement

The data that support the findings of this study are available from the corresponding author upon reasonable request.

References

1. S. M. Weinreb, Comprehensive Organic Synthesis, HeterodienophileAdditions to Dienes (Elsevier 1991).
2. G. W. Kirby, "Tilden Lecture. Electrophilic C-Nitroso-Compounds," Chemical Society Reviews 6 (1977): 1–24.
3. L. Brulíková, A. Harrison, M. J. Miller, and J. Hlavác,ˇ "Stereo- and Regioselectivity of the Hetero-Diels–Alder Reaction of Nitroso Derivatives with Conjugated Dienes," Beilstein Journal of Organic Chemistry 12 (2016): 1949–1980.
4. B. S. Bodnar and M. J. Miller, "The Nitrosocarbonyl Hetero-Diels–Alder Reaction as a Useful Tool for Organic Syntheses," Angewandte Chemie, International Edition 50 (2011): 5630–5647.
5. P. Bianchi and J.-C. M. Monbaliu, "Three Decades of Unveiling the Complex Chemistry of C-Nitroso Species with Computational Chemistry," Organic Chemistry Frontiers 9 (2022): 223–264.
6. D. Beaudoin and J. D. Wuest, "Dimerization of Aromatic C-Nitroso Compounds," Chemical Reviews 116 (2016): 258–286.
7. G. W. Kirby and J. G. Sweeny, "Formation and Dienophilic Reactions of Transient C-Nitrosocarbonyl Compounds," Journal of the Chemical Society, Perkin Transactions 1 (1981): 3250–3254.

Published in : ChemSusChem (2025), e202501565
DOI: 10.1002/cssc.202501565
Status : Postprint (Author's version)

8. G. W. Kirby, H. McGuigan, and D. McLean, "Intramolecular 'Ene' Reactions of Transient, Allylic, and Homoallylic C-Nitrosoformate Esters," Journal of the Chemical Society, Perkin Transactions 1 (1985): 1961–1966.
9. P. Quadrelli, G. Campari, M. Mella, and P. Caramella, "A Thermal Fragmentation of 1,2,4-Oxadiazole-4-Oxides to Nitriles and Nitrosocarbonyls," Tetrahedron Letters 41 (2000): 2019–2022.
10. G. W. Kirby and J. G. Sweeny, "Nitrosocarbonyl Compounds as Intermediates in the Oxidative Cleavage of Hydroxamic Acids," Journal of the Chemical Society, Chemical Communications (1973): 704–705.
11. M. G. Memeo and P. Quadrelli, "Generation and Trapping of Nitrosocarbonyl Intermediates," Chemical Reviews 117 (2017): 2108–2200.
12. A. D. Cohen, B.-B. Zeng, S. B. King, and J. P. Toscano, "Direct Observation of an Acyl Nitroso Species in Solution by Time-Resolved IR Spectrocopy," Journal of the American Chemical Society 125 (2003): 1444–1445.
13. A. G. Leach and K. N. Houk, "Transition States and Mechanisms of the Hetero-Diels–Alder Reactions of Hyponitrous Acid, Nitrosoalkanes, Nitrosoarenes, and Nitrosocarbonyl Compounds," Journal of Organic Chemistry 66 (2001): 5192–5200.
14. D. S. Zinad, A. Mahal, R. K. Mohapatra, A. K. Sarangi, andM. R. F. Pratama, "Medicinal Chemistry of Oxazines as Promising Agents in Drug Discovery," Chemical Biology & Drug Design 95 (2020): 16–47.
15. L.-H. Yan, X. Li, and B.-G. Wang, "Natural Products with 1,2-Oxazine Scaffold: Occurrence, Chemical Diversity, Bioactivity, Synthesis, and Biosynthesis," Natural Product Reports 40 (2023): 1874–1900.
16. G. Galvani, R. Lett, and C. Kouklovsky, "Mild Cleavage of N–O Bond of 3,6-Dihydro-1,2-Oxazines by Condensation of Aldehydes in Aqueous Media," Synlett 26 (2015): 1340–1344.
17. F. Pfrengle and H.-U. Reissig, "Amino Sugars and Their Mimetics via 1,2-Oxazines," Chemical Society Reviews 39 (2010): 549–557.
18. J. Streith and A. Defoin, "Azasugar Syntheses and Multistep Cascade Rearrangements via Hetero Diels-Alder Cycloadditions with Nitroso Dienophiles," Synlett 3 (1996): 189–200.
19. K. Okuro, K. Khumtaveeporn Tuan Dang, and H. Alper, "Cobalt Carbonyl Mediated Carbonylative ring Expansion Reactions of 3,6-Dihydro-2H-1,2-Oxazines," Tetrahedron Letters 37 (1996): 2713–2716.
20. N. Yasukawa, M. Kuwata, T. Imai, Y. Monguchi, H. Sajiki, andY. Sawama, "Copper-Catalyzed Pyrrole Synthesis from 3,6-Dihydro1,2-Oxazines," Green Chemistry 20 (2018): 4409–4413.
21. R. S. Givens, D. J. Choo, S. N. Merchant, R. P. Stitt, and B. Matuszewski, "Photochemistry of 3,6-Dihydro-1,2-Oxazines: A Versatile Route to Substituted Pyrroles," Tetrahedron Letters 23 (1982): 1327–1330.
22. J.-B. Behr, C. Chevrier, A. Defoin, C. Tarnus, and J. Streith, "Asymmetric Synthesis of Potent Glycosidase and Very Potent α-Mannosidase Inhibitors: 4-Amino-4-Deoxy-l-Erythrose and 4-Amino4,5-Dideoxy-l-Ribose," Tetrahedron 59 (2003): 543–553.
23. C. Arribas, M. C. Carreno, J. L. García-Ruano, J. F. Rodríguez,˜ M. Santos, and M. A. Sanz-Tejedor, "First Asymmetric Hetero DielsAlder Reaction of 1-Sulfinyl Dienes with Nitroso Derivatives. A New Entry to the Synthesis of Optically Pure 1,4-Imino-L-Ribitol Derivatives," Organic Letters 2 (2000): 3165–3168.
24. S. Krupkova, G. P. Aguete, L. Kocmanova, et al., "Solid-Phase Synthesis of ɣ-Lactone and 1,2-Oxazine Derivatives and Their Efficient Chiral Analysis," PLoS One 11 (2016): e0166558.
25. M. K. Manjula, K. M. L. Rai, S. L. Gaonkar, K. A. Raveesha, andS. Satish, "Synthesis of New Series of 5,6-Dihydro-4H-1,2-Oxazines via Hetero Diels–Alder Reaction and Evaluation of Antimicrobial Activity," European Journal of Medicinal Chemistry 44 (2009): 280–288.
26. G. Utecht and M. Jasi ´nski, "3,6-Dihydro-2H-1,2-Oxazines (microreview)," Chemistry of Heterocyclic Compounds 52 (2016): 143–145.

27. S. Iwasa, A. Fakhruddin, and H. Nishiyama, "Synthesis of Acylnitroso Intermediates and Their Synthetic Applications," Mini-Reviews in Organic Chemistry 2 (2005): 157–175.
28. M. A. EL-Atawy, D. Formenti, F. Ferretti, and F. Ragaini, "Synthesis of 3,6-Dihydro-2H-[1, 2]-Oxazines from Nitroarenes and Conjugated Dienes, Catalyzed by Palladium/Phenanthroline Complexes and Employing Phenyl Formate as a CO Surrogate," ChemCatChem 10(2018): 4707–4717.
29. C. P. Frazier, A. Bugarin, J. R. Engelking, and J. Read de Alaniz,"Copper-Catalyzed Aerobic Oxidation of N -Substituted Hydroxylamines: Efficient and Practical Access to Nitroso Compounds," Organic Letters 14 (2012): 3620–3623.
30. M. G. Memeo and P. Quadrelli, "A New Life for Nitrosocarbonyls in Pericyclic Reactions," Arkivoc 1 (2013): 418–423.
31. N. Momiyama and H. Yamamoto, "Enantioselective O- and N-Nitroso Aldol Synthesis of Tin Enolates. Isolation of Three BINAP–Silver Complexes and Their Role in Regio- and Enantioselectivity," Journal of the American Chemical Society 126 (2004): 5360–5361.
32. M. Baidya, K. A. Griffin, and H. Yamamoto, "Catalytic Enantioselective O-Nitrosocarbonyl Aldol Reaction of β-Dicarbonyl Compounds," Journal of the American Chemical Society 134 (2012): 18566–18569.
33. T. Kano, F. Shirozu, and K. Maruoka, "Metal-Free Enantioselective Hydroxyamination of Aldehydes with Nitrosocarbonyl Compounds Catalyzed by an Axially Chiral Amine," Journal of the American Chemical Society 135 (2013): 18036–18039.
34. Y. Li, S. Chakrabarty, and A. Studer, "An Efficient Approach to Chiral Allyloxyamines by Stereospecific Allylation of Nitrosoarenes with Chiral Allylboronates," Angewandte Chemie, International Edition 54 (2015): 3587–3591.
35. J.-C. Monbaliu, G. Dive, J. Marchand-Brynaert, and D. Peeters, "HDA Cycloadditions of 1-Diethoxyphosphonyl-1,3-Butadiene with Nitroso Heterodienophiles: A Computational Investigation," Journal of Molecular Structure: THEOCHEM 959 (2010): 49–54.
36. B. Maji and H. Yamamoto, "Copper-Catalyzed Asymmetric Synthesis of Tertiary α-Hydroxy Phosphonic Acid Derivatives with In Situ Generated Nitrosocarbonyl Compounds as the Oxygen Source," Angewandte Chemie International Edition 53 (2014): 14472–14475.
37. M. E. Shoman, J. F. DuMond, T. S. Isbell, et al., "Acyloxy Nitroso Compounds as Nitroxyl (HNO) Donors: Kinetics, Reactions with Thiols, and Vasodilation Properties," Journal of Medicinal Chemistry 54 (2011): 1059–1070.
38. J. Fahrer and M. Christmann, "DNA Alkylation Damage by Nitrosamines and Relevant DNA Repair Pathways," International Journal of Molecular Sciences 24 (2023): 4684.
39. P. Quadrelli, M. Mella, A. Gamba Invernizzi, and P. Caramella, "The Mild Oxidation of Nitrile Oxides Affords a Convenient Entry to Nitrosocarbonyl Intermediates, Versatile Tools in Organic Syntheses," Tetrahedron 55 (1999): 10497–10510.
40. J. Rowe and A. Ward, "Hydroxamic Acids. I. The Oxidation of Hydroxamic Acids and Their O-Alkyl Derivatives," Australian Journal of Chemistry 21 (1968): 2761–2761.
41. N. E. Jenkins, R. W. Ware, R. N. Atkinson, and S. B. King, "Generation of Acyl Nitroso Compounds by the Oxidation of N-Acyl Hydroxylamines with the Dessmartin Periodinane," Synthetic Communications 30 (2000): 947–953.
42. L. Palmer, C. Frazier, and J. Read de Alaniz, "Developments in Nitrosocarbonyl Chemistry: Mild Oxidation of N-Substituted Hydroxylamines Leads to New Discoveries," Synthesis 46 (2013): 269–280.
43. S. F. Martin, M. Hartmann, and J. A. Josey, "Diastereoselective [4+2] Cycloadditions of Acyl Nitroso Compounds," Tetrahedron Letters 33 (1992): 3583–3586.
44. G. E. Keck, "Intramolecular Dienophile Transfer. Diels-Alder Adducts of Acyl-Nitroso Compounds as Useful Reagents for Intramolecular Cycloadditions," Tetrahedron Letters 19 (1978): 4767–4770.

45. "Steel, Aluminum, Nickel, Rare earth, new energy, Copper Prices Charts and news-Shanghai Metals Market," accessed October, 2025, https://www.metal.com/.
46. M. F. A. Adamo and S. Bruschi, "Generation of Acylnitroso Dienophiles: A Study of Metal Catalysis," Journal of Organic Chemistry 72 (2007): 2666–2669.
47. J. A. K. Howard, G. Ilyashenko, H. A. Sparkes, and A. Whiting, "Development of New Transition Metal Catalysts for the Oxidation of a Hydroxamic Acid with In Situ Diels–Alder Trapping of the Acyl Nitroso Derivative," Dalton Transactions (2007): 2108–2111.
48. K. R. Flower, A. P. Lightfoot, H. Wan, and A. Whiting, "The Development and Application of Ruthenium Catalysed Oxidations of a Hydroxamic Acid and In Situ Diels–Alder Trapping of the Acyl Nitroso Derivative," Journal of the Chemical Society, Perkin Transactions 2 (2002): 2058–2064.
49. D. Atkinson, M. A. Kabeshov, M. Edgar, and A. V. Malkov, "Intramolecular Carbonyl Nitroso Ene Reaction Catalyzed by Iron(III) Chloride/Hydrogen Peroxide as an Efficient Tool for Direct Allylic Amination," Advanced Synthesis & Catalysis 353 (2011): 3347–3351.
50. G. T. Rice and M. C. White, "Allylic C-H Amination for the Preparation of Syn-1,3-Amino Alcohol Motifs," Journal of the American Chemical Society 131 (2009): 11707–11711.
51. R. I. McDonald and S. S. Stahl, "Modular Synthesis of 1,2-Diamine Derivatives by Palladium-Catalyzed Aerobic Oxidative Cyclization of Allylic Sulfamides," Angewandte Chemie 122 (2010): 5661–5664.
52. H. Lebel, K. Huard, and S. Lectard, "N-Tosyloxycarbamates as a Source of Metal Nitrenes: Rhodium-Catalyzed C-H Insertion and Aziridination Reactions," Journal of the American Chemical Society 127 (2005): 14198–14199.
53. I. Bauer and H.-J. Knölker, "Iron Catalysis in Organic Synthesis," Chemical Reviews 115 (2015): 3170–3387.
54. M.-Q. Liang and C.-D. Lu, "MgCl2-Catalyzed α-Amination of α-Alkylβ-Ketoesters via Oxidative N-Acylnitroso Aldol Reaction with Hydroxamic Acids," Synlett 25 (2014): 991–994.
55. D. Sandoval, C. P. Frazier, A. Bugarin, and J. Read de Alaniz, "Electrophilic α-Amination Reaction of β-Ketoesters Using N Hydroxycarbamates: Merging Aerobic Oxidation and Lewis Acid Catalysis," Journal of the American Chemical Society 134 (2012): 18948–18951.
56. A. Fakhruddin, S. Iwasa, H. Nishiyama, and K. Tsutsumi, "Ene Reactions of Acyl Nitroso Intermediates with Alkenes and Their Halocyclization," Tetrahedron Letters 45 (2004): 9323–9326.
57. A. Fakhruddin, A.-M. Abu-Elfotoh, K. Shibatomi, and S. Iwasa, "A New Synthetic Route to Acylnitroso Intermediates and Their Applications in HDA and Ene Reactions," Letters in Organic Chemistry 15 (2018): 196–205.
58. B. Kalita and K. M. Nicholas, "Copper-Catalyzed Allylic Hydroxyamination and Amination of Alkenes with Boc-Hydroxylamine," Tetrahedron Letters 46 (2005): 1451–1453.
59. R. S. Srivastava, "Copper-Catalyzed Allylic Amination of Olefins with Nitrosoarenes," Tetrahedron Letters 44 (2003): 3271–3274.
60. G. A. Hogan, A. A. Gallo, K. M. Nicholas, and R. S. Srivastava, "Cu(I)Catalyzed Allylic Amination of Olefins," Tetrahedron Letters 43 (2002): 9505–9508.
61. C.-M. Ho and T.-C. Lau, "Copper-Catalyzed Amination of Alkenes and Ketones by Phenylhydroxylamine," New Journal of Chemistry 24 (2000): 859–863.
62. Y. Hoshino, K. Suzuki, and K. Honda, "Vanadium-Catalyzed Oxidation of Tert-Butyl N-Hydroxycarbamate to Tert-Butyl Nitrosoformate and Its Diels–Alder Reaction with Simple and Functionalized Dienes," Synlett 23 (2012): 2375–2380.
63. G. Calvet, N. Blanchard, and C. Kouklovsky, "Synthesis of Polysubstituted Pyrroles from Nitroso-Diels-Alder Cycloadducts," Synthesis 19 (2005): 3346–3354.

64. K. R. Flower, H. Wan, A. Whiting, and A. P. Lightfoot, "Direct Evidence for a Ruthenium(iv) Oxo Complex-Mediated Oxidation of a Hydroxamic Acid in the Presence of Phosphine Oxide Donors," Chemical Communications 18 (2001): 1812–1813.
65. C. P. Chow and K. J. Shea, "Dual Function Catalysts. Dehydrogenation and Asymmetric Intramolecular Diels–Alder Cycloaddition of N -Hydroxy Formate Esters and Hydroxamic Acids: Evidence for a Ruthenium–Acylnitroso Intermediate," Journal of the American Chemical Society 127 (2005): 3678–3679.
66. J. A. K. Howard, G. Ilyashenko, H. A. Sparkes, A. Whiting, andA. R. Wright, "Mechanistic Insights into Transition Metal-Catalysed Oxidation of a Hydroxamic Acid with In Situ Diels–Alder Trapping of the Acyl Nitroso Derivative," Advanced Synthesis & Catalysis 350 (2008): 869–882.
67. T. L. Siddall, N. Miyaura, J. C. Huffman, and J. K. Kochi, "Isolation and Molecular Structure of Unusual Oxochromium(V) Cations for the Catalytic Epoxidation of Alkenes," Journal of the Chemical Society, Chemical Communications (1983): 1185–1186.
68. S. Iwasa, K. Tajima, S. Tsushima, and H. Nishiyama, "A Mild Oxidation Method of Hydroxamic Acids: Efficient Trapping of Acyl Nitroso Intermediates," Tetrahedron Letters 42 (2001): 5897–5899.
69. A. Fakhruddin, K. Phomkeona, A.-M. Abu-Elfotoh, K. Shibatomi, andS. Iwasa, "Ru(II)- and Ir(I) Catalyzed Hydrogen Peroxide Oxidation of Hydroxamic Acids and Their Subsequent Hetero Diels-Alder Cycloadditions with Chiral N-Dienyl Lactams," Letters in Organic Chemistry 7 (2010): 475–478.
70. S. Iwasa, A. Fakhruddin, Y. Tsukamoto, M. Kameyama, and H. Nishiyama, "Iridium(I)-Catalyzed Hydrogen Peroxide Oxidation of Hydroxamic Acids and Hetero Diels–Alder Reaction of the Acyl Nitroso Intermediates with Cyclopentadiene," Tetrahedron Letters 43 (2002): 6159–6161.
71. X. Tusun and C.-D. Lu, "The Oxidative Acylnitroso Hetero-DielsAlder Reaction Catalyzed by Dirhodium Caprolactamate," Synlett 23 (2012): 1801–1804.
72. M. O. Ratnikov, L. E. Farkas, E. C. McLaughlin, et al., "DirhodiumCatalyzed Phenol and Aniline Oxidations with T-HYDRO. Substrate Scope and Mechanism of Oxidation," Journal of Organic Chemistry 76 (2011): 2585–2593.
73. E. C. McLaughlin, H. Choi, K. Wang, G. Chiou, and M. P. Doyle,"Allylic Oxidations Catalyzed by Dirhodium Caprolactamate via Aqueous Tert -Butyl Hydroperoxide: The Role of the Tert-Butylperoxy Radical," Journal of Organic Chemistry 74 (2009): 730–738.
74. O. Carugo and K. D. Carugo, "When X-Rays Modify the Protein Structure: Radiation Damage at Work," Trends in Biochemical Sciences 30 (2005): 213–219.
75. E. G. Hrycay and S. M. Bandiera, "The Monooxygenase, Peroxidase, and Peroxygenase Properties of Cytochrome P450," Archives of Biochemistry and Biophysics 522 (2012): 71–89.
76. A. Samuni and S. Goldstein, "One-Electron Oxidation of Acetohydroxamic Acid: The Intermediacy of Nitroxyl and Peroxynitrite," Journal of Physical Chemistry A 115 (2011): 3022–3028.
77. E. Maimon, A. Samuni, and S. Goldstein, "Nitrogen Dioxide Reaction with Nitroxide Radical Derived from Hydroxamic Acids: The Intermediacy of Acyl Nitroso and Nitroxyl (HNO," Journal of Physical Chemistry A 122 (2018): 3747–3753.
78. U. Samuni, E. Maimon, and S. Goldstein, "A Kinetic Study of the Oxidation of Hydroxamic Acids by Compounds I and II of Horseradish Peroxidase: Effect of Transition Metal Ions," Journal of Coordination Chemistry 71 (2018): 1728–1737.
79. C. Lagercrantz and T. Larsson, "Spin Trapping of Methyl Radicals by the Acyl Nitroso Compound PH-C (=O)NO Formed in the Photochemical Reaction Between Benzohydroxamic Acid, Dimethyl Sulfoxide and Hydrogen Peroxide. An Epr Study," Free Radical Research 20 (1994): 181–187.
80. S. Uraoka, I. Shinohara, H. Shimizu, et al., "Hetero Diels–Alder Reaction and Ene Reaction of Acylnitroso Species In Situ Generated by Hypoiodite Catalysis," European Journal of Organic Chemistry 2018 (2018): 6199–6203.

Published in : ChemSusChem (2025), e202501565
DOI: 10.1002/cssc.202501565
Status : Postprint (Author's version)

81. A. Nakamura, J. Morimoto, M. Taniguchi, H. Aoyama, J. He, andT. Maegawa, "N-Bu_4NI/H_2O_2-Catalyzed Mild Conversion of Hydroxamic Acids to Carboxylic Acids," Tetrahedron Letters 126 (2023): 154656.
82. C. P. Frazier, J. R. Engelking, and J. Read de Alaniz, "CopperCatalyzed Aerobic Oxidation of Hydroxamic Acids Leads to a Mild and Versatile Acylnitroso Ene Reaction," Journal of the American Chemical Society 133 (2011): 10430–10433.
83. W. Oppolzer and V. Snieckus, "Intramolecular Ene Reactions in Organic Synthesis," Angewandte Chemie, International Edition in English 17 (1978): 476–486.
84. Y. Xu, M.-M. Alavanja, V. L. Johnson, G. Yasaki, and S. B. King, "Production of Nitroxyl (HNO) at Biologically Relevant Temperatures from the Retro-Diels–Alder Reaction of N-Hydroxyurea-Derived Acyl Nitroso-9,10-Dimethylanthracene Cycloadducts," Tetrahedron Letters 41 (2000): 4265–4269.
85. R. J. Boeckman and K. M. George, Encyclopedia of Reagents for Organic Synthesis (John Wiley & Sons, Ltd, 2009).
86. B. Gioia, F. Ruggieri, A. Biela, et al., "Regioselective and Stereoselective Synthesis of Parthenolide Analogs by Acyl Nitroso-Ene Reaction and Their Biological Evaluation against Mycobacterium Tuberculosis," International Journal of Molecular Sciences 24 (2023): 17395.
87. R. B. Lewis and J. Read de Alaniz, "Nitrosocarbonyl Hetero-Diels– Alder Cycloaddition with 2-Substituted 1,3-Butadienes," Tetrahedron 73 (2017): 4045–4051.
88. C. Xu, L. Zhang, and S. Luo, "Merging Aerobic Oxidation and Enamine Catalysis in the Asymmetric α-Amination of β-Ketocarbonyls Using N -Hydroxycarbamates as Nitrogen Sources," Angewandte Chemie International Edition 53 (2014): 4149–4153.
89. L. Zhang, C. Xu, X. Mi, and S. Luo, "Origins of the Enantio- and N/O Selectivity in the Primary-Amine-Catalyzed Hydroxyamination of 1,3Dicarbonyl Compounds with In-Situ-Formed Nitrosocarbonyl Compounds: A Theoretical Study," Chemistry - An Asian Journal 9 (2014): 3565–3571.
90. X. Xie, L. Zhang, Q. He, et al., "Copper-Catalyzed Aerobic Autoxidation of N -Hydroxycarbamates Probed by Mass Spectrometry," Chemistry - A European Journal 21 (2015): 14630–14637.
91. C. Xu, L. Zhang, and S. Luo, "Catalytic Asymmetric Oxidative α-C–H N, O-Ketalization of Ketones by Chiral Primary Amine," Organic Letters 17 (2015): 4392–4395.
92. I. Ramakrishna, G. S. Grandhi, H. Sahoo, and M. Baidya, "The Mukaiyama Aldol Reaction of In Situ Generated Nitrosocarbonyl Compounds: Selective C–N Bond Formation and N–O Bond Cleavage in One-Pot for α-Amination of Ketones," Chemical Communications 51 (2015): 13976–13979.
93. D. Sandoval, A. V. Samoshin, and J. Read de Alaniz, "Asymmetric Electrophilic α-Amination of Silyl Enol Ether Derivatives via the Nitrosocarbonyl Hetero-ene Reaction," Organic Letters 17 (2015): 4514–4517.
94. Y. Miura, H. Ouchi, M. Inai, et al., "Synthetic Studies on Pactamycin: A Synthesis of Johnson's Intermediate," Organic Letters 22 (2020): 3515– 3518.
95. J. T. Malinowski, R. J. Sharpe, and J. S. Johnson, "Enantioselective Synthesis of Pactamycin, a Complex Antitumor Antibiotic," Science 340 (2013): 180–182.
96. F. Zhao, P. Yu, Y. Chen, F. Liu, and K. N. Houk, "π-Facial Stereoselectivity in Acyl Nitroso Cycloadditions to 5,5-Unsymmetrically Substituted Cyclopentadienes: Computational Exploration of Origins of Selectivity and the Role of Substituent Conformations on Selectivity," Journal of Organic Chemistry 86 (2021): 17082–17089.
97. W. Yang, J. Sun, X. Xu, Q. Zhang, and Q. Liu, "Hydroxyamination of Aryl C–H Bonds with N-Hydroxycarbamate by Synergistic Rh/Cu Catalysis at Room Temperature," Chemical Communications 50 (2014): 4420–4422.

98. G. Song, F. Wang, and X. Li, "C–C, C–O and C–N Bond Formation via Rhodium(iii)-Catalyzed Oxidative C–H Activation," Chemical Society Reviews 41 (2012): 3651–3678.
99. Y. Lian, R. G. Bergman, L. D. Lavis, and J. A. Ellman, "Rhodium(III)Catalyzed Indazole Synthesis by C–H Bond Functionalization and Cyclative Capture," Journal of the American Chemical Society 135 (2013): 7122–7125.
100. L. Yang, C. A. Correia, and C. Li, "Grignard-Type Arylation of Aldehydes via a Rhodium-Catalyzed C-H Activation under Mild Conditions," Advanced Synthesis & Catalysis 353 (2011): 1269–1273.
101. W. Hou, B. Zhou, Y. Yang, H. Feng, and Y. Li, "Rh(III)-Catalyzed Addition of Alkenyl C–H Bond to Isocyanates and Intramolecular Cyclization: Direct Synthesis 5-Ylidenepyrrol-2(5 H)-Ones," Organic Letters 15 (2013): 1814–1817.
102. C. A. Parish, S. K. Smith, K. Calati, et al., "Isolation and Structure Elucidation of Parnafungins, Antifungal Natural Products that Inhibit mRNA Polyadenylation," Journal of the American Chemical Society 130 (2008): 7060–7066.
103. D. Chaiyaveij, L. Cleary, A. S. Batsanov, T. B. Marder, K. J. Shea, andA. Whiting, "Copper(II)-Catalyzed Room Temperature Aerobic Oxidation of Hydroxamic Acids and Hydrazides to Acyl-Nitroso and Azo Intermediates, and Their Diels–Alder Trapping," Organic Letters 13 (2011): 3442–3445.
104. D. Chaiyaveij, A. S. Batsanov, M. A. Fox, T. B. Marder, andA. Whiting, "An Experimental and Computational Approach to Understanding the Reactions of Acyl Nitroso Compounds in [4 + 2] Cycloadditions," Journal of Organic Chemistry 80 (2015): 9518–9534.
105. W. Yang, L. Huang, Y. Yu, D. Pflästerer, F. Rominger, andA. S. K. Hashmi, "Highly Diastereoselective and Regioselective Copper-Catalyzed Nitrosoformate Dearomatization Reaction under Aerobic-Oxidation Conditions," Chemistry - A European Journal 20 (2014): 3927–3931.
106. C. P. Frazier, D. Sandoval, L. I. Palmer, and J. Read de Alaniz,"Electrophilic α-Oxygenation Reaction of β-Ketoesters Using NHydroxycarbamates: Control of the Ambident Reactivity of Nitrosoformate Intermediates," Chemical Science 4 (2013): 3857–3862.
107. B. Maji and H. Yamamoto, "Asymmetric Synthesis of Tertiary α-Hydroxy Phosphonic Acid Derivatives under Aerobic Oxidation Conditions," Synlett 26 (2015): 1528–1532.
108. R. Engel, "Phosphonates as Analogues of Natural Phosphates," Chemical Reviews 77 (1977): 349–367.
109. L. Azema, R. Baron, and S. Ladame, "Targeting Enzymes with Phosphonate-Based Inhibitors: Mimics of Tetrahedral Transition States and Stable Isosteric Analogues of Phosphates," Current Enzyme Inhibition 2 (2006): 61–72.
110. Y. C. Teo, Y. Pan, and C. H. Tan, "Organic Dye-Photocatalyzed Acylnitroso Ene Reaction," ChemCatChem 5 (2013): 235–240.
111. C. P. Frazier, L. I. Palmer, A. V. Samoshin, and J. Read de Alaniz,"Accessing Nitrosocarbonyl Compounds with Temporal and Spatial Control via the Photoredox Oxidation of N-Substituted Hydroxylamines," Tetrahedron Letters 56 (2015): 3353–3357.
112. T. Basile, L. Capaldo, D. Ravelli, and P. Quadrelli, "Photocatalyzed Generation of Nitrosocarbonyl Intermediates Under Solar Light Irradiation," European Journal of Organic Chemistry 10 (2020): 1443–1447.
113. L. Y. Lam and C. Ma, "Transition-Metal Free Photocatalytic Synthesis of Acylsulfonamides," Organic Letters 27 (2025): 4732–4736.
114. C. Jäger, M. Haase, K. Koschorreck, V. B. Urlacher, and J. Deska,"Aerobic C–N Bond Formation through Enzymatic Nitroso-Ene-Type Reactions**," Angewandte Chemie, International Edition 62 (2023): e202213671.
115. G. E. Keck and R. Webb, "Carbon-Nitrogen Bond Formation AcylNitroso Compounds. Intramolecular Ene Processes," Tetrahedron Letters 20 (1979): 1185–1186.

116. S.-H. Huang, X. Tian, X. Mi, Y. Wang, and R. Hong, "Nitroso-ene Cyclization Enabled Access to 1-Azaspiro[4.4]nonane and Its Application in a Modular Synthesis toward (±)-Cephalotaxine," Tetrahedron Letters 56 (2015): 6656–6658.
117. C. Jäger, M. Nieger, K. Rissanen, and J. Deska, "Multienzymatic Synthesis of γ-Lactam Building Blocks from Unsaturated Esters and Hydroxylamine," European Journal of Organic Chemistry 26 (2023): e202300288.
118. C. Jäger, B. J. Gregori, J. A. S. Aho, M. Hallamaa, and J. Deska, "Peroxidase-Induced C–N Bond Formation via Nitroso Ene and Diels–Alder Reactions," Green Chemistry 25 (2023): 3166–3174.
119. C. M. Alder, J. D. Hayler, R. K. Henderson, et al., "Updating and Further Expanding GSK's Solvent Sustainability Guide," Green Chemistry 18 (2016): 3879–3890.
120. European Commission, "Critical Raw Materials Act," accessed October, 2025, https://single-market-economy.ec.europa.eu/sectors/ raw-materials/areas-specific-interest/critical-raw-materials/critical-rawmaterials-act_en.
121. D. Raabe, "The Materials Science behind Sustainable Metals and Alloys," Chemical Reviews 123 (2023): 2436–2608.
122. P. Nuss and M. J. Eckelman, "Life Cycle Assessment of Metals: A Scientific Synthesis," PLoS One 9 (2014): e101298.
123. C. Sambiagio and T. Noël, "Flow Photochemistry: Shine Some Light on Those Tubes!," Trends in Chemistry 2 (2020): 92–106.
124. C. A. Hone and C. O. Kappe, "The Use of Molecular Oxygen for Liquid Phase Aerobic Oxidations in Continuous Flow," Topics in Current Chemistry 377 (2019): 2.
125. M. B. Plutschack, B. Pieber, K. Gilmore, and P. H. Seeberger, "The Hitchhiker's Guide to Flow Chemistry," Chemical Reviews 117 (2017): 11796–11893.
126. T. Razzaq and C. O. Kappe, "Continuous Flow Organic Synthesis under High-Temperature/Pressure Conditions," Chemistry - An Asian Journal 5 (2010): 1274–1289.
127. A. Slattery, Z. Wen, P. Tenblad, et al., "Automated Self-Optimization, Intensification, and Scale-up of Photocatalysis in Flow," Science 383 (2024): 1–12.
128. S. D. A. Zondag, D. Mazzarella, and T. Noël, "Scale-Up of Photochemical Reactions: Transitioning from Lab Scale to Industrial Production," Annual Review of Chemical and Biomolecular Engineering 14 (2023): 283–300.
129. A. A. H. Laporte, T. M. Masson, S. D. A. Zondag, and T. Noël,"Multiphasic Continuous-Flow Reactors for Handling Gaseous Reagents in Organic Synthesis: Enhancing Efficiency and Safety in Chemical Processes," Angewandte Chemie, International Edition 63 (2024): e202316108.
130. S. Ozaki and M. Masui, "Oxidation of Hydroxylamine Derivatives. I. Anodic Oxidation of Hydroxamic Acids," Chemical and Pharmaceutical Bulletin 25 (1977): 1179–1185.
131. J. Fährmann and G. Hilt, "Alternating Current Electrolysis as Efficient Tool for the Direct Electrochemical Oxidation of Hydroxamic Acids for Acyl Nitroso Diels–Alder Reactions," Angewandte Chemie International Edition 60 (2021): 20313–20317.
132. C. Kingston, M. D. Palkowitz, Y. Takahira, et al., "A Survival Guide for the 'Electro-Curious," Accounts of Chemical Research 53 (2020): 72–83.
133. T. Noël, Y. Cao, and G. Laudadio, "The Fundamentals Behind the Use of Flow Reactors in Electrochemistry," Accounts of Chemical Research 52 (2019): 2858–2869.
134. J. K. Conrad, C. D. Pilgrim, S. M. Pimblott, S. P. Mezyk, andG. P. Horne, "Multiscale Modelling of the Radical-Induced Chemistry of Acetohydroxamic Acid in Aqueous Solution," RSC Advances 12 (2022): 29757–29766.

Published in : ChemSusChem (2025), e202501565
DOI: 10.1002/cssc.202501565
Status : Postprint (Author's version)

135. U. Hanefeld, F. Hollmann, and C. E. Paul, "Biocatalysis Making Waves in Organic Chemistry," Chemical Society Reviews 51 (2022): 594–627.
136. E. L. Bell, W. Finnigan, S. P. France, et al., "Biocatalysis," Nature Reviews Methods Primers 1 (2021): 46.

Biographies

Yi-Hsuan Tsai graduated from the University of Rosario (Argentina) with a Master's degree (2015) and a PhD degree (2020). She has been a postdoctoral fellow at the Center for Integrated Technology and Organic Synthesis (University of Liège, Belgium) where her research focused on studying and implementing nitrosocarbonyl chemistry in continuous flow. She is currently working at Ajinotomo Omnichem.

Carlotta Campalani completed her PhD at the University Ca' Foscari of Venice (Italy) working on carbon dots and their use in photocatalysis. After her PhD, she got a postdoctoral position at the Max Planck Institute for Chemical Energy Conversion in Mülheim an der Ruhr (Germany) to develop heterogeneous photocatalysts. She is now a postdoctoral fellow at the Center for Integrated Technology and Organic Synthesis (CiTOS) at the University of Liège (Belgium) where she works on the continuous flow synthesis of quantum dots.

Thomas Toupy graduated from the University of Liège with a Master's degree (2017) and a PhD degree (2022). He carried out his Master thesis and PhD research programs at the Center for Integrated Technology and Organic Synthesis on amination protocols toward the preparation of peptides and analogs. After a postdoctoral appointment at MIT with Prof. Allan Myerson, he joined Takeda.

Isaline Jacquemin graduated from the University of Liège with a Master's degree (2021). She carried out her Master thesis at the Center for Integrated Technology and Organic Synthesis on the generation of nitroso carbonyl derivatives. She then transitioned to industry.

Jean-Christophe M. Monbaliu is Full Professor of Organic Chemistry at the University of Liège and Principal Investigator at the WEL Research Institute. He heads the Center for Integrated Technology and Organic Synthesis (CiTOS) at the University of Liège.

Monbaliu also leads the first European Corning Advanced-Flow Reactor Qualified Lab. In 2022, Monbaliu founded FloW4all, a Flow Technology Platform in Wallonia that focuses on training, technology transfer, and services for Industry.